PUBLISHER :

Address of Publisher
& Editor's Office :

GDAŃSK UNIVERSITY
OF TECHNOLOGY
Faculty
of Ocean Engineering
& Ship Technology

ul. Narutowicza 11/12
80-952 Gdańsk, POLAND
tel.: +48 58 347 13 66
fax : +48 58 341 13 66
e-mail : office.pmr@pg.gda.pl

Account number :
BANK ZACHODNI WBK S.A.
I Oddział w Gdańsku
41 1090 1098 0000 0000 0901 5569

Editorial Staff :
Tadeusz Borzęcki Editor in Chief
e-mail : tadbor@pg.gda.pl
Przemysław Wierzchowski Scientific Editor
e-mail : e.wierzchowski@chello.pl
Jan Michalski Editor for review matters
e-mail : janmi@pg.gda.pl
Aleksander Kniat Editor for international relations
e-mail : olek@pg.gda.pl
Kazimierz Kempa Technical Editor
e-mail : kkempa@pg.gda.pl
Piotr Bzura Managing Editor
e-mail : pbzura@pg.gda.pl
Cezary Spigarski Computer Design
e-mail : biuro@oficynamorska.pl

Domestic price :
single issue : 20 zł

Prices for abroad :
single issue :
- in Europe EURO 15
- overseas US$ 20

ISSN 1233-2585

POLISH MARITIME RESEARCH
in internet
www.bg.pg.gda.pl/pmr/pmr.php

POLISH MARITIME RESEARCH
No 4(71) 2011 Vol 18

CONTENTS

Editorial

POLISH MARITIME RESEARCH is a scientific journal of worldwide circulation. The journal appears as a quarterly four times a year. The first issue of it was published in September 1994. Its main aim is to present original, innovative scientific ideas and Research & Development achievements in the field of :

Engineering, **Computing & Technology**, **Mechanical Engineering**,

which could find applications in the broad domain of maritime economy. Hence there are published papers which concern methods of the designing, manufacturing and operating processes of such technical objects and devices as : ships, port equipment, ocean engineering units, underwater vehicles and equipment as well as harbour facilities, with accounting for marine environment protection.
The Editors of POLISH MARITIME RESEARCH make also efforts to present problems dealing with education of engineers and scientific and teaching personnel. As a rule, the basic papers are supplemented by information on conferences , important scientific events as well as cooperation in carrying out international scientific research projects.

Scientific Board

POLISH MARITIME RESEARCH 4(71) 2011 Vol 18; pp. 3-13
10.2478/v10012-011-0020-0

Multi-objective optimization of high speed vehicle-passenger catamaran by genetic algorithm

Part II
Analysis of the results

Zbigniew Sekulski, Ph. D.
West Pomeranian University of Technology in Szczecin

ABSTRACT

Real ship structural design problems are usually characterized by presence of many conflicting objectives. Simultaneously, a complete definition of the optimum structural design requires a formulation of size-topology-shape-material optimization task unifying the optimization problems from the four areas and giving an effective solution of the problem. Any significant progress towards solving the problem has not been obtained so far. An objective of the present paper was to develop an evolutionary algorithm for multi-objective optimization of the structural elements of large spatial sections of ships. Selected elements of the multi-criteria optimization theory have been presented in detail. Methods for solution of the multi-criteria optimization problems have been discussed with the focus on the evolutionary optimization algorithms. In the paper an evolutionary algorithm where selection takes place based on the aggregated objective function combined with domination attributes as well as distance to the asymptotic solution, is proposed and applied to solve the problem of optimizing structural elements with respect to their weight and surface area for a high - speed vehicle-passenger catamaran structure, with taking into account several design variables such as plate thickness, scantlings of longitudinal stiffeners and transverse frames, and spacing between longitudinal and transversal members. Details of the computational models were kept at the level typical for conceptual design stage. Scantlings were analyzed by using the selected classification society rules. The results of numerical experiments with the use of the developed algorithm are presented. They show that the proposed genetic algorithm may be considered an efficient tool for multi-objective optimization of ship structures.

The paper has been published in the three parts: Part I: Theoretical background on evolutionary multi-objective optimization, Part II: Computational simulations, and Part III: Analysis of the results.

Keywords: ship structure; multi-objective optimization; evolutionary algorithm; genetic algorithm; Pareto domination, set of non-dominated solutions

ANALYSIS OF THE RESULTS AND CONCLUSIONS DRAWN FROM THE COMPUTATIONAL SIMULATIONS

Three series of the computer simulations, signed sym1, sym2 and sym3, confirmed effectiveness of the developed computational algorithm and computer code for solution of the formulated problem of ship structure topology-size multi-objective optimization. As a result of the calculations an approximation of the Pareto-optimum set containing, in each simulation, from a few to more than ten non-dominated solutions, was found. The obtained results do not allow to unequivocally conclude which of the examined factors: (1) objective function aggregation strategies, (2) domination attributes included into selection process, and (3) distance to asymptotic solution included into selection process, is most advantageous.

In the case of studying the influence of optimization criteria aggregation strategy, visual assessment of the shape of the obtained approximations of the Pareto-optimum set suggests an advantage of the strategy with random values of the weight coefficients w_s (sym1-2) and the least effectiveness of the strategy with fixed values of the weight coefficients w_s (sym1-1).

The effectiveness of the strategy with random selection of single optimization criteria in the selection process (sym1-3) is intermediate. In the case of the constrained problems it also turns out that the components of the penalty functions introduce a random contribution to the fitness function thus causing the strategy with the fixed weight coefficients w_s to be practically

a strategy similar to the two others and it also allows to find approximation of the Pareto-optimum set with the adequate accuracy.

From the found sets of the compromise solutions a user can select, in the next stage, one or a few solutions by applying additional premises which are not included in the optimization model. He can also select suggested non-dominated solutions the closest to the asymptotic solutions $\mathbf{f}^{\approx}$:

$$\mathbf{f}^{\approx}_{sym1\text{-}1} = [1086.28\ 7422.10]^{T}\cdot[\text{kN m}^2] \Rightarrow$$
$$\Rightarrow f_{1,sym1\text{-}1}(\mathbf{x}) = 1086.28\ \text{kN},\ f_{2,sym1\text{-}1}(\mathbf{x}) = 7422.10\ \text{m}^2$$

$$\mathbf{f}^{\approx}_{sym1\text{-}2} = [1113.65\ 7361.45]^{T}\cdot[\text{kN m}^2] \Rightarrow$$
$$\Rightarrow f_{1,sym1\text{-}2}(\mathbf{x}) = 1113.65\ \text{kN},\ f_{2,sym1\text{-}2}(\mathbf{x}) = 7361.45\ \text{m}^2$$

$$\mathbf{f}^{\approx}_{sym1\text{-}3} = [1153.68\ 7381.57]^{T}\cdot[\text{kN m}^2] \Rightarrow$$
$$\Rightarrow f_{1,sym1\text{-}3}(\mathbf{x}) = 1153.68\ \text{kN},\ f_{2,sym1\text{-}3}(\mathbf{x}) = 7381.57\ \text{m}^2$$

Since this way three solutions are obtained, the next question is which of them can be recommended as the best[1)]. Here the following procedure is suggested by this author: non-dominated solution sets obtained in subsequent simulations can be merged into a temporary solution set presented in Fig. 39a. In this set only a part of solutions is non-dominated ones, Fig. 39b. In the set of 15 non-dominated solutions obtained by using the results of three simulations, a distance of each of them from the asymptotic objective in normalized objective space, can be determined, Fig. 39c. The least distance equal to 1.082, was obtained for the solution $f_1(\mathbf{x}) = 1113.65$ kN and $f_2(\mathbf{x}) = 7361.45$ m^2 found in the simulation sym1-2 (random values of the weight coefficients w_1 and w_2 in the range [0, 1]). The solution can be recommended as a single solution of the formulated problem of multi-objective optimization.

Effectiveness of the three examined multi-objective optimization strategies which use optimization criteria values and functions representing violation degree of constraints,

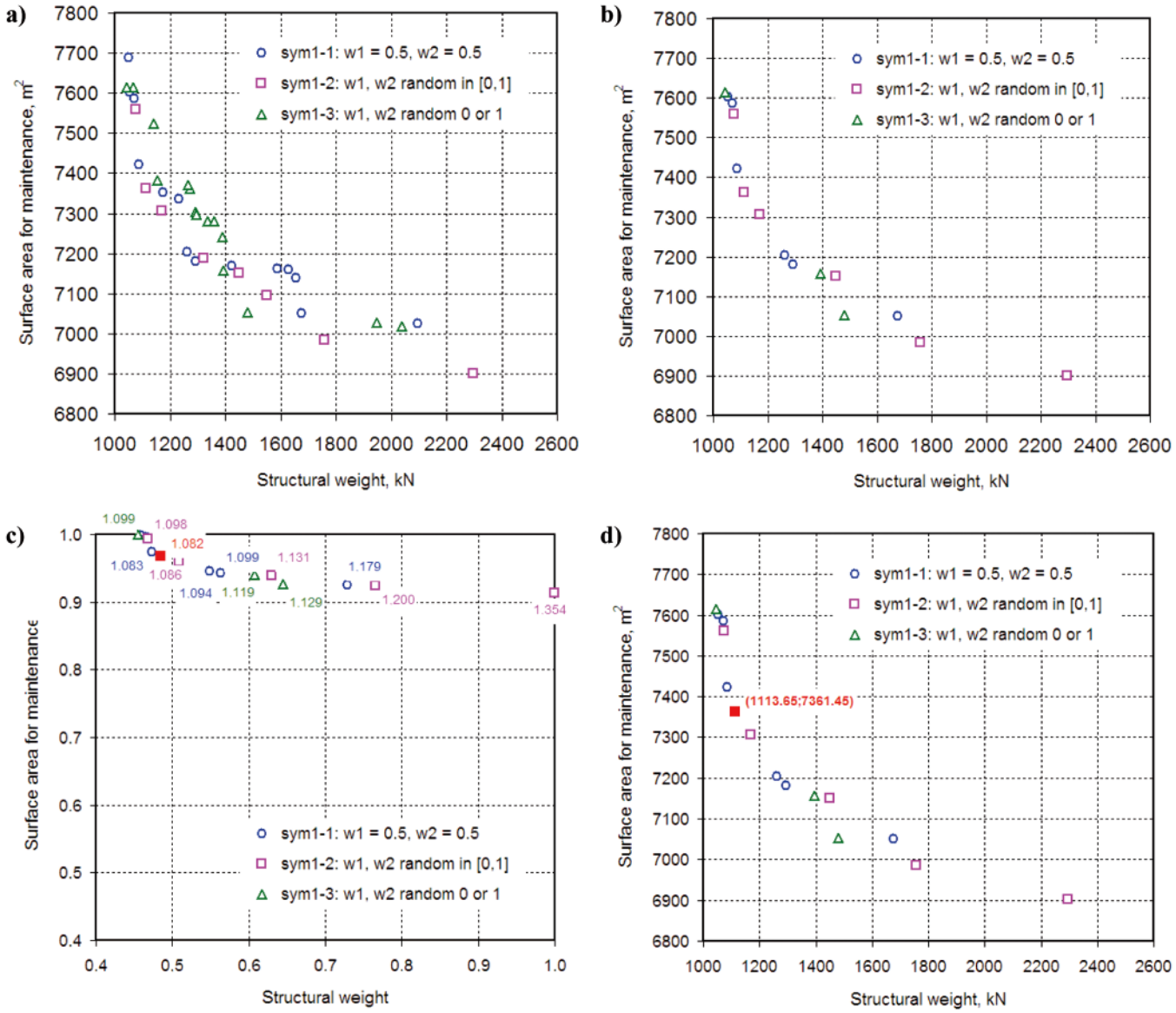

*Fig. 39. Selection of single, recommended solution of multi-objective optimization problem by using non-dominated solution sets obtained in the three series of computer simulations: **sym1-1**, **sym1-2**, **sym1-3**: **a)** temporary set composed of non-dominated solutions of each simulation, **b)** selection of non-dominated solutions in temporary set, **c)** determination of distance of non-dominated solutions from asymptotic objective in normalized objective space, **d)** values of optimization criteria for the found closest solution: $f_1(\mathbf{x}) = 1113.65$ kN and $f_2(\mathbf{x}) = 7361.45$ m^2*

[1)] Let us remember that in the multi-objective optimization there is not the single best solution of the problem and the formulated recommendation should be treated as a subjective choice by a person taking decision.

can be roughly evaluated also by assuming that the number of solutions produced by a given algorithm, that is a part of set of non-dominated solutions obtained on the basis of results produced by all algorithms, Fig. 39, is a measure of algorithm effectiveness. In the examined example the particular simulations: sym1-1, sym1-2 and sym1-3 have brought respectively 6, 6 and 3 non-dominated solutions into set of non-dominated solutions. On this basis a conclusion may be suggested that the strategies of fixed values of the optimization criteria weight coefficients $\mathbf{w_1 = w_2 = 0.5}$ and random values of the weight coefficients $\mathbf{w_1}$ **and** $\mathbf{w_2}$ in the range [0, 1] show similar effectiveness whereas the strategy of random values of the weight coefficients $\mathbf{w_1}$ **and** $\mathbf{w_2}$ equal to **0** or **1** proved to be the least effective. The issue of examining the effectiveness of multi-objective evolutionary algorithm is very relevant and not fully solved hence it requires a separate research which exceeds however content of this case study.

The conducted analysis of computer simulation results of the problem of ship structure multi-objective optimization in question allows to state that in the studied cases the most effective strategies were the following: (1) that with random values of the weight coefficients $\mathbf{w_1}$ and $\mathbf{w_2}$ in the range [0, 1], and that with fixed values of the optimization criteria weight coefficients $\mathbf{w_1 = w_2 = 0.5}$. Less effective was the strategy with random values of the weight coefficients $\mathbf{w_1}$ **and** $\mathbf{w_2}$ **equal to 0** or **1**.

The recommended non-dominated solution was obtained for the values of design variables specified in Tab. 8. The corresponding dimensions of the ship cross-section are given in Fig. 40.

From the study of influence of dominance attributes and distance from asymptotic solution on the effectiveness of the algorithms of sym2-1, sym2-2 and sym2-3, also satisfactory results were achieved as follows:

$$\mathbf{f}^{\approx}_{sym2\text{-}1} = [1105.95\ 7345.11]^T \cdot [\text{kN m}^2] \Rightarrow$$
$$\Rightarrow f_{1,sym2\text{-}1}(\mathbf{x}) = 1105.95\ \text{kN},\ f_{2,sym2\text{-}1}(\mathbf{x}) = 7345.11\ \text{m}^2$$

$$\mathbf{f}^{\approx}_{sym2\text{-}2} = [1192.04\ 7327.41]^T \cdot [\text{kN m}^2] \Rightarrow$$
$$\Rightarrow f_{1,sym2\text{-}2}(\mathbf{x}) = 1192.04\ \text{kN},\ f_{2,sym2\text{-}2}(\mathbf{x}) = 7327.41\ \text{m}^2$$

$$\mathbf{f}^{\approx}_{sym2\text{-}3} = [1060.03\ 7485.93]^T \cdot [\text{kN m}^2] \Rightarrow$$
$$\Rightarrow f_{1,sym2\text{-}3}(\mathbf{x}) = 1060.03\ \text{kN},\ f_{2,sym2\text{-}3}(\mathbf{x}) = 7485.93\ \text{m}^2$$

In the case of necessity to identify a single solution from a series of simulations one can apply the earlier described procedure of aggregation of set of non-dominated solutions obtained in particular simulations and identify the non-dominated solution nearest the asymptotic solution.

The performed calculation investigations have positively verified the effectiveness of the combined fitness multi-objective evolutionary algorithm developed by this author, as well as the calculation tool built for solving the unified ship structure topology-size multi-objective optimization problem. Particular computer simulations have produced a dozen or somewhat more of non-dominated solutions which constitute the set of trade-off solutions from among which decision makers may choose one or more of them for further development. The algorithm developed as a part of the underlying work allows also to pinpoint a single variant closest to the asymptotic solution which may be proposed as a single solution of the multi-objective optimization problem.

Fig. 41 presents the comprehensive results of the multi-objective optimization of the ship hull structure: (1) general arrangement and main particulars of an example ship, (2) optimization criteria, (3) simulation main parameters and control variables, (4) values of optimization criteria for the obtained non-dominated variants, (5) values of optimization criteria for the variant closest to the asymptotic solution, and (6) structural dimensions and scantlings for this variant.

Tab. 8. *Values of design variables recommended as a result of multi-objective optimization*

No.	Symbol	Description	Value
1	x_1	serial No. of mezzanine deck plate	5
2	x_2	serial No. of mezzanine deck bulb	6
3	x_3	serial No. of mezzanine deck T-bulb	48
4	x_4	number of web frames	13
5	x_5	number of mezzanine deck stiffeners	29
6	x_6	serial No. of superstructure I plate	8
7	x_7	serial No. of superstructure I bulb	5
8	x_8	serial No. of superstructure I T-bulb	47
9	x_9	number of superstructure I stiffeners	5
10	x_{10}	serial No. of inner side plate	6
11	x_{11}	serial No. of inner side bulb	2
12	x_{12}	serial No. of inner side T-bulb	48
13	x_{13}	number of inner side stiffeners	21
14	x_{14}	serial No. of bottom plate	9
15	x_{15}	serial No. of bottom bulb	5
16	x_{16}	serial No. of bottom T-bulb	52
17	x_{17}	number of bottom stiffeners	16
18	x_{18}	serial No. of outer side plate	5
19	x_{19}	serial No. of outer side bulb	2
20	x_{20}	serial No. of outer side T-bulb	52
21	x_{21}	number of outer side stiffeners	30
22	x_{22}	serial No. of wet deck plate	8
23	x_{23}	serial No. of wet deck bulb	6
24	x_{24}	serial No. of wet deck T-bulb	51
25	x_{25}	number of wet deck stiffeners	36
26	x_{26}	serial No. of main deck plate	10
27	x_{27}	serial No. of main deck bulb	1
28	x_{28}	serial No. of main deck T-bulb	46
29	x_{29}	number of main deck stiffeners	26
30	x_{30}	serial No. of superstructure II plate	8
31	x_{31}	serial No. of superstructure II bulb	5
32	x_{32}	serial No. of superstructure II T-bulb	47
33	x_{33}	number of superstructure II stiffeners	5
34	x_{34}	serial No. of upper deck plate	10
35	x_{35}	serial No. of upper deck bulb	1
36	x_{36}	serial No. of upper deck T-bulb	48
37	x_{37}	number of upper deck stiffeners	36

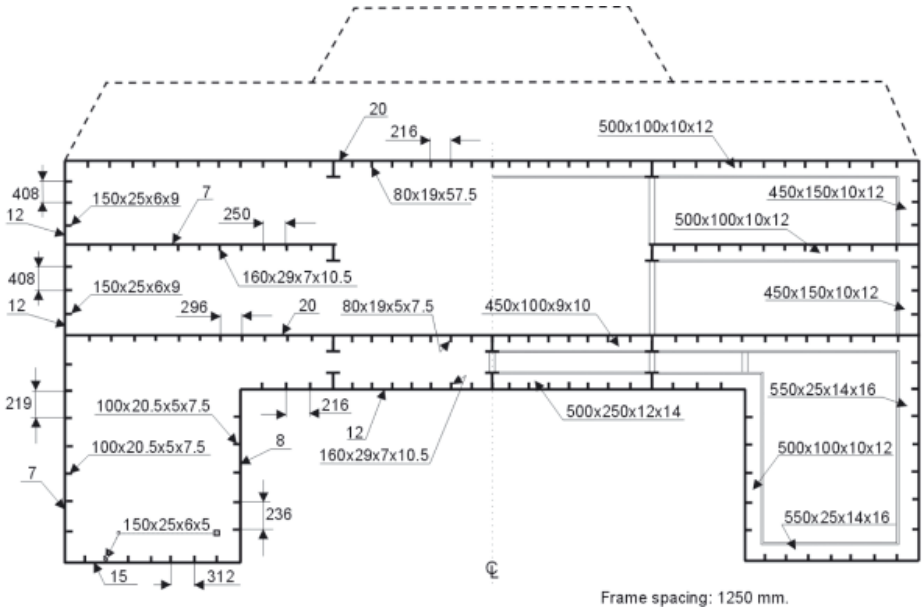

Fig. 40. *Ship structural dimensions and scantlings recommended as a result of multi-objective optimization; structural material: for plates - 5083-H111 Al alloy, for profiles - 6082-T6 Al alloy*

PERFORMANCE ASSESSMENT OF THE DEVELOPED MULTI-OBJECTIVE OPTIMIZATION ALGORITHM

The question should be answered if the proposed combined fitness multi-objective evolutionary algorithm (Eq. 28) is more efficient than the evolutionary algorithms used in the process of selection of only optimization criteria (in the form of scalar substitute optimization criteria) and functions representing the degree of constraint violation (Eq. 8). Unfortunately the answer cannot be simple and unequivocal.

In practical problems the ship structural multi-objective optimization which produces a set of Pareto-optimum solutions may be very computation time-consuming or even impossible to be performed. In the cases the evolutionary algorithms of multi-objective optimization do not guarantee identification of Pareto-optimum compromises but can help identifying a satisfactory approximation, i.e. a set of solutions hoped to be not too far distant from searched front of optimum solutions (in the sense of Pareto). However in this case methods are necessary to evaluate how good produced solutions of formulated problems are. And, this leads to the question: how to compare effectiveness of different algorithms? In the context of the presented work the question may be formulated as follows: how to compare effectiveness of the studied evolutionary multi-objective optimization of ship hull structure, assumed for different evaluation strategies of fitness function.

In the case of the evolutionary algorithms of multi-objective optimization, statistical in their nature, evaluation of obtained results and comparison of effectiveness of optimization algorithms implementing different strategies is a very difficult task, arousing much controversy and misunderstanding. Whereas visual and qualitative comparison of the sets approximating Pareto front is commonly used for deduction of quality of evolutionary multi-objective optimization, in the case of quantitative methods the searching of proper standards are just under way [Knowles, Thiele, Zitzler (2006)].

Generally accepted procedures enabling to compare quality of solutions obtained by different algorithms (usually in many runs) or solutions of the same algorithm obtained in many runs, quantitatively taking into account their statistical characteristics are necessary [Sarker, Coello Coello (2002)], [Knowles, Thiele, Zitzler (2006)].

The problem is extremely difficult also because in this case, as opposed to single-objective optimization, it is necessary to compare not individual solutions, but vectors representing sets of non-dominated solutions under assumption that they are an approximation of a practically unknown set of Pareto-optimum solutions, referred to as a front of Pareto-optimum solutions. In consequence, most comparative studies are based on different methodologies and assumptions, and therefore results obtained from such studies are difficult to be used in mutual comparisons [Knowles, Thiele, Zitzler (2006)].

In the case of single-objective optimization the selection of quality measure is obvious and simple: optimization criterion. The quantity is unequivocally defined, optimization criterion value calculated for every test solution, and smaller or greater depending on the task, which corresponds to better solution. In the case of multi-objective optimization it is not clear what „better" means: is it that located closer to the front of optimum solutions, covering a wider range of solution characteristics, or something else? And, it should be realized that the front of Pareto-optimum solutions is unknown. That is why it is difficult to define proper quality measure for approximations of an unknown front of Pareto-optimum solutions. Therefore for comparing and evaluating results of qualitative evaluation of multi-objective evolutionary algorithms, graphical presentation of obtained non-dominated solutions has been first of all used until recently [Veldhuizen (1999)].

In recent years in this field a certain progress has been made and several papers concerning the quantitative comparing of different approximations of Pareto-optimum set can be found. The most popular is the unary quality measure, i.e. that which attributes, to every single approximation set, one numerical value which reflects a specified quality aspect [Veldhuizen, Lamont (2000)], [Zitzler, Thiele, Laumanns, Fonseca, Grunert da Fonseca (2002)]. To increase the deducing strength the unary quality measures are usually used jointly, to cope of taking into account different aspects of the notion of "quality". Other methods are based on binary quality measures which assign numerical values to pairs of solutions, [Zitzler, Thiele (1998)], [Hansen, Jaszkiewicz (1998)].

Third group of evaluation methods, completely different in conceptual respect, is the method of attainment function,

High-speed vehicle-passenger catamaran, Auto Express 82 type

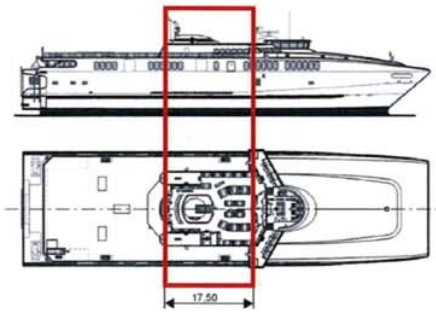

Main particulars:
- length overall, L = 90.0 m,
- breadth, B = 23.0 m,
- maximum depth, H = 11.7 m,
- length of midship block-section subject to optimisation, 17.0 m.

Properties of structural material:
- aluminium alloys,
- 5083-H111 alloy for plates ($R_{0,2}$ = 125 N/mm^2),
- 6082-T6 alloy for bulb extrusions ($R_{0,2}$ = 250 N/mm^2).

Multi-objective topology and size optimisation of ship structure by evolutionary algorithm with combined fitness function, *CFMOEA*, based on genetic algorithm

Combined fitness function:

$$f(\mathbf{x}) = w_1 f_1(\mathbf{x}) + w_2 f_2(\mathbf{x}) + w_{rank}\, rank(\mathbf{x}) + w_{count}\, count(\mathbf{x}) + w_{distance}\, distance(\mathbf{x}) + \sum_{k=1}^{n_c} (w_k \cdot penalty_k(\mathbf{x}))$$

Optimization criteria:
- structural weight $f_1(\mathbf{x})$, kN,
- surface area for cleaning and painting $f_2(\mathbf{x})$, m^2.

Parameters of *CFMOEA* simulation:
- sym2-1,
- number of individuals n_i = 5,000,
- number of generations n_g = 10,000,
- $w_1 = w_2 = 0.0$,
- $w_{rank} = 3.0$, $w_{count} = 0.0$, $w_{distance} = 0.0$.

The best (recommended) solution:
- structural weight $f_1(\mathbf{x}_4)$ = 1106 kN,
- surface area $f_2(\mathbf{x}_4)$ = 7345 m^2.

Non-dominated solutions:
(1) $f_1(\mathbf{x}_1)$ = 1069 kN, $f_2(\mathbf{x}_1)$ = 7790 m^2,
(2) $f_1(\mathbf{x}_2)$ = 1077 kN, $f_2(\mathbf{x}_2)$ = 7742 m^2,
(3) $f_1(\mathbf{x}_3)$ = 1085 kN, $f_2(\mathbf{x}_3)$ = 7518 m^2,
(4) $f_1(\mathbf{x}_4)$ = 1106 kN, $f_2(\mathbf{x}_4)$ = 7345 m^2,
(5) $f_1(\mathbf{x}_5)$ = 1316 kN, $f_2(\mathbf{x}_5)$ = 7231 m^2,
(6) $f_1(\mathbf{x}_6)$ = 1391 kN, $f_2(\mathbf{x}_6)$ = 7130 m^2,
(7) $f_1(\mathbf{x}_7)$ = 1607 kN, $f_2(\mathbf{x}_7)$ = 7074 m^2,
(8) $f_1(\mathbf{x}_8)$ = 1767 kN, $f_2(\mathbf{x}_8)$ = 7074 m^2,
(9) $f_1(\mathbf{x}_9)$ = 1968 kN, $f_2(\mathbf{x}_9)$ = 7044 m^2,
(10) $f_1(\mathbf{x}_{10})$ = 2244 kN, $f_2(\mathbf{x}_{10})$ = 7022 m^2.

Midship section structural arrangements and scantlings of the best solution

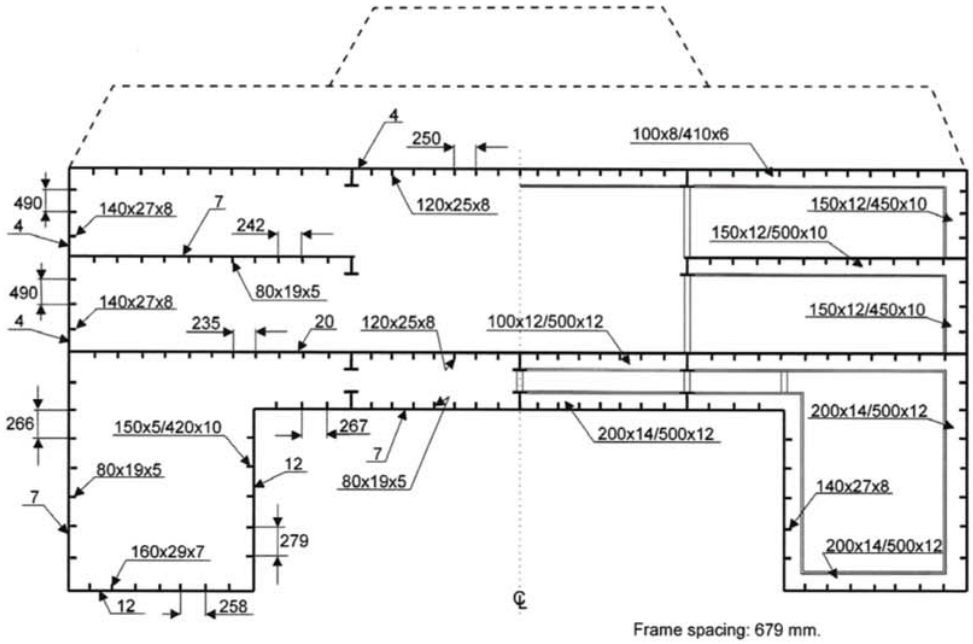

1 of 2 / 2011-09-02 10:30
by Zbigniew Sekulski, West Pomeranian University of Technology, Szczecin (Poland) - Faculty of Maritime Technology

Fig. 41. *Result of the multi-objective evolutionary optimization of the ship structure with respect to the structural weight f_1 and surface area of structural members for maintenance (cleaning and painting) f_2 (sym2-1)*

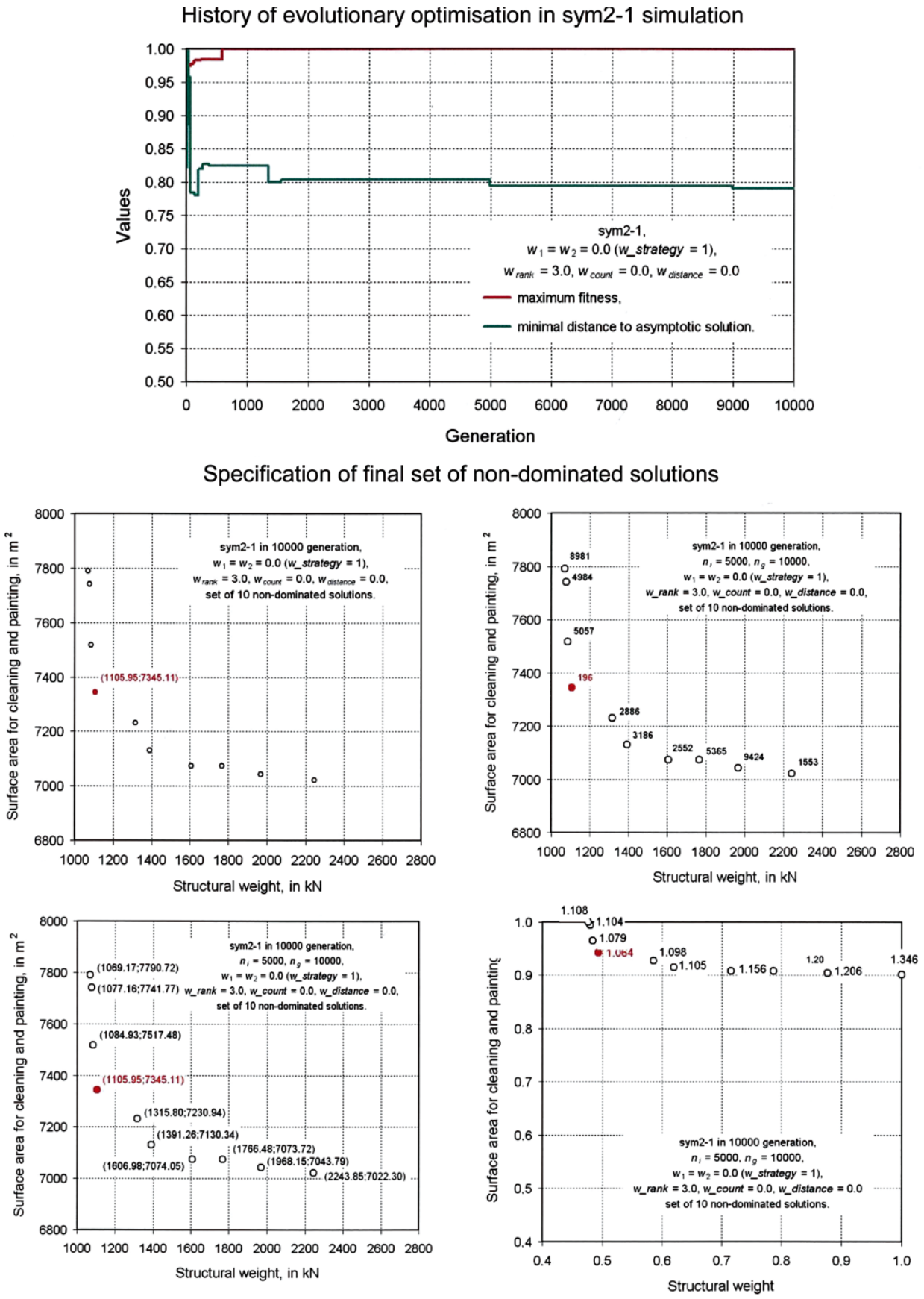

2 of 2 / 2011-09-02 10:30

by Zbigniew Sekulski, West Pomeranian University of Technology, Szczecin (Poland) - Faculty of Maritime Technology and Transport

Fig. 41 cont. *Result of the multi-objective evolutionary optimization of the ship structure with respect to the structural weight f_1 and surface area of structural members for maintenance (cleaning and painting) f_2 (sym2-1), which contains: evolution of the highest value of fitness function and the lowest value of non-dominated solution distance from asymptotic one; structure of the set of non-dominated solutions; number of generations in which particular non-dominated solutions were found; detailed structure of the set of non-dominated solutions; structure of the set of non-dominated solutions in normalized objective space*

[Fonseca, Fleming (1996)], in which the probability of achieving any chosen objectives in evaluation space is assessed on the basis of the knowledge of many approximation sets.

Besides the above mentioned diversity of methods it is still unclear what mutual relations of certain quality measures are like (what is their mutual connection) and what their relative advantages and disadvantages are [Zitzler, Thiele, Laumanns, Fonseca, Grunert da Fonseca (2002)]. In consequence there are no agreed opinions stating which quality measure or measures should be used in specific cases [Zitzler, Thiele, Laumanns, Fonseca, Grunert da Fonseca (2002)].

To define a reliable evaluation methodology is very important for its application to algorithm validation. However, as far as the problem of multi-objective optimization is concerned there are several reasons due to which it is difficult to evaluate obtained results. Firstly, from evolutionary algorithms many solutions are obtained instead of only one, usually as many as possible solutions belonging to the set of non-dominated solutions, approximation set of Pareto-optimum solutions, are aimed at. Secondly, evolutionary algorithms are stochastic, therefore for effectiveness evaluation it is necessary to run many simulations and subject obtained results to statistical analysis; in this case drawn conclusions will also have stochastic characteristics. Thirdly, we may be interested in measuring different aspects of quality; for example, we may be more interested in possessing a robust, but slower, algorithm convergent to Pareto front practically in every case, than in a faster algorithm but convergent to Pareto front only occasionally (in case of specific types of tasks); we also may be interested in evaluating behaviour of evolutionary algorithm in the course of simulation, trying to determine its capability of maintaining diversity and gradual convergence to set of solutions close to Pareto front. This short discussion shows how difficult is to develop effectiveness measures for multi-objective optimization evolutionary algorithms.

The next problem in the discussion is the question: what should be measured? It is very important to determine what kind of results will be subjected to measurement, evaluation and analysis, and to define quality measures according to a task.

It is obvious that in the formulating of a good quality measure for multi-objective optimization evolutionary algorithm the following should be considered [Zitzler, Deb, Thiele (1999)]:

1. the minimizing of distance between approximation of Pareto front, obtained by the algorithm, and a real Pareto-optimum front of solutions, (of course if so is known, what in practice of optimizing engineering objects does not happen),
2. the maximizing of diversity of obtained non-dominated solutions, i.e. the arranging of non-dominated solutions in approximation set over empirical compromise area, as smoothly and homogeneously as possible,
3. the maximizing of number of solutions in the set which approximates the Pareto-optimum set. [Zitzler, Thiele, Laumanns, Fonseca, Grunert da Fonseca (2002)], [Zitzler, Laumanns, Bleuler (2002)], [Zitzler, Thiele, Laumanns, Fonseca, Grunert da Fonseca (2003)], [Fonseca, Knowles, Thiele, Zitzler (2005)], [Knowles, Thiele, Zitzler (2006)] presented the most extensive (in the author's opinion) review of problems related to evaluation of effectiveness of randomized multi-objective optimization algorithms. Assuming that a set of incomparable solutions (called an approximation set), is a result of operation of multi-objective optimization evolutionary algorithm, they proposed a mathematical basis for studying multi-objective optimization effectiveness algorithms.

In particular [Zitzler, Thiele, Laumanns, Fonseca, Grunert da Fonseca (2002)] showed that if we have two sets of solutions, a and B, which approximate Pareto-optimum set of solutions, then we cannot elaborate a finite set of quality measures, which can indicate if the approximation a of Pareto-optimum set is better that the approximation B, in every case. Elaborated quality measures may be applied only to specific aspects of the quality concept, therefore the only thing left to deduct is that the approximation a is not worse that the approximation B, which means that either the approximation a is better than the approximation B, or the approximations a and B are incomparable with regard to a specified quality measure. This statement cannot be generalized in a way indicating that the approximation a is always better than the approximation B. So if it is impossible to state in a close and exact quantitative way the supremacy of one approximation set over the other, therefore it is impossible to state the supremacy of one algorithm over the other. Choice of one of them is determined by the efficiency in every specific case it was used.

[Sarker, Coello Coello (2002)] made a review of propositions they considered the most important and enabling to measure the three above listed aspects of the notion „quality", subjected to evaluation. They also observed that there is no method that would allow to measure the three aspects with one value only. Unfortunately, attempts to elaborate a single measure for grasping them together have not been successful so far because they concern very different algorithm characteristics. That is why the attempts to reduce them to one measure may lead to misunderstandings. Therefore the using of different quality measures to estimate different aspects of algorithm behaviour seems more proper in practice[2)].

On the basis of visual assessment of approximating sets attained in particular simulations, Fig. 42, it can be stated that the best solutions, i.e. approximation sets, were obtained in the simulations**: sym**2-1 ($w_1 = w_2 = 0.0$, $w_{rank} = 3.0$, $w_{count} = 0.0$, $w_{distance} = 0.0$), sym1-2 (w_1, w_2 are random in the range [0, 1], $w_{rank} = 0.0$, $w_{count} = 0.0$, $w_{distance} = 0.0$) and sym2-3 ($w_1 = w_2 = 0.0$, $w_{rank} = 0.0$, $w_{count} = 0.0$, $w_{distance} = 3.0$). Solutions obtained from the simulations are arranged the most uniformly, hence they can be expected to be a good representation of searched Pareto-optimum front. In the case of the remaining simulations: sym1-1 ($w_1 = w_2 = 0.5$, $w_{rank} = 0.0$, $w_{count} = 0.0$, $w_{distance} = 0.0$), sym1-3 (w_1, w_2 are random 0 or 1, $w_{rank} = 0.0$, $w_{count} = 0.0$, $w_{distance} = 0.0$) and sym2-2 ($w_1 = w_2 = 0.0$, $w_{rank} = 0.0$, $w_{count} = 3.0$, $w_{distance} = 0.0$), the found solutions are arranged less uniformly, hence they represent Pareto-optimum front in a worse manner. Therefore it can be approximately stated that out of six conducted research simulations the following were found more effective: the simulation (1) that took into consideration influence of dominance attribute, i.e. dominance rank, the simulation (2) that took distance of the asymptotic solution into consideration, and the simulation in which the selection process is controlled only by optimization criteria. Less effective were found the simulations (4) and (5) in which selection process was controlled only by optimization criteria, the simulation (6) that took into consideration the influence of dominance attribute, i.e. dominance count. Thus in the group of more effective strategies there were two simulations which use the combined fitness and one simulation which realizes the strategy of random combination of objective function without

[2)] Let's notice that fulfillment of mentioned algorithm quality aspects can be considered as multi-objective task of algorithm optimization (optimizer).

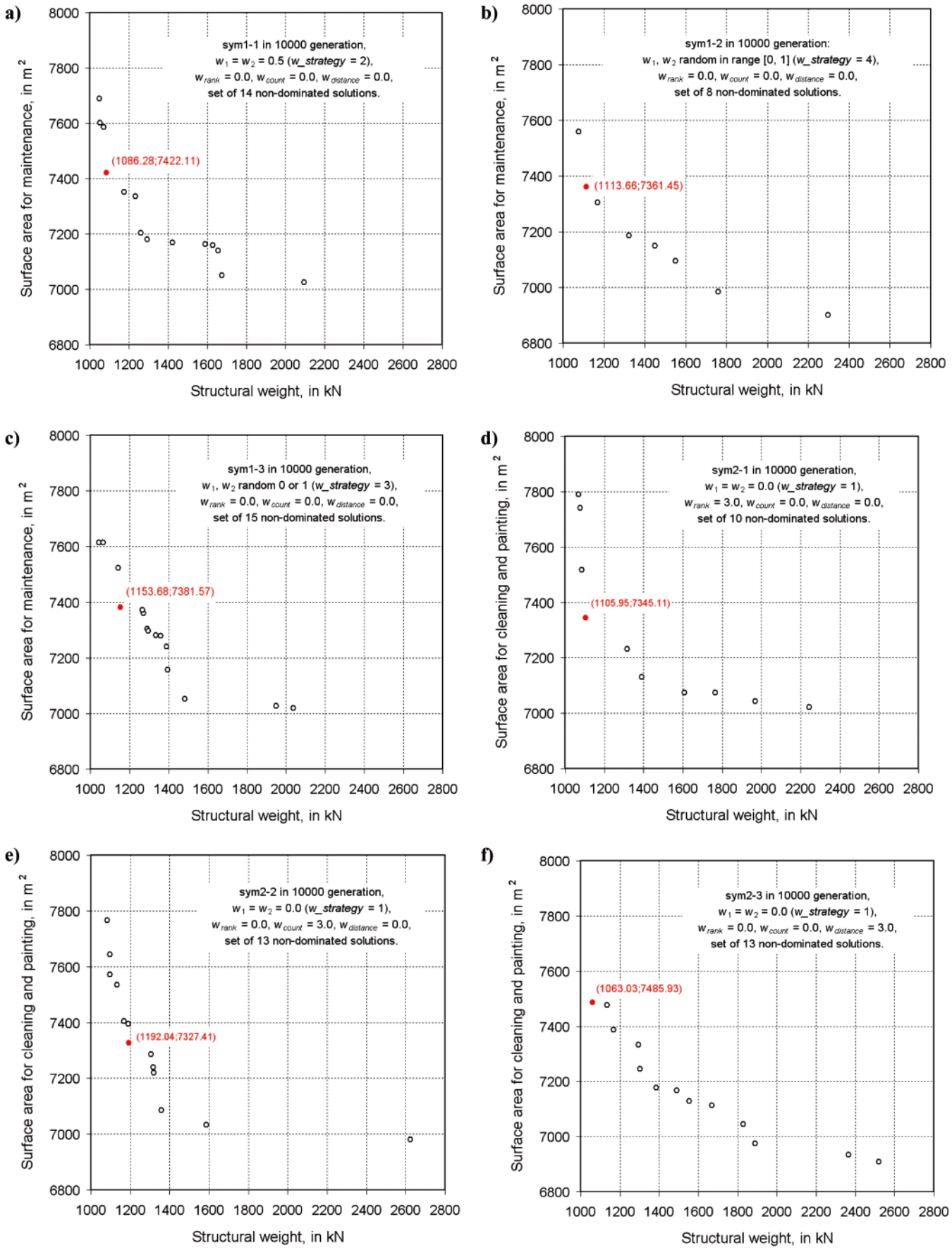

Fig. 42. *Specification of the sets of non-dominated solutions obtained during the performed genetic multi-objective optimization simulations of ship structure with respect to the structure weight f_1 and the surface area f_2; black circles represent non-dominated solutions, red dots represent non-dominated solutions closest to the asymptotic one*

taking into consideration domination attributes. On the basis of such superficial quality analysis can be proposed the statement that the combined fitness multi-objective optimization algorithm can be a more efficient strategy for multi-objective optimization of ship structure than scalarization of objective function strategy, without taking into consideration domination attributes in selection process.

The conducted series of computer simulations confirmed efficiency of the developed computational algorithm and computer program for solving the formulated unified problem of topology and optimization of ship structure dimensions. As a result of the calculations, were elaborated approximations of the set of Pareto-optimum solutions which in particular contain simulations of non-dominated solutions, from several to a dozen or somewhat more in number. The obtained results do not allow to unequivocally determine superiority of any examined strategies of fitness function evaluation. For formulating more detailed quantitative conclusions further systematic statistical studies performed on much larger number of samples, are necessary.

In the case of ship structure optimization the problem of efficiency assessment of elaborated algorithms is additionally complicated by the necessity of formulating many constraints and including them to the fitness function. In the task considered in this publication forty constraints were assumed. The constraint represented in optimization model in the form of proper components of penalty function, $n_c = 40$, very strongly limit solution space available for searching; this way they also distort image of influence of the assumed fitness function computing strategies on algorithm convergence and the quality of attained solutions and therefore on the efficiency of the studied algorithms.

From practical point of view it is interesting to notice which of the formulated constraints appears active in optimization process and which does not. In the first case to allocate large computational outlay to control them is justified. In the other case such outlay may appear useless from the point of view of effectiveness of optimization process and in some cases it is possible even to resign from controlling them. In the case of the optimization model used in this work the constraints in the form given by the inequality (21) concerning the required section moduli values of web frames in the three structural regions: side outboard region, bottom region and wet deck region, appeared active. In the case of the remaining constraints dealing first of all with the required thickness values of plates and dimensions of frames, the formulated constraints are satisfied with a large excess.

The final conclusion can be formulated as follows: one cannot formulate a finite number of quantitative measures which allow putting in order the set of Pareto-front approximating sets in relation to the quality, and therefore one cannot formulate objective quality/efficiency measures of the proposed multi-objective optimization evolutionary algorithms. Thus one cannot prove objectively and unequivocally the supremacy of one of the algorithms proposed and discussed in this work or realization strategies of one of them. It depends on a potential user whether he / she would consider the presented concept interesting, elaborate its computer realization and finally verify its efficiency in his / her specific case.

SUMMARY AND CONCLUSIONS

The problem of minimization of weight and total surface area of the complete three-dimensional midship block-section of the high- speed catamaran hull was presented and discussed in detail. The strength criteria for checking ship structure were taken from the selected classification rules. The calculation tool for solving the formulated unified problem of the multi-objective optimization of topology and scantlings of the sea-going ship hull structure was developed with the accuracy typical for the preliminary design stage.

The application of the genetic algorithm concept to solve the formulated optimization problem was presented. In the study it was proved that the genetic algorithm allows to include, in the multi-objective optimization model, a large number of design variables of real ship structure. The introducing of constraints related to strength, fabrication and standardization is not difficult and may cover a more representative set of criteria.

The aggregation method was proved effective even in the case of the fixed values of the weight coefficients since in the case of the constrained problem the components of the penalty function introduce a random influence to the fitness function. The method is thus closer to that based on the random weight coefficients of the optimization criteria.

This author has discussed crucial role of Pareto domination relation in process of evolution of feasible solutions for ship structure towards Pareto-front containing non-dominated variants of the ship structure. Using the concept of d omination in the set of feasible solutions this author has proposed his own definitions of the concept of domination rank as well as domination count, enabling this way to take into account relation between a feasible variant and other feasible variants. Basing on the ideas the author has proposed an evolutionary algorithm for solving the problem of topology-size multi-objective optimization of hull structure of sea-going ship, which uses, in selection process, the combined fitness function which allows taking into account, in selection process, the following items: (1) optimization criteria, (2) dominance attributes, (3) distance to the asymptotic solution as well as (4) penalty functions for violating assumed constraints. The computational program which makes it possible to perform ship structure multi-objective optimization with an accuracy appropriate for preliminary design stage, was elaborated. By using the tool and elaborated computational model of hull structure, series of computer simulations were conducted for the fast catamaran passenger-vehicle ferry of Auto Express 82 design. The results of the performed computations and subsequent discussion gave reasons for the statement that the elaborated algorithm may be considered an efficient tool for multi-objective optimization of ship structures in the preliminary design stage.

It should be remembered that the developed multi-objective optimization algorithm is based on the random processes therefore the obtained results should be interpreted in the statistical sense. It means that the simulations and their results may appear sometimes not representative. a slight change of the developed models or control parameters may result in a different course of simulation and lead to different results. In this context further systematic studies on algorithm efficiency controlled by a particular component of combined fitness function, are necessary.

Further systematic investigations of effectiveness of the proposed strategies, including repeated computations different to each other only by evolution history, aimed at statistical confirmation of the effectiveness, are deemed necessary.

REFERENCES

1. Abraham, A., Jain, L. and Goldberg, R., 2005. *Evolutionary Multiobjective Optimization*. Springer.
2. Back, T., 1996. *Evolutionary Algorithms in Theory and Practice*. Oxford University Press, New York.
3. Binh, T.T. and Korn, U., 1997. MOBES: A Multiobjective Evolution Strategy for Constrained Optimization Problems.

In: The Third International Conference on Genetic Algorithms (Mendel 97), 25-27 June 1997, Brno, Czech Republic, 176-182.
4. Darwin, Ch., 1859. *Origin of Species*. John Murray, London.
5. Coello Coello, C.A., Lamont, G.B. and Veldhuizen, D.A., 2007. *Evolutionary Algorithms for Solving Multi-objective Problems*. Springer.
6. Cohon, J.L., 1978. *Multiobjective Programming and Planning*. New York, Academic Press.
7. Coley, D.A., 1999. *An Introduction to Genetic Algorithms for Scientists and Engineers*. World Scientific, Singapore.
8. Das, P.K., 1993. Reliability – Based Design Procedure of Stiffened Cylinder Using Multiple Criteria Optimisation Techniques. *In: Proceedings of Offshore Technology Conference, OTC 1993*, Vol. 3, No. 7236, 297-313.
9. Das, P.K., Tolikas, C., Morandi, A.C., Zanic, V. and Warren, N.F., 1993. Multiple Criteria Synthesis Technique Applied to the Reliabilty Based Structural Design of Hull Components of A Fast Swath Ship. *In: Proceedings of Second International Conference on Fast Sea Transportation, FAST '93*, Japan, Tokyo, Vol. 1, 473-487.
10. Davis, L. 1991. *Handbook of Genetic Algorithms*. New York: Van Nostrand.
11. De Jong, K., 1995. On Decentralizing Selection Algorithms. *In: Proceedings of the Sixth International Conference on Genetic Algorithms*, 15-19 July 1995, Pittsburgh, PA, USA, Morgan Kaufmann Publishers, San Francisco, 17-23.
12. Deb, K., 2001. *Multi-Objective Optimization using Evolutionary Algorithms*. John Wiley & Sons.
13. Deb, K., Agrawal, S., Pratab, A. and Meyarivan, T., 2000. *A Fast Elitist Non-Dominated Sorting Genetic Algorithm for Multi-Objective Optimization*: NSGA-II. KanGAL Report 200001, Indian Institute of Technology, Kanpur, India.
14. Edgeworth, F.Y., 1881. *Mathematical Physics: An Essay on the Application of Mathematics to the Moral Sciences*. Paul Keagan, London, England.
15. Eschenauer, H., Koski, J. and Osyczka, A., 1990. *Multicriteria Design Optimisation*. Berlin: Springer-Verlag, Berlin.
16. Fonseca, C.M. and Fleming, P.J., 1993. Genetic Algorithms for Multiobjective Optimization: Formulation, Discussion and Generalization. *In: 5th International Conference on Genetic Algorithms, Proceedings*, 416-423.
17. Fonseca, C.M. and Fleming, P.J., 1996. On the Performance Assessment and Comparison of Stochastic Multiobjective Optimizers. *In: Parallel Problem Solving from Nature – PPSN IV*, September 1996, Berlin, Germany, Lecture Notes in Computer Science, Springer-Verlag, Berlin, Germany, 585-593.
18. Fonseca, C.M., Knowles, J.D., Thiele, L. and Zitzler, E., 2005. A Tutorial on the Performance Assessment of Stochastic Multiobjective Optimizers. Invited talk. *In: Evolutionary Multi-Criterion Optimization Conference (EMO 2005)*, 9-11 March 2005, Guanajuato, Mexico, Lecture Notes in Computer Science 3410, Springer 2005,
19. Fox, R.L., 1971. *Optimization Methods for Engineering Design*. Addison-Wesley Publishing Company, Inc., Reading.
20. Goldberg, D.E., 1989. *Genetic Algorithms in Search, Optimization and Machine Learning*. Addison-Wesley Longman Publishing Co., Inc. Boston, MA, USA.
21. Goldberg, D.E. and Deb K., 1991. A Comparative Analysis of Selection Schemes Used in Genetic Algorithms. *In: Foundations of Genetic Algorithms*. Morgan Kaufmann Publishers, San Mateo, 69-93.
22. Hajela, P. and Lin, C.Y., 1992. Genetic Search Strategies in Multicriterion Optimal Design. *Structural Optimization*, 4: 99-107.
23. HANSA, 1997. *Polish fast ferry "Boomerang"*. 6:26-29.
24. Hansen, M.P. and Jaszkiewicz, A., 1998. *Evaluating the quality of approximations of the non-dominated set*. Technical report, Institute of Mathematical Modeling, Technical University of Denmark, IMM Technical Report IMM-REP-1998-7.
25. Horn, J., Nafpliotis, N. and Goldberg, D.E., 1994. A Niched Pareto Genetic Algorithm for Multiobjective Optimization. *In: First IEEE Conference on Evolutionary Computation*, IEEE World Congress on Computational Intelligence, 1: 82-87.
26. Hughes, E.J., 2003. Multiple Single Objective Sampling. *In: Proceedings of 2003 Congress on Evolutionary Computation, CEC 2003*, 8 - 12 December 2003, Canberra, Australia, 2678-2684.
27. Hughes, E.J., 2005. Evolutionary Many-objective Optimization: Many Once or One Many? *In: Proceedings of 2005 Congress of Evolutionary Computation*, CEC 2005, 2-4 September 2005, Edinbourgh, Scotland, UK, IEEE Press, 222-227.
28. Hutchinson, K., Todd, D. and Sen, P., 1998. An evolutionary multiple objective strategy for the optimisation of made-to-order products with special reference to the conceptual design of high speed mono hull roll-on/roll-off passenger ferries. *In: Proceedings of International Conference of Royal Institution of Naval Architects*.
29. Ishibuchi, H. and Murata, T., 1996. Multi-objective genetic local search algorithm. *In: Proceedings of IEEE International Conference on Evolutionary Computation (ICEC'96)*, Piscataway, NJ, IEEE Press, 119-124.
30. Jang, C.D. and Shin, S.H., 1997. A Study on the Optimal Structural Design for Oil Tankers Using Multi Objective Optimization. *In: Proceedings of 6th International Marine Design Conference*, IMDC'97, Newcastle, 23-25 June 1997, University of Newcastle, United Kingdom, Vol. 1, Penshaw Press, 217-231.
31. Jaszkiewicz, A., 2004. On the Computational Efficiency of Multiple Objective Metaheuristics: The Knapsack Problem Case Study. *European Journal of Operational Research*, 158:418-433.
32. Jianguo. W. and Zuoshui. X., 1996. Symmetric Solution of Fuzzy Multi-Objective Optimization for Ship Structure. *Journal East China Shipbuilding Institute*, 10(1): 1-7.
33. Kitamura, M., Nobukawa, H. and Yang, F., 2000. Application of a genetic algorithm to the optimal structural design of a ship's engine room taking dynamic constraints into consideration. *Journal of Marine Science and Technology*, Vol. 5, 131-146.
34. Klanac, A., Ehlers, S. and Jelovica, J., 2009. Optimization of crashworthy marine structures. *Marine Structures*, Vol. 22, 670-690.
35. Knowles, J. and Corne. D., 1999. The Pareto Archived Evolution Strategy: a New Baseline Algorithm for Multiobjective Optimisation. *In*: *1999 Congress on Evolutionary Computation, CEC99,* Washington, D.C., 6-9 July 1999, IEEE Service Center, 98-105.
36. Knowles, J.D., Thiele, L. and Zitzler, E., 2006. *A tutorial on the Performance Assessment of Stochastic Multiobjective Optimizers*. Computer Engineering and Networks Laboratory, ETH Zurich, Switzerland, TIK-Report No. 214.
37. Kursawe, F., 1991. A variant of evolution strategies for vector optimization. *In*: Proceedings of the 1st Workshop on Parallel Problem Solving from Nature (PPSN I), 1-3 October 1990, Dortmund, Berlin, Springer-Verlag, 1991, 193–197.
38. Leyland, G., 2002. *Multi-objective Optimization Applied to Industrial Energy Problems*. PhD Thesis, École Polytechnique Fédérale de Lausanne.
39. Man, K.F., Tang, K.S. and Kwong, S., 1999. *Genetic Algorithms*. Springer-Verlag, London.
40. Michalewicz, Z., 1996. *Genetic Algorithms + Data Structures = Evolution Programs*. Berlin-Heidelberg: Springer-Verlag.
41. Murata, T. and Ishibuchi, H., 1995. MOGA: Multi-objective genetic algorithms. *In: Proceedings of the Second IEEE International Conference on Evolutionary Computation*, 289-294. In Proceedings of the Second IEEE International Conference on Evolutionary Computation, IEEE Press, 289-294.
42. Okada, T. and Neki, I., 1992. Utilization of Genetic Algorithm for Optimizing the Design of Ship Hull Structure. *Journal of the Society of Naval Architect of Japan*, 171: 71-83.
43. Osyczka, A., 2002. *Evolutionary Algorithms for Single and Multicriteria Design Optimization*. Heidelberg: Physica-Verlag.
44. Pareto, V., 1896. *Cours D'Economie Politique, Volume 1*. Lausanne: F. Rouge.
45. Parsons, M.G. and Singer, D., 2000. A Fuzzy Logic Agent for Design Team Communications and Negotiations. *In: Conference on Computer Applications and Information Technology in the Maritime Industries, COMPIT 2000,* March 2000, Potsdam/Berlin.

46. Purshouse, R.C. and Fleming, P.J., 2003. Evolutionary Many-Objective Optimization: An Exploratory Analysis. *In: Proceedings of 2003 Congress on Evolutionary Computation*, CEC2003, 8-12 Dec 2003, Canberra, Australia, IEEE, Piscataway, N.J., USA, 2066-2073.
47. Ray, T. and Sha, O.P., 1994. Multicriteria Optimisation Model for a Containership Design. *Marine Technology*, 31(4): 258-268.
48. Reklaitis, G.V., Ravindran, A. and Ragsdell, K.M., 1983. *Engineering Optimization. Methods and Applications*. New York: John Wiley and Sons, New York.
49. Ryan, D.M., 1974. Penalty and Barrier Functions. *In*: P.E. Gill and W. Murray (Eds.) *Numerical Methods for Constrained Optimization*, Academy Press, London.
50. Sarker, R. and Coello Coello, C.A., 2002. Evolutionary Optimization, Chapter 7, Assessment methodologies for multiobjective evolutionary algorithms. *In*: R. Sarker, M. Mohammadian, X. Yao (Editors) *Evolutionary Optimization*, Academic Publishers, Boston, 177-195.
51. Sarker, R., Mohammadian, M. and Yao, X., (Eds.), 2002. *Evolutionary Optimization, Part III, Multi-objective Optimization*. Boston: Kluwer Academic Publishers.
52. Schaffer, J.D., 1985. Multiple Objective Optimization with Vector Evaluated Genetic Algorithms. *In: Proceedings of an International Conference on Genetic Algorithms and Their Applications*, 24-26 July 1985, Carnegie-Mellon University, Pittsburgh, Pa, 93-100.
53. Sekulski, Z., 2010. Multi-objective topology and size optimization of high-speed vehicle-passenger catamaran structure by genetic algorithm. *Marine Structures*, Vol. 23, 405-433.
54. Sen, P. and Yang, J.B., 1995. An Investigation Into the Influence of Preference Modelling in Ship Design with Multiple Objectives. *In: Proceedings, PRADS '95*, Vol. 2, Society of Naval Architecture of Korea, 1252-1263.
55. Sen, P. and Yang, J.B., 1998. *Multiple Criteria Decision Support in Engineering*. London: Springer-Verlag.
56. Shi, W.B., 1992. In-Service Assessment of Ship Structures: Effect of General Corrosion on Ultimate Strength. *In: Spring Meteting, RINA*.
57. Significant Ships, 1997. *Boomerang: catamaran ferry for Baltic Service*, 21-21.
58. Srinivas, N. and Deb, K., 1995. Multiobjective Optimization Using Nondominated Sorting in Genetic Algorithms. *Evolutionary Computation*, 2(3): 221-248.
59. Stadler, W., 1988. Multiobjective Optimization in Engineering and in the Sciences. New York: Plenum Press.
60. Statnikov, R.B. and Matosov, J.B., 1995. Multicriteria Optimization and Engineering. New York: Chapman&Hall.
61. Trincas, G., Zanic, V. and Grubisic, I., 1994. Comprehensive Concept Design of Fast RO-RO Ships by Multi-Atribute Decision-Making. *In: Proceedings, IMDC '94*, Delft, 403-417.
62. UNITAS, 1995. Rules for the Construction and Classification of High Speed Craft.
63. Vanderplaats, G.N., 1984. Numerical Optimization Techniques for Engineering Designs. New York: McGraw-Hill.
64. Veldhuizen Van, D.A., 1999. *Multiobjective Evolutionary Algorithms: Classifications, Analyses, and New Innovations*. Ph. D. thesis, Air Force Institute of Technology, Wright-Patterson AFB, Ohio.
65. Veldhuizen Van, D.A. and Lamont, G.B., 2000. On measuring multiobjective evolutionary algorithm performance. *In*: A. Zazala, R. Eberhart (Eds.) *Congress on Evolutionary Computation (CEC 2000)*, vol. 1, Piscataway, NY, IEEE Press, 204-211.
66. Zitzler, E., 1999. *Evolutionary Algorithms for Multiobjective Optimization: Methods and Applications*. Disertation for degree of Doctor of Technical Sciences, Swiss Federal Institute of Technology Zurych.
67. Zitzler, E., Deb, K. and Thiele, L., 1999. *Comparison of Multiobjective Evolutionary Algorithms: Empirical Results*. TIK-Report, No. 70, Computer Engineering and Communication Networks Lab, Swiss Federal Institute of Technology, Zurych, Switzerland.
68. Zitzler, E., Deb, K. and Thiele, L., 2000. Comparison of multiobjective evolutionary algorithms: Empirical results. *Evolutionary Computation*, 8(2): 173–195.
69. Zitzler, E., Laumanns, M. and Bleuler, S., 2002. A tutorial on evolutionary multiobjective optimization. *In Workshop on multiple objective metaheuristics (MOMH 2002)*, Springer-Verlag, Berlin.
70. Zitzler, E., Laumanns, M. and Thiele, L., 2001. SPEA-2: Improving the Strength Pareto Evolutionary Algorithm. Evolutionary Methods for Design. *In: Proceedings of the EUROGEN'2001 Conference on Optimization and Control with Applications to Industrial Problems*, 19-21 September 2001, International Center for Numerical Methods in Engineering, Greece, p. 95-100.
71. Zitzler, E. and Thiele, L., 1998. Multiobjective Optimization Using Evolutionary Algorithms – A Comparative Case Study. *In: Parallel Problem Solving from Nature – PPSN*, Amsterdam, 292-301.
72. Zitzler, E. and Thiele, L., 1998. Multiobjective Optimization Using Evolutionary Algorithms – A Comparative Case Study. *In*: *Proceedings of the PPSN V - Fifth International Conference on Parallel Problem Solving from Nature*, Amsterdam, The Netherlands, 27-30 September 1998, Springer, Berlin, Germany, 292-301.
73. Zitzler, E. and Thiele, L., 1999. Multiobjective Evolutionary Algorithms: A Comparative Case Study and Strength Pareto Approach. *IEEE Transactions on Evolutionary Computation*, 3(4): 257-271.
74. Zitzler, E. and Thiele, L., Laumanns, M., Fonseca, C.M., Grunert da Fonseca V., 2002. *Performance Assessment of Multiobjective Optimizers: An Analysis and Review*. TIK-Report No. 139, Swiss Federal Institute of Technology (ETH) Zurich, Switzerland.
75. Zitzler, E., Thiele, L., Laumanns, M., Fonseca, C.M. and Grunert da Fonseca V., 2003. Performance Assessment of Multiobjective Optimizers: An Analysis and Review. *IEEE Transactions on Evolutionary Computation*, 7(2):117-132.

CONTACT WITH THE AUTHOR

Zbigniew Sekulski, Ph. D.
West Pomeranian University of Technology, Szczecin
Faculty of Marine Technology
Al. Piastów 41
71-065 Szczecin, POLAND
e-mail: zbigniew.sekulski@zut.edu.pl

POLISH MARITIME RESEARCH 4(71) 2011 Vol 18; pp. 14-22
10.2478/v10012-011-0021-z

An Experimental and Numerical Study of Tip Vortex Cavitation

J.A. Szantyr, Prof.
P. Flaszyński, Ph. D.
K. Tesch, Ph. D.
Gdansk University of Technology
W. Suchecki, Ph. D.
S. Alabrudziński, Ph. D.
Warsaw University of Technology

ABSTRACT

The article presents the results of the research project concerning tip vortex cavitation. This form of cavitation is very important in operation of many types of rotary hydraulic machines, including pumps, turbines and marine propellers. Tip vortex cavitation generates noise, vibration and erosion. It should be eliminated or significantly limited during the design of these types of machines. The objective of the project was to develop an accurate and reliable method for numerical prediction of tip vortex cavitation, which could serve this purpose. The project consisted of the laboratory experiments and numerical calculations. In the laboratory experiments tip vortex cavitation was generated behind a hydrofoil in the cavitation tunnel and the velocity field around the cavitating kernel was measured using the Particle Image Velocimetry method. Measurements were conducted in three cross-sections of the cavitating tip vortex for a number of angles of attack of the hydrofoil and for several values of the cavitation index. In the course of numerical calculations two commercial CFD codes were used: Fluent and CFX. Several available approaches to numerical modeling of tip vortex cavitation were applied and tested, attempting to reproduce the experimental conditions. The results of calculations were compared with the collected experimental data. The most promising computational approach was identified.

Keywords: rotary hydraulic machinery; cavitation; numerical methods; experimental techniques

INTRODUCTION

One of the most important problems in design of different types of rotary hydraulic machines, such as marine propellers, water turbines and pumps is the as accurate as possible prediction of cavitation properties of these machines. Such a prediction enables elimination or significant limitation of the cavitation phenomena at the design stage. Among different types of cavitation, the tip vortex cavitation plays a very important role, because it is responsible for generation of intensive noise and vibration and also often causes erosion of the machinery elements. Development of accurate and reliable method for numerical prediction of tip vortex cavitation is the objective of research described below.

The mechanism of formation of the cavitating tip vortex is shown schematically in Fig. 1. Combination of the inflow velocity to the hydrofoil and intensive rotation of the liquid around the vortex leads to the region of strongly reduced pressure, with minimum at the centre of the vortex just behind the tip of the foil. The complicated contradictory phenomena of concentration and dissipation of vorticity plays an important role in this process. Cavitation nuclei, i.e. micro-bubbles naturally present in the liquid, are pushed by the pressure distribution into the centre of the vortex, where in sufficiently low pressure they undergo rapid growth, leading to formation of the cavitating kernel of the vortex.

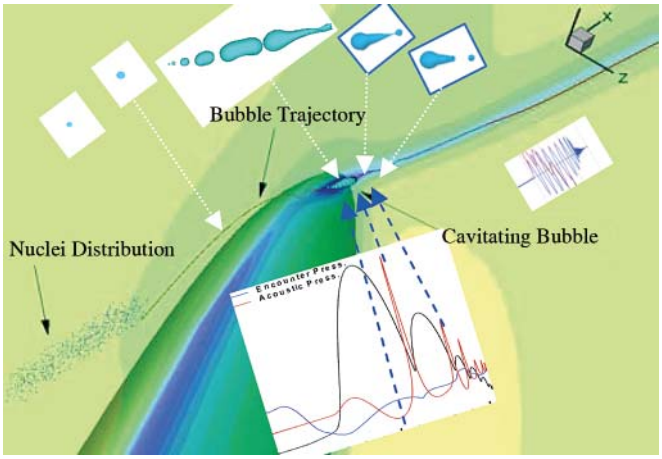

Fig. 1. Scheme of formation of the cavitating tip vortex

The accurate determination of the pressure distribution in close vicinity of the tip vortex is the obvious pre-requisite for effective prediction of the tip vortex cavitation. The methods for calculation of the velocity and pressure around a tip vortex were the subject of earlier research published in [1, 2, 3, 6].

The continuation research, presented in this article, consists of the experimental and numerical parts. The purpose of the experimental part is to supply information about the velocity field around the cavitating tip vortex, necessary for development of the numerical methods and data concerning the geometry of the cavitating vortex for experimental verification of the numerical results. In the numerical part of the research project two commercial computer CFD codes were used and several available models of turbulence were tested. The detailed presentation of the experimental and numerical research is included in the following sections of the article.

EXPERIMENTAL MEASUREMENTS OF THE VELOCITY FIELD AROUND THE CAVITATING TIP VORTEX

The experiments were conducted in the cavitation tunnel of the Department of Energy and Industrial Apparatus of the Gdansk University of Technology, shown in Fig. 2. This tunnel has a rectangular measuring section having the dimensions 3.0*0.35*0.45 meters. The maximum flow velocity in the tunnel is 6 meters per second. The velocity measurements around the cavitating tip vortex were performed using the Particle Image Velocimetry method and they were conducted by the team from the Warsaw University of Technology, Faculty of Civil Engineering, Mechanics and Petrochemistry. The PIV equipment set-up is also shown in Fig. 2.

Fig. 2. *Cavitation tunnel during PIV measurements*

The hydrofoil model used in the experiments was specially designed on the basis of the typical contemporary marine propeller blade geometry, which was developed onto a plane surface (cf. Fig. 3). The span of the hydrofoil was selected equal to 225 mm in order to ensure that the cavitating tip vortex was located approximately in the centre line of the measuring section. The hydrofoil was manufactured of bronze and mounted vertically in the tunnel by means of the mechanism enabling accurate control of the angle of attack.

The PIV measurements were conducted for a number of conditions, resulting from combinations of angle of attack and flow velocity. These conditions are listed in Table 1, together with the locations of three measurement planes. These planes were perpendicular to the tunnel axis and they were located 50, 200 and 300 mm behind the tip of the hydrofoil, in order to visualize the process of development of the cavitating tip vortex. The combination of all conditions listed in Table 1 produced 27 measurements of flow velocity (3 velocities * 3 angles of attack * 3 measuring planes). During the experiments the static pressure in the tunnel was kept constant at 15 [kPa] and the variation in the cavitation index were obtained through changes in the flow velocity. The cavitation index σ is defined according to the formula:

$$\sigma = \frac{p - p_{\upsilon}}{\frac{1}{2}\rho V^2} \tag{1}$$

where:
- p – the static pressure in the tunnel
- p_{υ} – the critical vapour pressure
- ρ – the liquid density
- V – the flow velocity

Tab. 1. *Conditions for PIV measurements*

Distance behind the hydrofoil tip [mm]	Flow velocities [m/s]	Cavitation indices [-]	Angles of attack [deg]
50	4.32, 5.09, 5.87	1.393, 1.003, 0.755	4, 8, 12
200	4.32, 5.09, 5.87	1.393, 1.003, 0.755	4, 8, 12
300	4.32, 5.09, 5.87	1.393, 1.003, 0.755	4, 8, 12

PIV method enables determination of the velocity vectors on the basis of measurement of displacement of particles between two correlated pictures created by the laser light (cf. Fig. 5) and registered consecutively in a short time interval

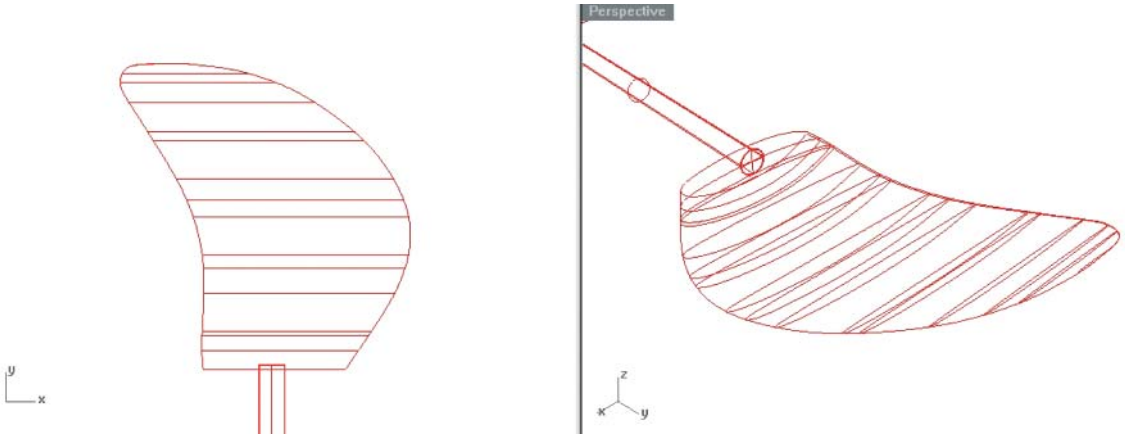

Fig. 3. *Design of the model hydrofoil*

by the camera. In order to provide sufficient number of micro-particles in the flow, necessary for effective PIV measurements, the water in the tunnel was seeded with a silver metallic paint. The deflection of the light beam when crossing the window-water boundary was taken into account. The results of PIV measurements were stored in computer files and then filtered and re-calculated using specialized software.

The scheme of the PIV measuring system is shown in Fig. 4. The distances of the camera K from the measuring section were kept constant b = 570 mm and c = 668 mm. The distance of the laser L from the measuring section was constant and equal to a = 440 mm. The distances of the measuring plane from the hydrofoil tip were varied: d = 50, 200 and 300. The system was arranged in such a way that the angle between the laser light plane and the camera axis was approximately equal to 45 degrees in all measurements.

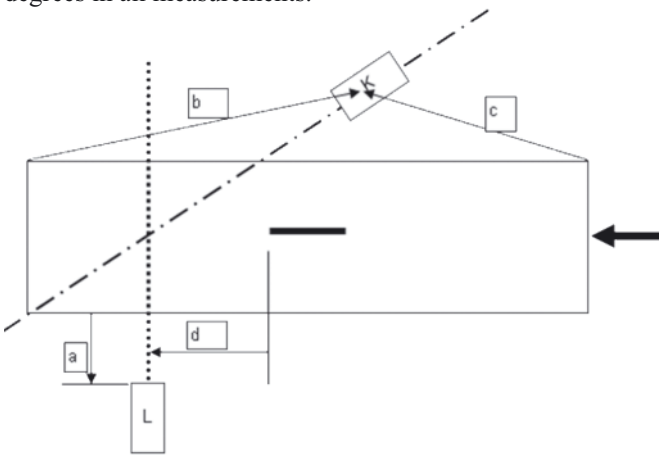

Fig. 4. *Scheme of the measuring system*

Fig. 5 shows the laser light in the measuring plane 50 mm behind the hydrofoil tip during the PIV measurements. Apart from the PIV measurements the photographic registration of the cavitating tip vortex was performed. The complete description of the measurements may be found in [5].

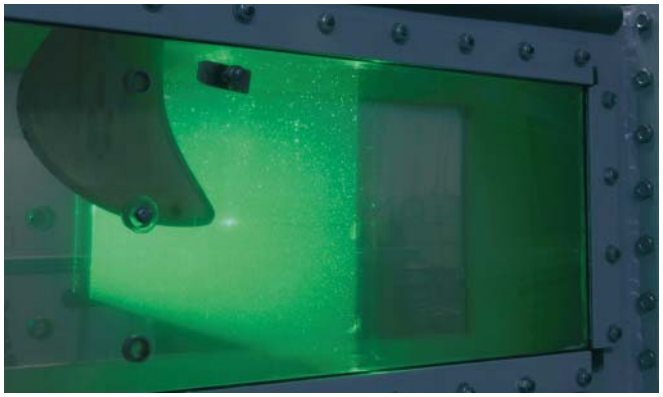

Fig. 5. *The PIV measurement plane behind the tip of the hydrofoil*

NUMERICAL PREDICTION OF THE CAVITATING TIP VORTEX

The purpose of the first stage of calculations in the research project, described in this article, was to test and compare different CFD programs and different turbulence models from the point of view of their ability to predict accurately the geometry of the cavitating kernel of the tip vortex. One flow condition was selected for this comparison, namely hydrofoil angle of attack equal to 8 degrees and the velocity of flow equal to 5.2 m/s. The geometry of the computation domain taken into account in the CFD calculation is shown in Fig. 6 It may be seen that quite a large section of the cavitation tunnel, especially in front of the hydrofoil, was modeled numerically. The inlet confuser was taken into account in the simulations in order to obtain the similar velocity distribution upstream the hydrofoil as in the measurements. Calculations were performed using two commercial CFD programs: Ansys/Fluent v12 and Ansys/CFX. In order to demonstrate the practical accuracy of numerical prediction of the cavitating tip vortex, the authors of calculations were not familiar with the experimental results beforehand. They prepared and performed the calculations using their best experience.

The unstructured computational grid for Fluent is constructed of about 4.7 million of hexahedral elements. The mesh was created in Hexpress/Numeca mesh generator. The density of element distribution is increased near the tunnel walls in order to keep y=1. In view of the anticipated presence of the tip vortex the grid had also significantly increased density in the region behind the hydrofoil tip – see Fig. 7. In computations the MUSCL (Monotone Upstream-Centered Schemes for Conservation Laws) scheme was used and 4 turbulence models were tested:

- standard k – ε model
- k – ε RNG
- k – ω SST
- Reynolds Stress Model (RSM)

Boundary conditions were set as follows:

– at the inlet plane:
  - mass flow rate 437 kg/s (it corresponds to velocity at the test section ~5.2 m/s)
  - total temperature 283 K
  - turbulence intensity 1%
  - turbulent viscosity ratio 10

– at the outlet plane
  - static pressure 15 kPa

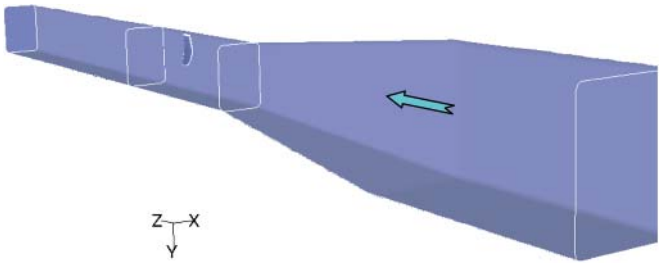

Fig. 6. *The domain of flow taken into account in CFD calculations*

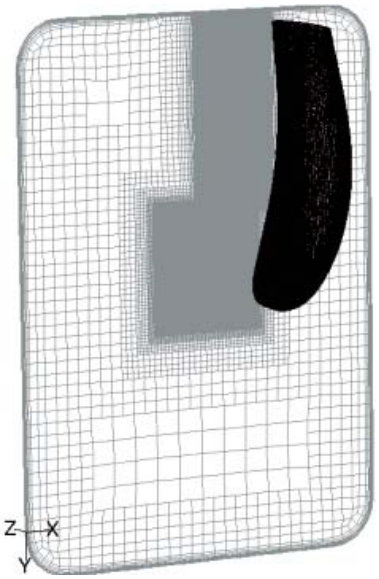

Fig. 7. *Discretization of the hydrofoil and the plane behind it used in Fluent*

A mixed two-phase model was used in the calculations of the cavitating flow. Cavitation was determined on the basis of Rayleigh-Plesset equation in Zwart-Gerber-Belamri formulation [7]. The gaseous phase was treated as a compressible medium according to the perfect gas model.

Calculations performed using the Ansys/CFX program were performed on the basis of unstructured grid having about 9 million elements, including about 8.2 million tetrahedral elements and about 0.8 million prismatic elements in the boundary layer. Part of this grid located in the vicinity of the hydrofoil is shown in Fig. 8. The gaseous phase was treated as a incompressible medium in case of Ansys/CFX simulations.

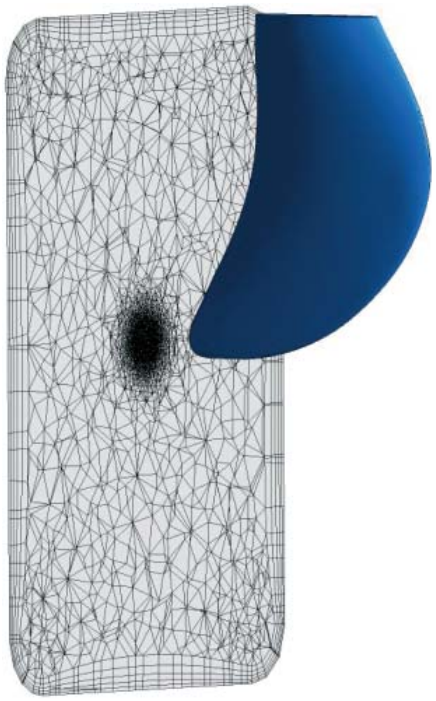

Fig. 8. *Discretization of the hydrofoil and plane behind it used in CFX*

In the calculations by CFX the same turbulence models were used as in Fluent case.

The comprehensive description of CFD calculations may be found in [4].

COMPARISON OF THE EXPERIMENTAL AND NUMERICAL RESULTS

Comparison of the registered and calculated geometry of the cavitating tip vortex

The photograph of the cavitating tip vortex in the analyzed flow condition (angle of attack 8 degrees, velocity of flow 5.2 m/s) is shown in Fig. 9, while the results of corresponding CFD calculations are presented in Figs. 10, 11 and 12. The detailed analysis of the figures leads to the following observations:

- there are significant differences between Fluent and CFX predictions, even when using the same turbulence model; these differences may be attributed to the markedly different structure in the computational grid between both programs,
- similarly important differences may be found in predictions by each of the programs (Fluent or CFX) while using different turbulence models,
- CFX results are much less dependent of the turbulence model than the Fluent ones,
- the differences in performance between Fluent and CFX for the same turbulence models result most likely from the different structures of the computational grids and numerical schemes implemented in the solvers
- k-ε RNG turbulence model seems to be the best suited for prediction of tip vortex cavitation and it performs equally well both in Fluent and CFX,
- standard k-ε turbulence model in Fluent case gives the shortest cavitating zone what is highly related to the dissipative nature of this model
- CFX results for standard k-ε and SST turbulence model give surprisingly the same results
- both programs predicted some sheet cavitation at the root of the hydrofoil which was not observed in the experiment.

Fig. 9. *Photograph of the cavitating tip vortex in the selected flow configuration*

Comparison of the measured and calculated velocity field near the cavitating vortex

The measurements and calculations of the velocity field in the close vicinity of the cavitating tip vortex were performed for the same selected flow condition. The results are presented in the form of velocity vectors in the X-Y plane (i.e. plane

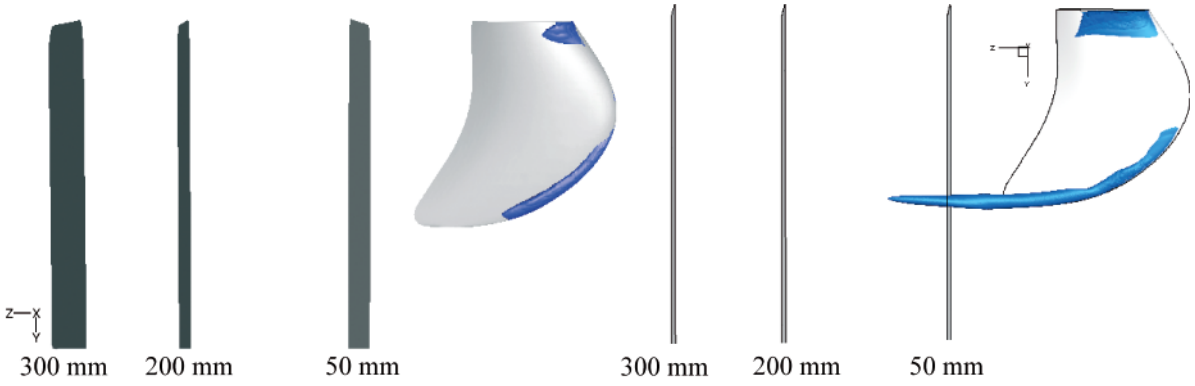

Fig. 10. *Calculated cavitation - k-ε standard turbulence model – Fluent (left) and CFX (right)*

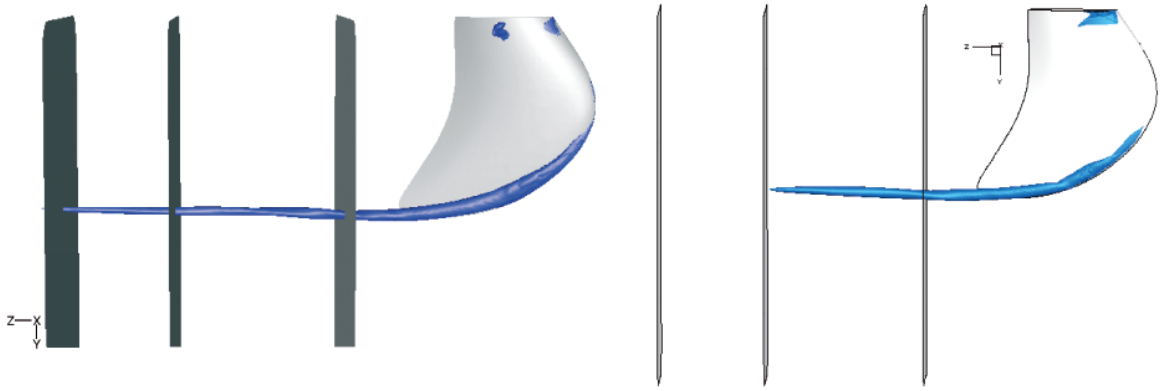

Fig. 11. *Calculated cavitation – k-ε RNG turbulence model – Fluent (left) and CFX (right)*

Fig. 12. *Calculated cavitation – k-ω SST turbulence model– Fluent (left) and CFX (right)*

perpendicular to the axis of the cavitating vortex) and they are grouped together according to the distance of this plane from the hydrofoil tip. Figs. 13, 14, 15, 16 show the results for 50 mm distance, Figs 17, 18, 19, 20 – for 200 mm distance and Figs. 21, 22, 23 and 24 – for 300 mm distance. The results of measurements are presented (Figs. 13, 17 and 21) according to two different procedures of averaging (left and right section of the Figures) of the velocity field. The processing of experimental data in each flow conditions was done by PIV measurements of approximately 20 to 25 instantaneous velocity fields and their time averaging. Two final types of velocity fields were obtained for each measuring conditions by subtracting either space averaged velocity vector or only the horizontal component of this vector from the time averaged velocity field. The origin of the coordinating system for each PIV intersection distance from hydrofoil was in taken in the center of the cavitating tip vortex. The homogeneous high velocity area in the vicinity of the origin should be analyzed with respect of remarks described in the conclusions section of this article.

Close inspection of the results for the plane located 50 mm behind the hydrofoil tip leads to several interesting observations:

- measurements indicate presence of two almost equally strong vortex kernels; such a situation may happen in specific flow cases, but in this case it is not confirmed by photographs and by calculations,
- predictions by CFX look almost the same for all turbulence models, what corresponds to the results of calculation of cavitation described above,
- predictions by Fluent depend strongly on the turbulence model,
- predictions by Fluent and CFX agree quite well with each other for k-ε RNG turbulence model,
- Fluent results show existence of the wake downstream of the hydrofoil, such effect is less visible in prediction by CFX, what arises from the mesh structure.

Analysis of Figs 17 – 20, describing the situation at 200 mm behind the hydrofoil, may be summarized in the following way:

- the measurements indicate the advancing process of concentration and merging of the two initially detected vortex kernels into one,
- calculation by Fluent and CFX indicate the process of turbulent dissipation of vorticity and resulting weakening of the vortex,
- this calculated process of dissipation of turbulent vorticity depends strongly on the model of turbulence; it seems to be overestimated in case of standard k-ε and k-ω SST models, what leads to prediction of too short cavitating tip vortex (cf. Figs. 9 – 12), because the calculated intensity of the vortex falls too rapidly with distance from the hydrofoil,
- the k-ε RNG turbulence model produces very similar results both in Fluent and CFX, moreover, they agree reasonably with the results of measurements as far as the maximum values of velocity are concerned.
- Fluent results still indicate existence of the wake downstream of the hydrofoil, its interaction with the vortex results in an asymmetric structure of the vortex, it is better shown for k-ε RNG and SST models (less dissipative than standard k-ε).

The situation at 300 mm behind the hydrofoil tip, shown in Figs. 21 – 24, may be summarized in the following way:

- measurements show a single strong vortex of a rather unnatural rectangular cross-section,
- as far as the calculations are concerned, only the results obtained from Fluent with k-ε RNG turbulence model produce maximum values of velocity comparable with that determined in the measurements,
- all other calculations predict too intensive dissipation of vorticity, what is confirmed by the cavitation prediction shown in Figs. 10 – 12
- the interaction of the tip vortex with the wake is still present in Fluent results.

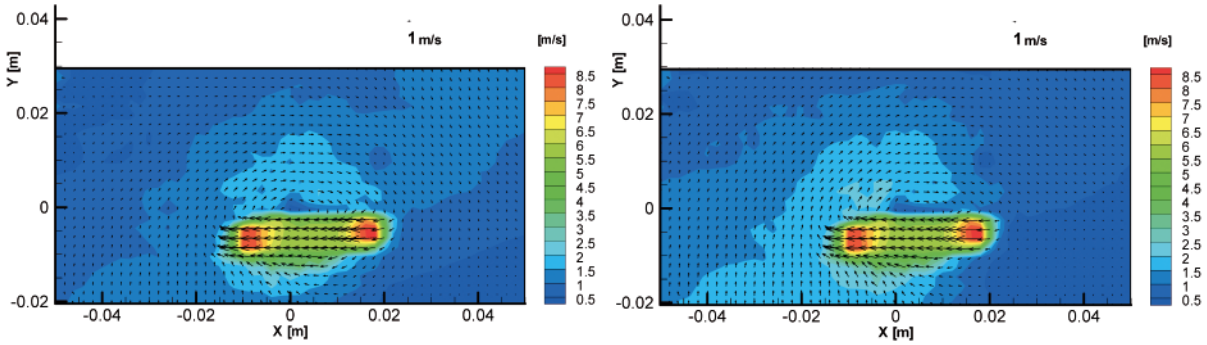

Fig. 13. Measured velocity field in plane the X-Y at the distance 50 mm behind the hydrofoil tip

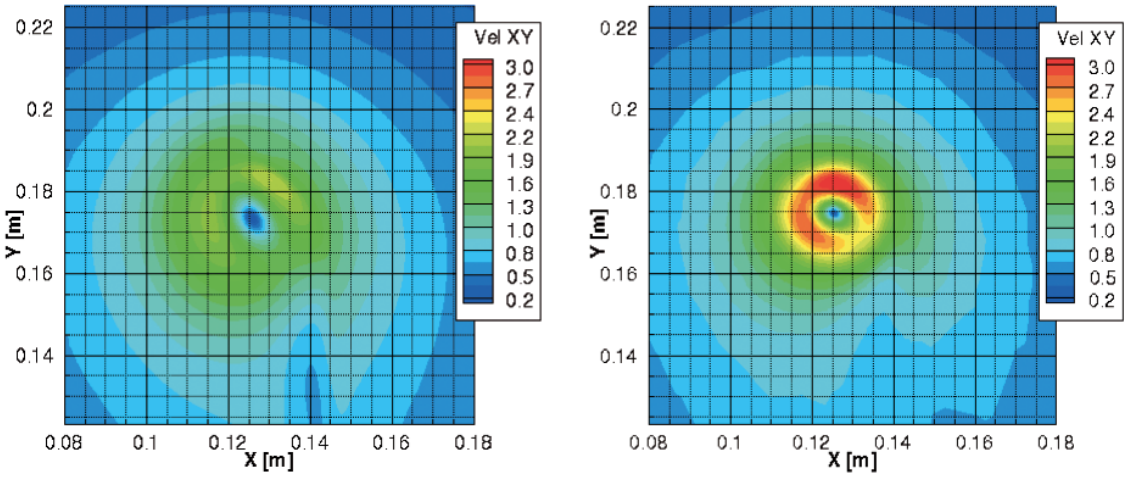

Fig. 14. Calculated velocity field in the plane X-Y at the distance 50 mm behind the hydrofoil tip – k-ε standard turbulence model – Fluent (left), CFX (right)

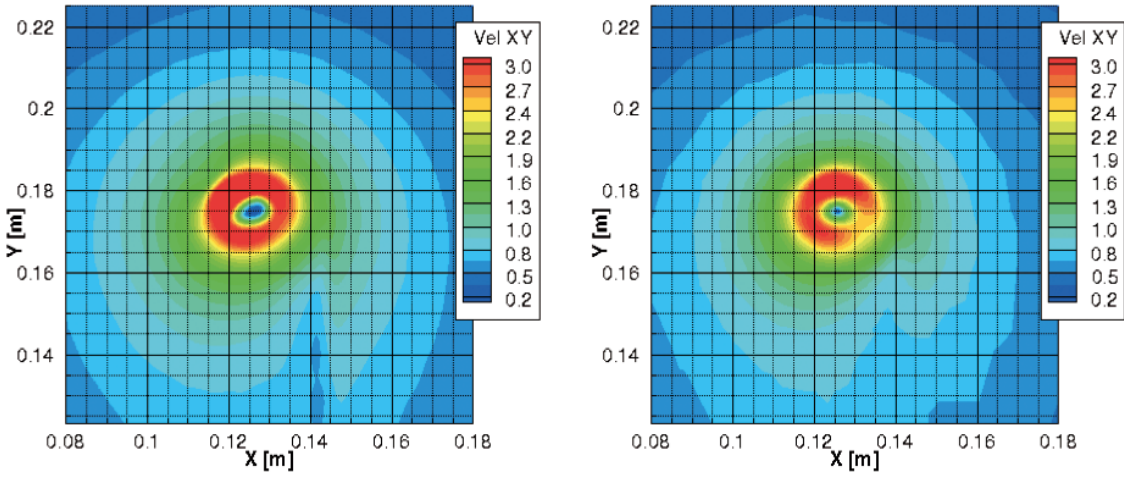

Fig. 15. Calculated velocity field in the plane X-Y at the distance 50 mm behind the hydrofoil tip – k-ε RNG turbulence model – Fluent (left), CFX (right)

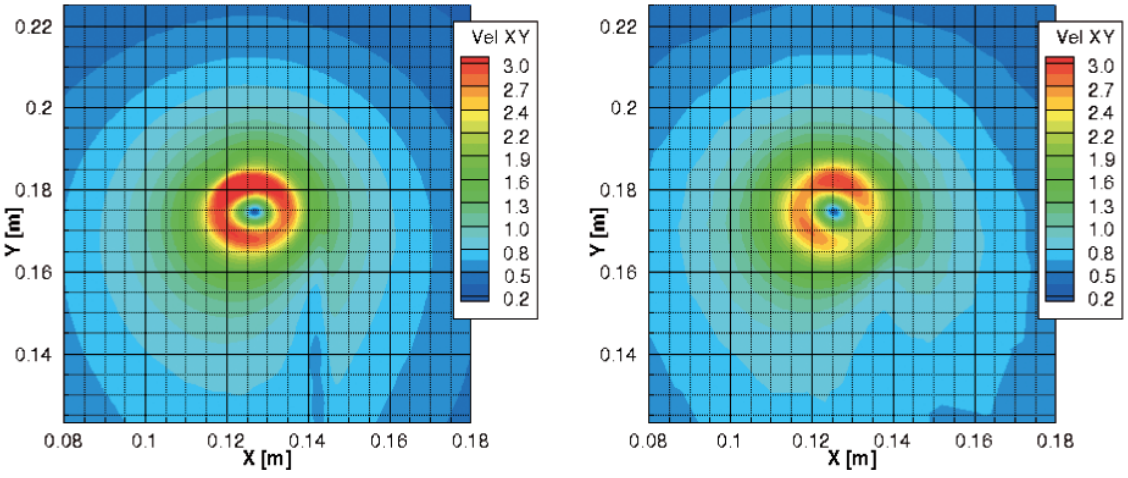

Fig. 16. Calculated velocity field in the plane X-Y at the distance 50 mm behind the hydrofoil tip – k-ω SST turbulence model – Fluent (left), CFX (right)

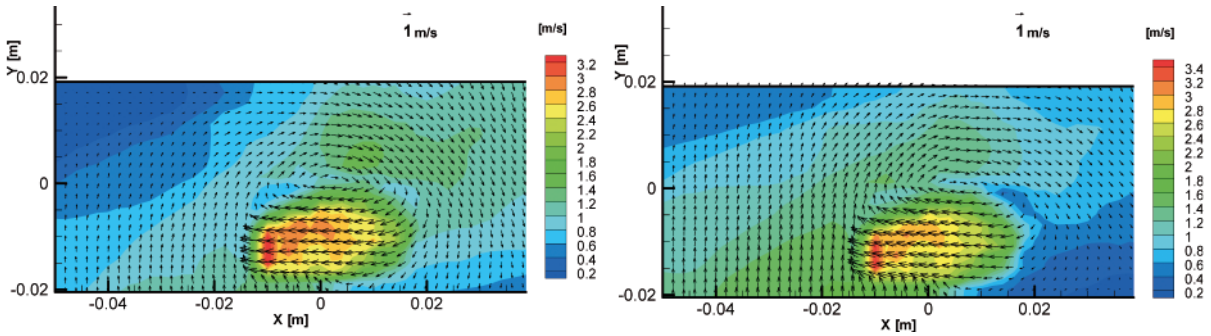

Fig. 17. Measured velocity field in plane X-Y at the distance 200 mm behind the hydrofoil tip

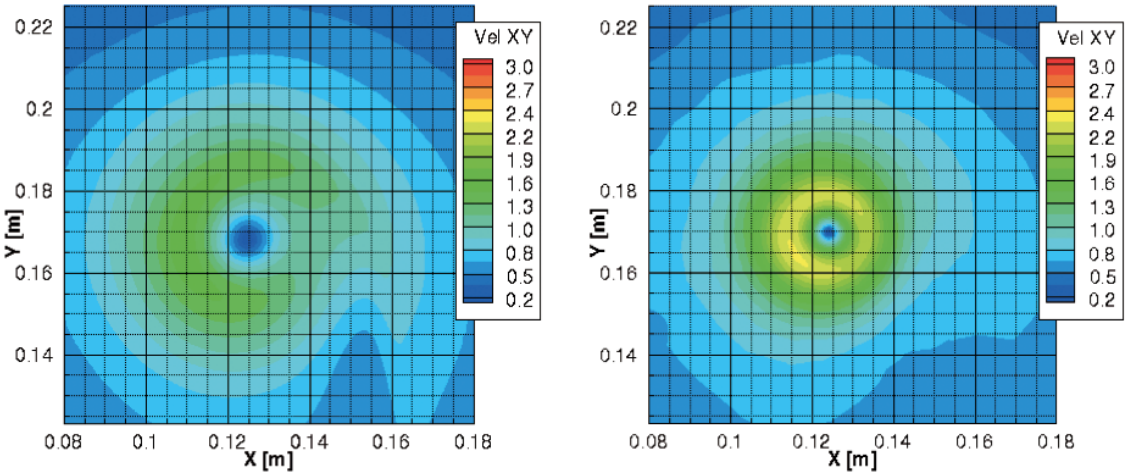

Fig. 18. Calculated velocity field in the plane X-Y at the distance 200 mm behind the hydrofoil tip – k-ε standard turbulence model – Fluent (left), CFX (right)

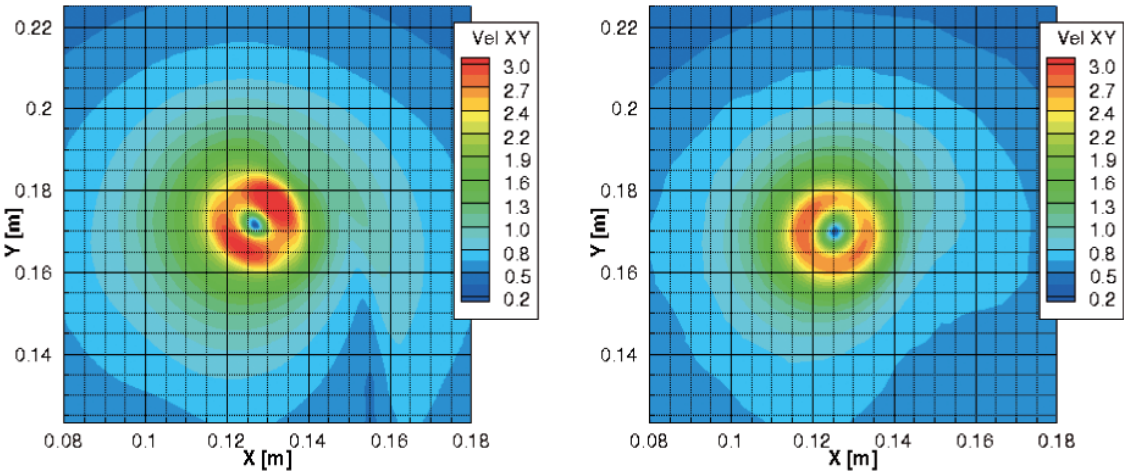

Fig. 19. Calculated velocity field in the plane X-Y at the distance 200 mm behind the hydrofoil tip – k-ε RNG turbulence model – Fluent (left), CFX (right)

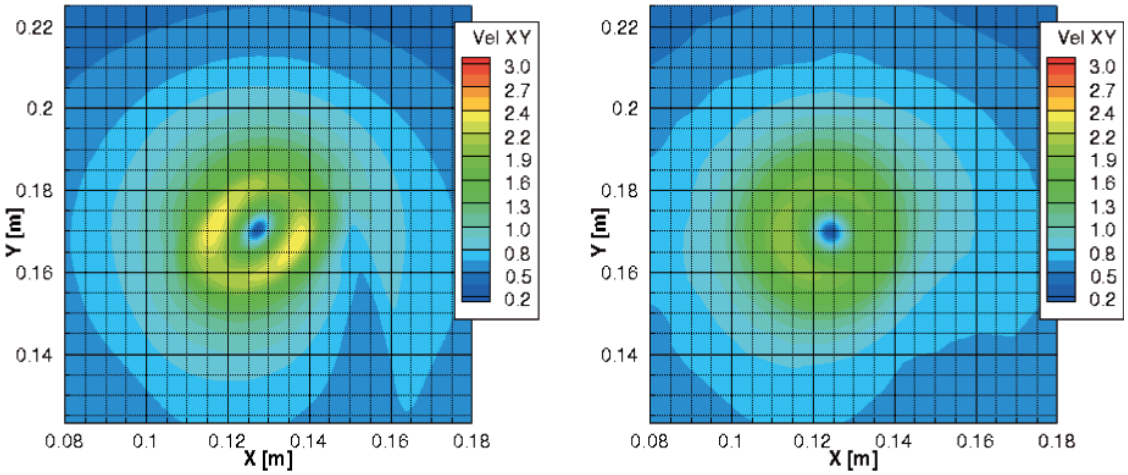

Fig. 20. Calculated velocity field in the plane X-Y at the distance 200 mm behind the hydrofoil tip – k-ω SST turbulence model – Fluent (left), CFX (right)

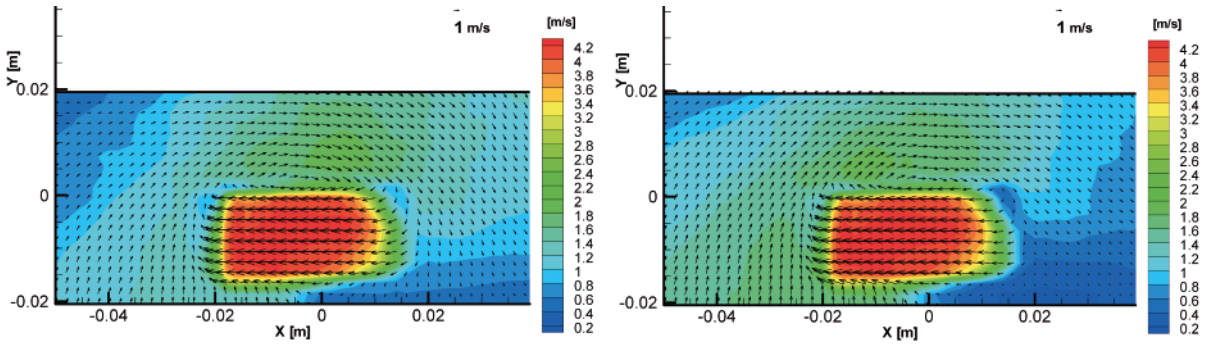

Fig. 21. Measured velocity field in the plane X-Y at the distance 300 mm behind the hydrofoil tip

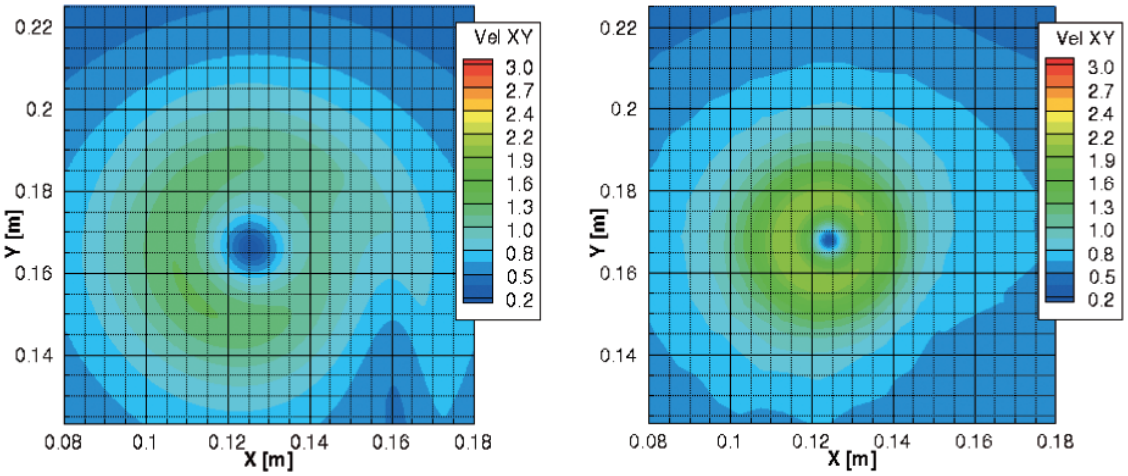

Fig. 22. Calculated velocity field in the plane X-Y at the distance 300 mm behind the hydrofoil tip – k-ε standard turbulence model – Fluent (left), CFX (right)

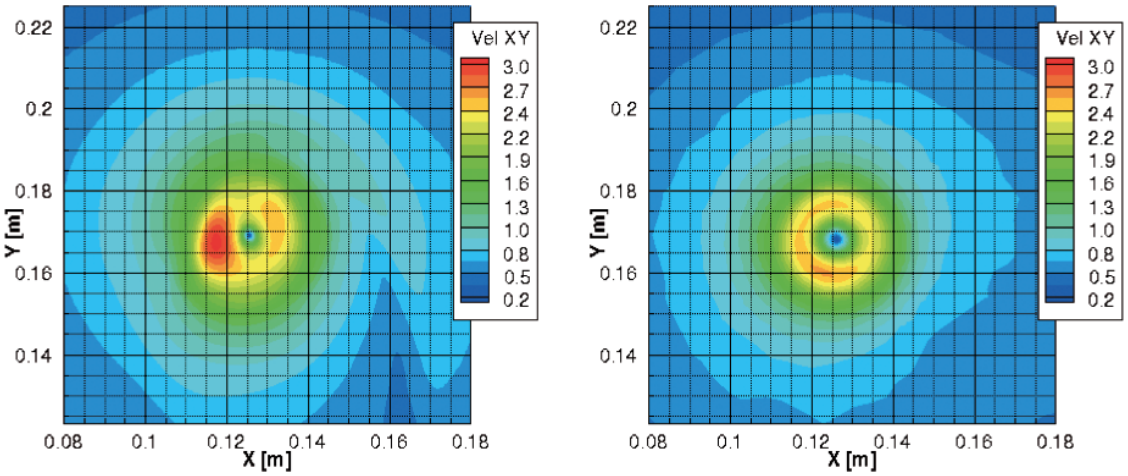

Fig. 23. Calculated velocity field in the plane X-Y at the distance 300 mm behind the hydrofoil tip – k-ε RNG turbulence model – Fluent (left), CFX (right)

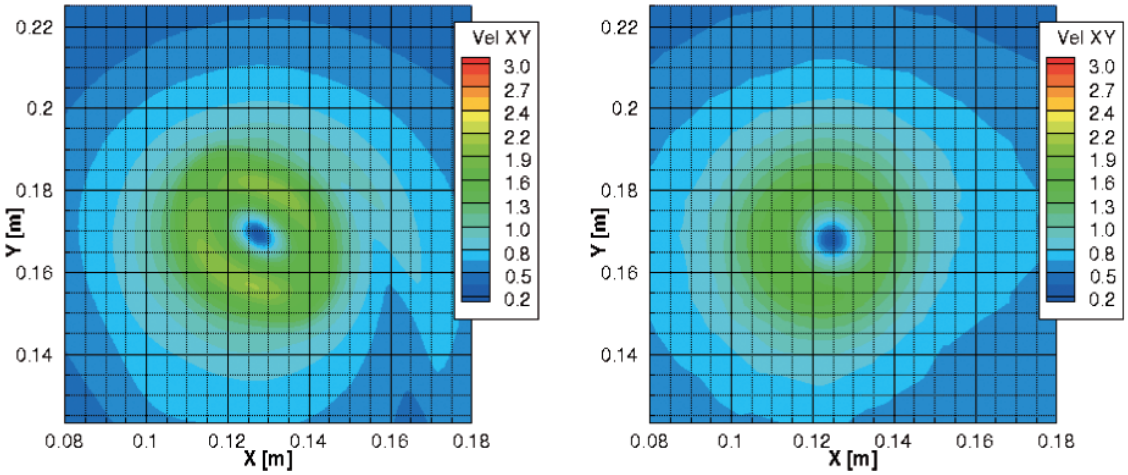

Fig. 24. Calculated velocity field in the plane X-Y at the distance 300 mm behind the hydrofoil tip – k-ω SST turbulence model – Fluent (left), CFX (right)

CONCLUSIONS

The detailed analysis of the results of measurements, observations and CFD calculations presented in this article leads to the following conclusions:

- the contemporary commercial CFD codes are generally capable of predicting the geometry of the cavitating tip vortices generated by hydrofoils reasonably well,
- the accuracy of CFD prediction of the geometry of the cavitating tip vortex depends strongly on the turbulence models and on the grid structure, hence only the grids constructed especially for vortex-dominated flows should be used, together with turbulence models especially suited for modeling of such flows [1, 2, 3, 6],
- in view of the above presented results the turbulence model k-ε RNG seems to be best suited for CFD prediction of tip vortex cavitation, despite the fact that according to [3] the k-ω SST performed best in prediction of non-cavitating vortex flows,
- the measurements of the velocity field in the vicinity of the cavitating tip vortex by means of PIV methods seem to be a difficult and challenging task, especially due to the following reasons:
  - unsteady oscillations of the cavitating kernel of the vortex,
  - uncontrolled content of cavitation nuclei (i.e. gas and vapour filled micro-bubbles) carried by the flowing water,
  - shading of part of the measuring plane by the cavitating kernel,
  - difficulties in homogeneous PIV seeding due to the large volume of fluid inside the cavitation tunnel and complex flow conditions near cavitating tip vortex (centrifugal force acting on seeding particles)
- due to the above listed reasons the velocity distribution predicted numerically at the following sections is significantly different from the measurements.

Acknowledgement

The research described in this article has been conducted with the support of the Research Grant No. N N504 088738 of the Polish Ministry of Science and Higher Education.

BIBLIOGRAPHY

1. Dymarski P., Szantyr J., Flaszyński P., Kraskowski M., Biernacki R.: *Modelling of Tip Vortex Behind a Blade using Different Turbulence Models and Different RANSE Solvers*, Proc. of the 11th Numerical Towing Tank Conference, Brest, France, September 8-10, 2008
2. Flaszyński P., Szantyr J., Dymarski P., Kraskowski M.: *Numerical Prediction of Vortex Generated by a Hydrofoil*, Proc. Of the International Symposium on Marine Propulsors, Trondheim, Norway, June 22-24, 2009
3. Flaszyński P., Szantyr J.: Biernacki R., Dymarski P., Kraskowski M.: *A Method for the Accurate Numerical Prediction of the Tip Vortices Shed from Hydrofoils*, Polish Maritime Research No. 2(65), Vol. 17, 2010, pp.10-17
4. Flaszyński P., Tesch K.: *Research Report – Task 2 Calculations for the Selected Flow Configuration Using Different Cavitation Models* (in Polish), Gdansk University of Technology 2011
5. Suchecki W., Alabrudziński S.: Research Report – *Task 1 Experimental Measurements of the Geometry of the Cavitating Vortex Kernel and Velocity in its Close Vicinity* (in Polish), Warsaw University of Technology 2011
6. Szantyr J., Biernacki R., Flaszyński P., Dymarski P., Kraskowski M.: *An Experimental and Numerical Study of The Vortces Generated by Hydrofoils*, Polish Maritime Research No. 3(61), Vol. 16, 2009, pp.11-17
7. Zwart P.J., Gerber A.G., Belamri T.: *A Two-Phase Flow Model for Predicting Cavitation Dynamics*, Fifth International Conference on Multiphase Flow, Yokohama, Japan, 2004

CONTACT WITH THE AUTHORS

J.A. Szantyr, Prof. e-mail: jas@pg.gda.pl
P. Flaszynski, Ph.D. e-mail: pflaszyn@pg.gda.pl
K.Tesch, Ph.D. e-mail: krzyte@pg.gda.pl
Faculty of Mechanical Engineering
Gdansk University of Technology
Narutowicza 11/12
80-231 Gdańsk, POLAND

W. Suchecki, Ph.D. email: suchecki@pl.onet.pl
S. Alabrudziński, Ph. D. e-mail: salabrudzinski@pw.plock.pl
Faculty of Civil Enginering,
Mechanics and Petrochemistry
Warsaw University of Technology
Łukasiewicza 17
09-400 Płock, POLAND

POLISH MARITIME RESEARCH 4(71) 2011 Vol 18; pp. 23-27
10.2478/v10012-011-0022-y

Vibration Analysis of Grid-Stiffened Circular Cylindrical Shells with Full Free Edges

J. E. Jam, Ph. D.
M. Yusef Zadeh, Ph. D. Res. Scientist
H. Taghavian, M. Sc.
B. Eftari, M. Sc.
Composite Materials and Technology Center, Tehran, IRAN

ABSTRACT

Free vibration of grid stiffened circular cylindrical shells is investigated based on the first Love's approximation theory using Galerkin method. Full free edges are considered for boundary conditions. An equivalent stiffness model (ESM) is used to develop the analytical solution of the grid stiffened circular cylindrical shell. The effect of helical stiffeners orientation and some of the geometric parameters of the structure have been shown. The accuracy of the analysis has been examined by comparing results with those available in the literature and finite element approach.

Keywords: Free vibration; Grid Structure; Cylindrical Shells; Stiffener; Galerkin Method

INTRODUCTION

Grid stiffened cylindrical shells are applicable in many industries such as aerospace industries. Stiffened cylindrical shells play a big role in aerospace industries in fuselage and fuel tank applications. This has resulted in an extensive research work in the field of cylinders with stiffening structures [1–8].

Grid stiffened cylindrical shells are widely used in engineering fields. These structures are subjected to external dynamic loads. These external dynamic loads can cause the undesirable resonance and it can lead to fatigue. Moreover, dynamic characteristics must be used on design of structure because only vibration (not fatigue) could severely damage the sensitive equipment in airplanes, launch vehicles and etc. Therefore, it is essential to understand the dynamic behavior of these structures. Theoretical methods of analyzing the grid stiffened structures are classified into two main types, depending upon whether the stiffeners are treated by averaging their properties over the shell surface to conventional materials or by considering them as discrete elements. The first method, so-called smeared stiffener theory, is particularly applicable only when large numbers of stiffeners are closely and evenly spaced. The second method, so-called discrete stiffener theory, is more general as it can accommodate any stiffener distribution. Numerous researches have been developed to study the vibrational behavior of stiffened cylindrical shells. Mustafa and Ali [9] predicted natural frequencies for the stiffened cylindrical shells using the Rayleigh-Ritz procedure. In this procedure they used only one term in assuming the displacement functions satisfying the simply supported boundary condition. One-term approximation is sufficient for the analysis of the cylindrical shells with simply supported boundary condition. However, it can lead to much error to obtain the exact solution of stiffened shells with any other boundary conditions. Yang and Zhou [10] presented the transfer function method to analyze the ring-stiffened shell. Lee and Kim [11, 12] investigated the effect of rotation speeds and boundary conditions on the frequencies for the orthogonally stiffened composite cylindrical shells treating the materials of stiffeners as equivalent isotropic. The mentioned papers were, however, limited to the shells with the uniform dimensional and evenly spaced stiffeners. In fact, non-uniform dimensional and unevenly spaced stiffeners are used much more in structural reinforcements. Wang *et al*. [13] solved the free vibration problem for the isotropic cylindrical shells with varying ring-stiffener distribution using the extended Ritz method. Egle and Sewall [14], in different boundary conditions, have analyzed the effect of stiffeners on natural frequencies of stiffened cylindrical shells. In this research, stiffeners are considered as discrete elements, energy method and Hamilton principle are used to obtain equations of motion. Rinehart and Wang [15] have studied the changes in natural frequencies of cylindrical shells affected by stringers stiffeners, based on Vlasov thin walled beam theory. By both, considering the stiffeners as discrete elements and using energy method, they have obtained the equations of motion.

Unlike the previous study, the vibrations of stiffened cylindrical shells with grid structure under full free boundary conditions are analyzed in this paper. The stiffness matrix of the whole structure is determined by stiffness matrix of grid structures. Then, equilibrium equations are considered based

on the classical shell theory. Strain-displacement relations are written based on the first approximation of Love theory and then by replacement in stress-strain relations, equilibrium equations based on displacement parameters are obtained. After simplification of equilibrium equations, the shell frequency equation is obtained by using Galerkin method. Finally, according to the following assumptions, the effect of stiffener geometry and mass of grid stiffened cylindrical shell on natural frequencies is presented:

1. The thickness of ribs is small compared with length of the ribs. So the transverse strain of stiffeners is much smaller than that of longitudinal strain and can be negligible.
2. The strain is uniform across the cross-sectional area of the stiffeners. Hence, a uniform stress distribution is assumed across the cross-sectional area of the stiffeners.
3. The load on the stiffener/shell is transferred through shear forces between the stiffeners and shell.

$$\begin{Bmatrix} N_x \\ N_\theta \\ N_{\theta x} \\ M_x \\ M_\theta \\ M_{\theta x} \end{Bmatrix}^s = AE \begin{bmatrix} 2\frac{c^3+1}{a} & 2\frac{cs^2}{a} & 0 & \frac{c^3+1}{a}t & \frac{cs^2}{a}t & 0 \\ \frac{2c^2s}{b} & 2\frac{s^3+1}{b} & 0 & \frac{c^2st}{b} & \frac{s^3+1}{b}t & 0 \\ 0 & 0 & \frac{2s^2c}{a} & 0 & 0 & \frac{s^2ct}{a} \\ \frac{c^3+1}{a}t & \frac{cs^2t}{a} & 0 & \frac{c^3+1}{2a}t^2 & cs^2\frac{t^2}{2a} & 0 \\ \frac{sc^2t}{b} & \frac{s^3+1}{b}t & 0 & sc^2\frac{t^2}{2b} & (s^3+1)\frac{t^2}{2b} & 0 \\ 0 & 0 & \frac{s^2ct}{a} & 0 & 0 & sc^2\frac{t^2}{2a} \end{bmatrix} \begin{bmatrix} \varepsilon_x^o \\ \varepsilon_\theta^o \\ \gamma_{x\theta}^o \\ k_x \\ k_\theta \\ k_{\theta x} \end{bmatrix} \tag{2}$$

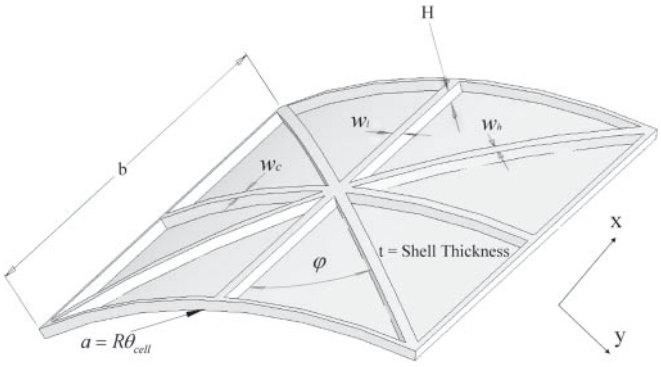

Fig. 1. *Grid stiffener and shell design parameters*

The above matrix elements are the functions of the strain and curvature parameters of the shell. We denote these stiffness parameters by A^s, B^s and D^s which corresponds to the extensional, coupling and bending matrices, respectively. Here, the superscript *s* stands for stiffener. By the matrix summation of force and moment, coming from the stiffener Grid structure and cylindrical shell, the force and the moment of the whole structure will be obtained.

$$\begin{bmatrix} N \\ M \end{bmatrix} = \begin{bmatrix} N^s + N^{sh} \\ M^s + M^{sh} \end{bmatrix} \tag{3}$$

N^{sh} and M^{sh} are the force and moment contribution of the shell, respectively. Forces and moments, which affect the shell,

ANALYTICAL METHOD

Equivalent Stiffness Matrix of the Stiffener and Shell

To calculate the natural frequencies of the whole structures, first, the stiffness matrix of grid structures must be determined. This matrix is composed of three separated matrices A^s, B^s and D^s which can be explained like below:

$$\begin{bmatrix} N \\ M \end{bmatrix}^s = \begin{bmatrix} A^s & B^s \\ B^s & D^s \end{bmatrix} \begin{bmatrix} \varepsilon^0 \\ k \end{bmatrix} \tag{1}$$

Based on geometrical variables of grid structures which presented in Fig. 1, stiffness matrix of grid structures can be obtained as below [16]:

relate to the occurred strain by stiffness matrix A^{sh}, B^{sh} and D^{sh}. Based on shell mechanical properties, these matrices are:

$$A_{ij}^{sh} = \frac{Et}{1-\nu^2}\begin{bmatrix} 1 & \nu & 0 \\ \nu & 1 & 0 \\ 0 & 0 & \frac{1-\nu}{2} \end{bmatrix} \quad B_{ij}^{sh} = [0]$$
$$D_{ij}^{sh} = \frac{Et^3}{12(1-\nu^2)}\begin{bmatrix} 1 & \nu & 0 \\ \nu & 1 & 0 \\ 0 & 0 & \frac{1-\nu}{2} \end{bmatrix} \quad i, j = 1,2,6 \tag{4}$$

Substituting the force and moment expressions for the stiffener network from Eq. 2, and the force and moment expressions for the shell from Eq. 4, the total structure constitutive equation given by Eq. 5 results:

$$\begin{bmatrix} N \\ M \end{bmatrix} = \begin{bmatrix} A^s + A^{sh} & B^s + B^{sh} \\ B^s + B^{sh} & D^s + D^{sh} \end{bmatrix} \begin{bmatrix} e^0 \\ k \end{bmatrix} \tag{5}$$

Formulation

The cylindrical shell under consideration is with constant thickness t, radius R and length L. The reference surface of the shell is taken to be at its middle surface where an orthogonal coordinate system (x, θ, z) is fixed. As shown in Fig. 2, the

x axis is taken in the axial direction of the shell, where the θ and z axises are in the circumferential and radial directions of the shell, respectively. The displacements of the shell are defined by u, v, w in the x, θ, z directions respectively.

The equations of motion for a cylindrical shell can be written by the Love theory as:

$$\begin{bmatrix} L_{11} & L_{12} & L_{13} \\ L_{21} & L_{22} & L_{23} \\ L_{31} & L_{32} & L_{33} \end{bmatrix} \begin{Bmatrix} u \\ v \\ w \end{Bmatrix} = \begin{Bmatrix} 0 \\ 0 \\ 0 \end{Bmatrix} \tag{6}$$

where:

$L_{ij}(i, j = 1, 2, 3)$ – the differential operators with respect to x and θ.

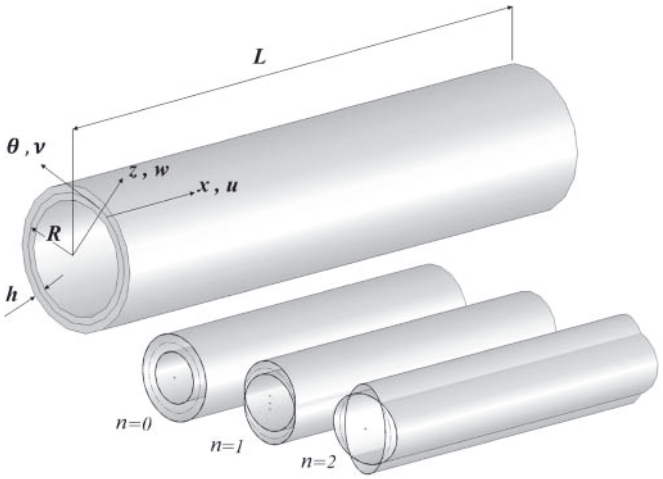

Fig. 2. *Co-ordinate system and circumferential modal shape [17]*

Boundary Conditions

Due to the satisfaction of the boundary conditions, the displacement u, v and w can be explained as double Fourier series [19]:

$$\begin{aligned} u(x,\theta,t) &= \sum_m \sum_n A_{mn} \frac{\partial \varphi_u(x)}{\partial x} \cos(n\theta)\cos(\omega t) \\ v(x,\theta,t) &= \sum_m \sum_n B_{mnv} \varphi(x) \sin(n\theta)\cos(\omega t) \\ w(x,\theta,t) &= \sum_m \sum_n C_{mnw} \varphi(x) \cos(n\theta)\cos(\omega t) \end{aligned} \tag{7}$$

In recent equations, A_{mn}, B_{mn} and C_{mn} are coefficients of natural modes' shape, which obtained from solving free vibration. For solving free vibrations, $T_{mn}(t) = e^{\omega_{mn} t}$ is considered as a function of time, m is the number of axial half-wavelength, n is the number of circumferential half-wavelength and ω_{mn} is the natural frequency in mode of mn. To satisfy boundary conditions, axial and circumferential functions are explained as below:

$$\begin{cases} \varphi_i(x) = \alpha_1 \cosh\left(\dfrac{\lambda_m x}{L}\right) + \alpha_2 \cos\left(\dfrac{\lambda_m x}{L}\right) - \sigma_m \left(\alpha_3 \sinh\left(\dfrac{\lambda_m x}{L}\right) - \alpha_4 \sin\left(\dfrac{\lambda_m x}{L}\right)\right) \ (i = u, v, w) \\ \phi_v(\theta) = \sin(n\theta) \qquad \phi_u(\theta) = \phi_w(\theta) = \cos(n\theta) \end{cases} \tag{8.a}$$

In above equations α_i are constant coefficients which determined according to boundary conditions. λ_m is the root of non-linear equations and σ_m is the dependant parameter on λ_m which obtained according to boundary conditions. Free-Free supported conditions can be defined as below:

$$\frac{\partial^2 \varphi(x)}{\partial x^2} = \frac{\partial^3 \varphi(x)}{\partial x^3} = 0 \tag{8.b}$$

Free Vibration Analysis

Using Galerkin method and substituting Eq. 7 into Eq. 6, it can be written as:

$$\begin{bmatrix} c_{11} & c_{12} & c_{13} \\ c_{21} & c_{22} & c_{23} \\ c_{31} & c_{32} & c_{33} \end{bmatrix} \begin{Bmatrix} A_{mn} \\ B_{mn} \\ D_{mn} \end{Bmatrix} = 0 \tag{9}$$

where:

$C_{ij}(i, j = 1, 2, 3)$ – the parameters from the L_{ij} after they are operated with the x and θ.

For non-trivial solutions, one sets the determinant of the characteristic matrix in Eq. 9 to zero:

$$\det(C_{ij}) = 0 \ (i, j = 1, 2, 3) \tag{10}$$

So the frequency equation can be obtained as:

$$\beta_1 \omega^6 + \beta_2 \omega^4 + \beta_3 \omega^2 + \beta_4 = 0 \tag{11}$$

where:

$\beta_i(i, j = 1, 2, 3)$ – the coefficients of Eq. 10.

Solving Eq. 11, one obtains three positive roots and three negative roots. The three positive roots are the angular natural frequencies of the cylindrical shell in the axial, circumferential and radial directions. The lowest of the three positive roots represents the flexural vibration, and the other two are in-plane vibrations.

NUMERICAL RESULTS AND DISCUSSION

Numerical implementation of the present analysis was performed using general-purpose computation package MATLAB. To check the accuracy of the present analysis, the results obtained are compared with those in the [17]. A comparison of the values of the frequency of a free vibrating cylindrical shell with the F-F boundary conditions is given in Table 1.

Tab. 1. *Comparison of values of the natural frequency ω_n for a cylindrical shell with F-F supported boundary conditions*
m = 1; R/h = 374; L/R = 2.63; h = 0.6477 mm;
E = 70 GPA; ν = 0.3; ρ = 2700 Kg/m³

m	n	Reference [17]	Present	Difference (%)
1	7	251.4	267.9	6.56
	8	243.5	243.0	0.20
	9	257.1	252.4	1.82
	10	280.2	284.5	1.53
	11	340.3	331.2	2.67

In the parameter, E is Young's modulus of elasticity, ν is the Poisson ratio, ρ is the density, R is the radius and ω is the frequency. The comparisons are carried out for the parameter of L/R = 2.63 and for the cases of R/h = 374 and t = 6.477x10^{-4} m. Using the method outlined earlier, numerical results are obtained for the six model of grid-stiffened cylinder with four families of ribs and geometric and mechanical parameters given in Tables 2 and 3.

Tab. 2. Dimensions of the considered structures (mm, kg)

m_{TOT}	$m_{stiffener}$	m_{shell}	t_{shell}	R	L	φ	$w_h=w_c=$ $=w_l=w$	H	
19.794	3.450	16.344	5	300	653	30°	6	6	Model 1
21.007	4.663	16.344	5	300	653	30°	7	7	Model 2
25.681	9.337	16.344	5	300	653	30°	10	10	Model 3
36.647	20.302	16.344	5	300	653	30ş	15	15	Model 4
20.944	4.430	16.344	5	300	640	45ş	6	6	Model 5
22.505	6.161	16.344	5	300	653	60ş	6	6	Model 6

Tab. 3. Mechanical properties of the models (Aluminum)

Modulus of elasticity	Poisson's ratio	Density
E (GPa)	ν	ρ kg/m³
70	0.3	2700

The obtained results are compared to the solution of the same problem when the considered structures are modeled with a finite element analysis package *ANSYS*. One of the generated mesh by this package is shown in Fig. 3.

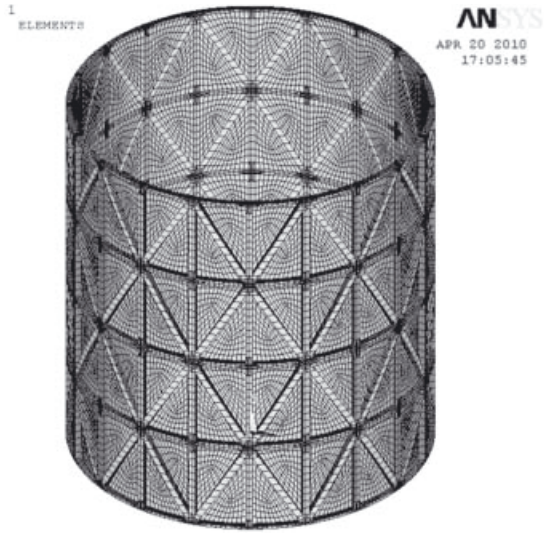

Fig. 3. *The mesh generated for a grid stiffened cylindrical shell using ANSYS*

Based on a technical report [18], natural frequencies of a grid-stiffened shell can be approximated by equivalent of thickness. In this method, a conventional shell with the same weight as grid part is predicted. An equivalent shell will be produced by the replacement of this shell with grid part. The obtained frequencies of this equivalent shell can be a proper approximation for natural frequencies of the main structure. In Figs. 4-9, a comparison between the results obtained by ETM (Equivalent Thickness Method), FEM and present method is presented. These figures have shown that the present method gives more exact answers than ETM.

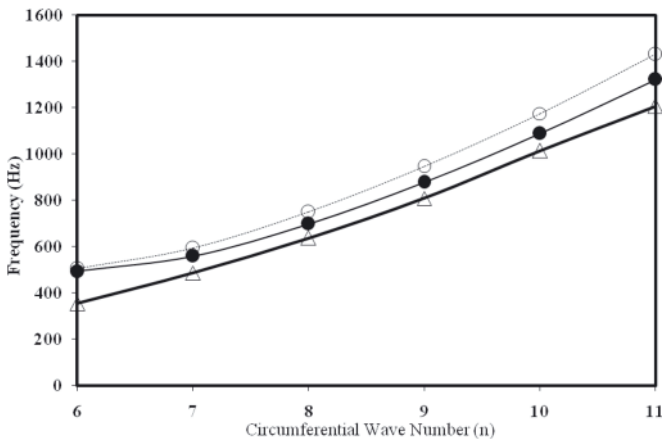

Fig. 4. *Values of natural frequency for Model (1) with Free-Free boundary conditions in three methods. Δ FEM; ● Present Method; ○ ETM (Equivalent Thickness Method); m = 1*

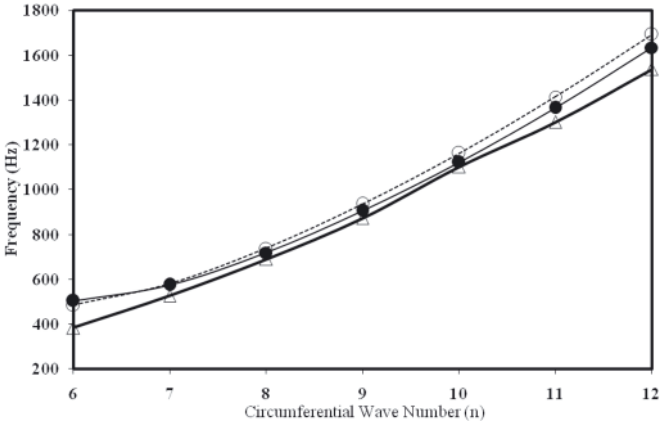

Fig. 5. *Values of natural frequency for Model (2) with Free-Free boundary conditions in three methods. Δ FEM; ● Present Method; ○ ETM (Equivalent Thickness Method); m = 1*

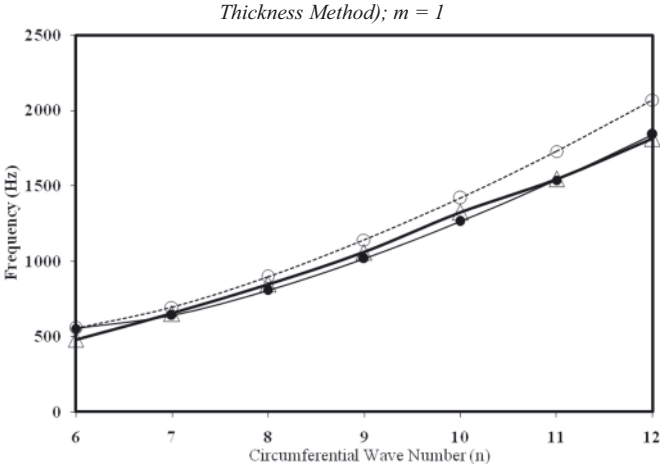

Fig. 6. *Values of natural frequency for Model (3) with Free-Free boundary conditions in three methods. Δ FEM; ● Present Method; ○ ETM (Equivalent Thickness Method); m = 1*

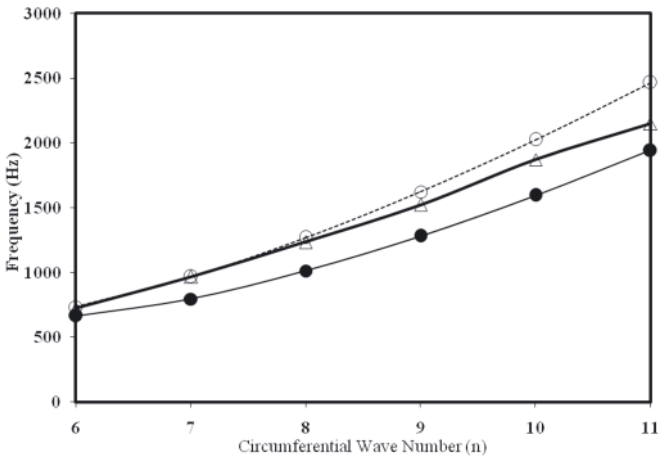

Fig. 7. *Values of natural frequency for Model (4) with Free-Free boundary conditions in three methods. Δ FEM; ● Present Method; ○ ETM (Equivalent Thickness Method); m = 1*

Fig. 10 shows the changes relative to natural frequencies of six predicted models, according to the angle of helical ribs. As shown in this figure, when the angle of helical rib increases, the amount of natural frequencies of structures will be increased.

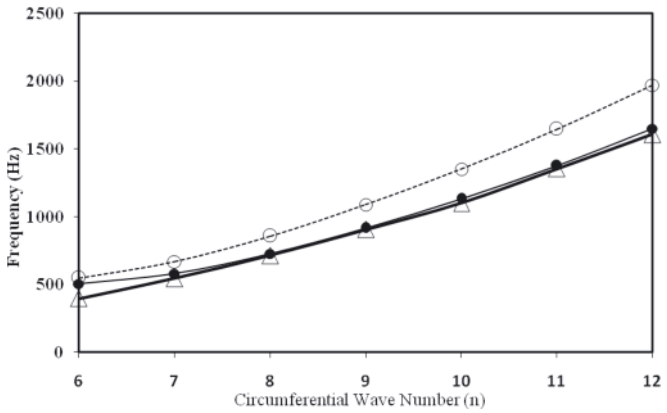

Fig. 8. *Values of natural frequency for Model (5) with Free-Free boundary conditions in three methods. Δ FEM; ● Present Method; ○ ETM (Equivalent Thickness Method); m = 1*

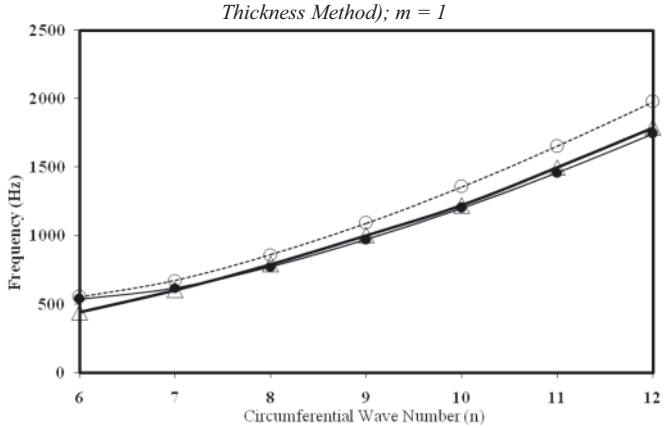

Fig. 9. *Values of natural frequency for Model (6) with Free-Free boundary conditions in three methods. Δ FEM; ● Present Method; ○ ETM (Equivalent Thickness Method); m = 1*

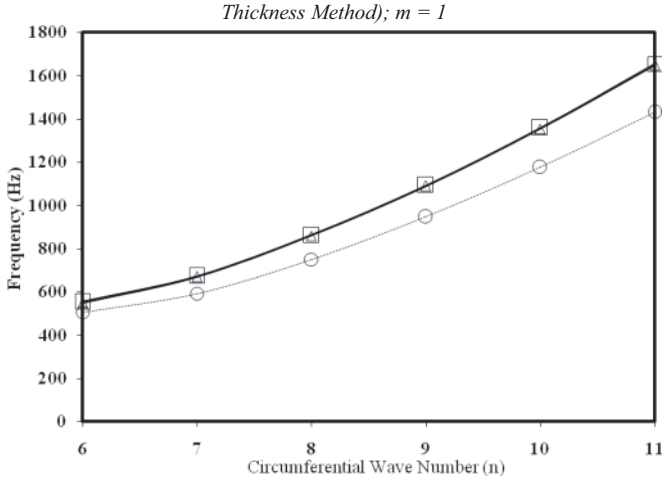

Fig. 10. *Comparison of natural frequencies of three predicted models according to the angle of helical ribs. ○ φ = 30 (Model 1); Δ φ = 45 (Model 5); □ φ = 60 (Model 6); m = 1*

Note: In this comparison Model 5 is smaller length than the remaining ones (about 2%). According to difference between configurations of models, the resulted value from FEM modeling is the minimum height discrepancy can be obtained.

CONCLUSION

The article has presented the analysis of grid stiffened cylindrical shell using Galerkin method. Comparison of the results by the present method and numerical finite element method was carried out. The six finite element models for grid stiffened cylindrical shell were created. The shell was fully free-free at both ends. The second six natural frequencies were obtained with the *ANSYS*. These results were compared with the present method and the agreement between them was good. Based on comparisons of the mentioned method, it is concluded that the present method is more convenient, more effective and more accurate.

BIBLIOGRAPHY

1. Helms J. E., Li G., Smith B. H.: *Analysis of grid stiffened cylinders*, ASME/ETCE, USA, 2001.
2. Navin J., Norman F. K., Damodar R.: *Formulation of an improved smeared stiffener theory of buckling analysis of grid-stiffened composite panels*, NASA Technical Memorandum 110162, USA, 1995.
3. Phillips J. L., Gurdal Z.: *Structural analysis and optimum design of geodesically stiffened composite panels*, Report NASA CCMS-90-50 (VPI-E-90-08), Grant NAG-1-643, USA, 1990.
4. Brush D. O., Almroth B. O.: *Buckling of bars, plates, and shells*, McGraw-Hill, New York, 1975.
5. Bruhn E. F.: *Analysis and design of flight vehicle structures*, Jacobs Publishing, Carmel, 1973.
6. Ramm E.: *Buckling of shells*, Springer, Berlin,1982.
7. Gerdon G., Gurdal Z.: *Optimal design of geodesically stiffened composite cylindrical shells*, Journal of AIAA, 23(11) (1985), 1753–61.
8. Troisky M.S.: *Stiffened plates, bending, stability and vibration*, Elsevier, Amsterdam, 1976.
9. B. A. J. Mustafa and R. Ali: *An energy method for free vibration analysis of stiffened circular cylindrical shells*, Computers and Structures 32 (1989), 355-363.
10. B. Yang and J. Zhou*: Analysis of ring-stiffened cylindrical shells*, Journal of Applied Mechanics 62 (1995), 1005-1014.
11. Y. S. Lee and Y. W. Kim: Vibration analysis of rotating composite cylindrical shells with orthogonal stiffeners, Computers and Structures, 69 (1998), 271-281.
12. Y. S. LEE and Y.W. KIM: *Effect of boundary conditions on natural frequencies for rotating composite cylindrical shells with orthogonal stiffeners*, Advanced in Engineering Software 30 (1999), 649-655.
13. M. Wang, S. Swaddiwudhipong and J. Tian: *Ritz method for vibration analysis of cylindrical shells with ring stiffeners*, Journal of Engineering Mechanics 123 (1997), 134-142.
14. D. M. Egle, J. L. Sewall: *An analysis of the free vibration of orthogonally stiffened cylindrical shells with stiffener separated as discrete elements*, AIAA Journal 3 (1968), 518± 26.
15. S. A. Rinehart, J. T. S Wang: *Vibration of Simply Supported Cylindrical Shells with Longitudinal Stiffeners*, Journal of Sound and Vibration 24 (1972), 151-163.
16. Samuel Kidane, Guoqiang Li, Jack Helms, Su-Seng Pang, Eyassu Woldesenbet: *Buckling Load Analysis of Grid Stiffened Composite Cylinders*, Journal of Composites, PartB 34 (2003), 1–9.
17. Arthur Leissa*: Vibration of Shells. Columbus*, Acoustical Society of America, Ohio, 1993.
18. Hassan Mahfuz*: Final Report on Innovative Manufacturing and Structural Analysis of Composite Isogrid Structures for Space Applications,* AFRL-SR-AR-TR-04, USA, 2004.
19. M. M. Najafizadeh, M. R. Isvandzibaei: *Vibration of Functionally Graded Cylindrical Shells Based on Higher Order Shear Deformation Plate Theory With ring Support*, Acta Mech Journal, 191 (2007), 75-91.

CONTACT WITH THE AUTHORS

J. E. Jam, Ph. D.
tel.: 98-21-22952286
fax: 98-21-22936578
e-mail address: jejam@mail.com
M. Yusef Zadeh, Ph. D. Res. Scientist
H. Taghavian, M. Sc.
B. Eftari, M. Sc.
Composite Materials and Technology Center,
MUT, Tehran, IRAN

POLISH MARITIME RESEARCH 4(71) 2011 Vol 18; pp. 28-35
10.2478/v10012-011-0023-x

Theoretical and mathematical models of the torque of mechanical losses in the pump used in a hydrostatic drive

Zygmunt Paszota, Prof.
Gdansk University of Technology

ABSTRACT

The paper presents theoretical and mathematical models of the torque of mechanical losses in the pump with theoretical (constant) capacity q_{Pt} per one shaft revolution (with constant theoretical working volume V_{Pt}) and geometrical (variable) capacity q_{Pgv} per one shaft revolution (with variable volume V_{Pgv}). The models may be used in the laboratory and simulation investigations of the pump energy efficiency and the hydrostatic drive efficiency.

Key words: hydrostatic drive; displacement pump; energy efficiency

INTRODUCTION

The paper is a continuation of the work presented in references [1 ÷ 18], aimed at creating a method of evaluation of the losses and energy efficiency of hydrostatic drives as well as the used displacement machines (pump and hydraulic motors). The method is based on mathematical models of energy losses in the pumps, in hydraulic motors and in other elements of a hydrostatic drive system.

The description of pump losses and energy efficiency is based on the **diagram of power increase in the drive system opposite to the direction of power flow, replacing the Sankey diagram of power decrease in the direction of power flow** [18]. The Sankey diagram of decrease (division) of power in a drive system in the direction of power flow is the main reason of incorrect evaluation of the energy losses, a. o. in the displacement pumps and hydraulic motors used in hydrostatic drive systems.

During the operation of a hydrostatic drive system, the energy losses **force the increase of power in the system** – from useful power P_{Mu} required by the hydraulic motor driven machine to the power P_{Pc} consumed by the pump on the pump shaft.

In the description of power flow in a drive system and the powers of energy losses connected with the flow, the notions: „power decrease", „power division", „power loss" should not be used.

The notion associated with the power of energy losses in a drive system is „increase of power".

Figure 1 presents a diagram of power increase in a displacement pump opposite to the direction of power flow, which replaces the Sankey diagram of power decrease in the direction of power flow.

The aim of the paper is to present the theoretical and mathematical models of mechanical losses in the pump „working chambers – shaft" assembly. Pump is a displacement machine with theoretical (constant) capacity q_{Pt} per one shaft revolution (with constant theoretical working volume V_{Pt}) or with geometrical (variable) capacity q_{Pgv} per one shaft revolution (with variable geometrical working volume V_{Pgv}).

The models may be used in the laboratory and simulation investigations of the pump mechanical losses, allowing to evaluate the pump energy efficiency and the hydrostatic drive efficiency .

THEORETICAL MODELS OF THE TORQUE M_{PM} OF MECHANICAL LOSSES IN THE PUMP „WORKING CHAMBERS - SHAFT" ASSEMBLY

The pump shaft torque M_P (required by the pump of its driving motor) **must be greater than the torque M_{Pi} indicated in the pump working chambers because of the necessity of balancing also the torque M_{Pm} of mechanical losses in the „working chambers – shaft" assembly. The assembly forms the working chambers and changes their capacity and also connects the working chambers with the shaft**. Therefore, the torque M_P required on the pump shaft is a sum of the torque M_{Pi} indicated in the working chambers and the torque M_{Pm} of mechanical losses in the pump „working chambers – shaft" assembly:

$$M_P = M_{Pi} + M_{Pm} \tag{1}$$

Torque M_{Pm} of mechanical losses in a pump with variable capacity q_{Pgv} per one shaft revolution is, at the maximum value of q_{Pgv} i.e. $q_{Pgv} = q_{Pt}$ (with $b_P = q_{Pgv}/q_{Pt} = 1$), equal to the torque

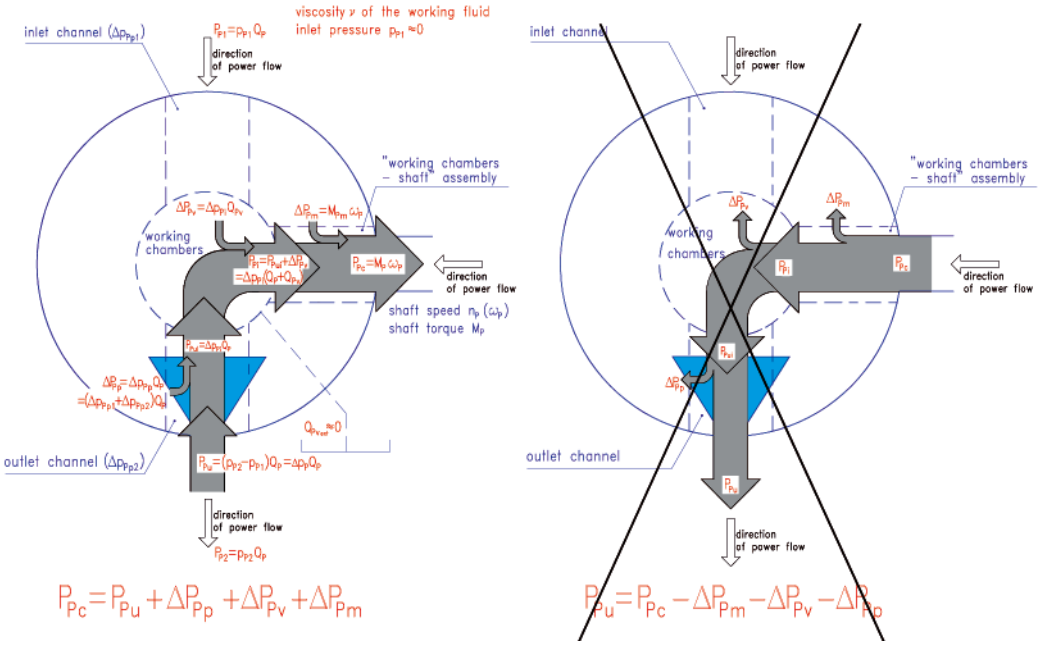

Fig. 1. *Diagram of power increase in a displacement pump opposite to the direction of power flow, replacing the Sankey diagram of power decrease in the direction of power flow*

of mechanical losses in that pump working as a pump with constant capacity q_{Pt} per one shaft revolution. The theoretical and mathematical models describing the torque M_{Pm} of mechanical losses in a pump with variable capacity q_{Pgv} per one shaft revolution may be based on models of M_{Pm} describing the torque of mechanical losses in a pump with constant capacity q_{Pt} per one shaft revolution (with $b_P = 1$). Considering the models describing the torque of pump mechanical losses, we assume, that the pump is driven with practically constant rotation speed n_p, and the decrease of shaft speed (decrease of the pump driving motor speed as a result of the increase of torque M_P loading the motor shaft) to a value $n_P < n_{P0}$ (n_{P0} – rotational speed of unload pump driving motor) is negligible from the point of view of the impact of speed n_P on the value of torque M_{Pm} of mechanical losses.

Torque M_{Pm} of mechanical losses in the pump is mainly an effect of friction forces between elements of the „working chambers – shaft" assembly, depending, among other, on the torque M_{Pi} indicated in the working chambers – $M_{Pi} = q_{Pgv}\,\Delta p_{Pi}/2\Pi = b_P\,q_{Pt}\,\Delta p_{Pi}/2\Pi$.

Friction forces between elements of the „working chambers – shaft" assembly are, to some extent, also an effect of the load on those elements of the inertia forces from rotational and reciprocating motion and depend on the pump capacity q_{Pgv} per one shaft revolution (b_P coefficient).

In the piston (axial or radial) pumps with casing (crankcase) filled with liquid, friction forces also occur between elements of the „working chambers – shaft" assembly and the liquid and depend on the liquid viscosity ν.

The value of torque $M_{Pm|\Delta ppi,bp,\nu n}$ of mechanical losses in the pump „working chambers – shaft" assembly, loaded with indicated increase Δp_{Pi} of pressure in the working chambers, in the pump operating at the capacity $q_{Pgv} = b_p\,q_{Pt}$ per one shaft revolution and discharging the working liquid with (constant) reference viscosity ν_n, can be described as a sum of torque $M_{Pm|\Delta ppi,bp,\nu n}$ of mechanical losses in the unloaded pump (torque of the losses when the indicated increase Δp_{Pi} of pressure in the pump working chambers is equal to zero – $\Delta p_{Pi} = 0$) and increase $M_{Pm|\Delta ppi,bp,\nu n}$ of torque of mechanical losses, the increase being an effect of loading the assembly structure elements with torque M_{Pi} indicated in the pump working chambers (torque M_{Pi} appearing when the indicated increase Δp_{Pi} of pressure in the pump working chambers is greater than zero – $\Delta p_{Pi} > 0$):

$$M_{Pm|\Delta p_{Pi},b_P,\nu_n} = M_{Pm|\Delta p_{Pi}=0,b_P,\nu_n} + \Delta M_{Pm|\Delta p_{Pi},b_P,\nu_n} \qquad (2)$$

Torque M_{Pi} indicated in the pump working chambers is proportional to the increase Δp_{Pi} of pressure in the chambers and to the active volume of the chambers created during one pump shaft revolution, which is equal to the theoretical capacity q_{Pt} per one shaft revolution in a pump with constant capacity per one shaft revolution or to the geometrical capacity $q_{Pgv} = b_P\,q_{Pt}$ per one shaft revolution in a pump with variable capacity per one shaft revolution.

Therefore, the „working chambers – shaft" assembly structure elements are loaded:

– in a pump with theoretical (constant) capacity q_{Pt} per one shaft revolution – with indicated torque:

$$M_{Pi} = \frac{q_{Pt}\Delta p_{Pi}}{2\Pi}$$

– in a pump with geometrical (variable) capacity q_{Pgv} per one shaft revolution – with indicated torque:

$$M_{Pi} = \frac{q_{Pgv}\Delta p_{Pi}}{2\Pi} = \frac{b_P q_{Pt}\Delta p_{Pi}}{2\Pi}$$

which, in effect, causes a differentiated intensity of the increase $M_{Pm|\Delta ppi,bp,\nu n}$ of the torque of mechanical losses, determined, with different values of coefficient $b_P = q_{Pgv}/q_{Pt}$, as a function of the increase Δp_{Pi} of pressure in the pump working chambers.

In the theoretical and mathematical models describing the torque $M_{Pm|\Delta ppi,bp,\nu n}$ of mechanical losses a hypothesis is assumed, that the **increase $M_{Pm|\Delta ppi,bp,\nu n}$ of the torque of mechanical losses in the pump is proportional to the torque M_{Pi} indicated in its working chambers** (Fig. 2 and 5).

The impact of inertia forces of the „working chambers – shaft" assembly elements, performing the rotational and reciprocating motion in the pump, on the torque M_{Pm} of mechanical losses can be presented, under the assumption that rotational speed n_P of the pump driving motor changes only in a small range, as a function of capacity q_{Pgv}

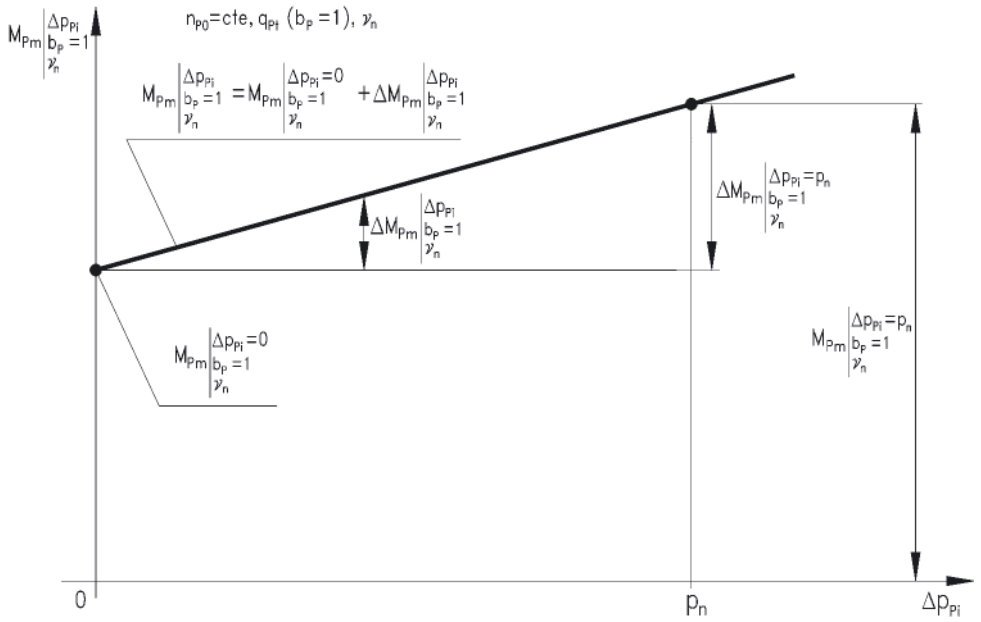

Fig. 2. Torque $M_{Pm|\Delta p_{Pi},b_P=1,\nu_n}$ of mechanical losses in the pump with constant capacity q_{Pt} per one shaft revolution (b_P =1), with working liquid reference viscosity ν_n, as a function of the indicated increase Δp_{Pi} of pressure in the pump working chambers – graphical interpretation of theoretical model (2)

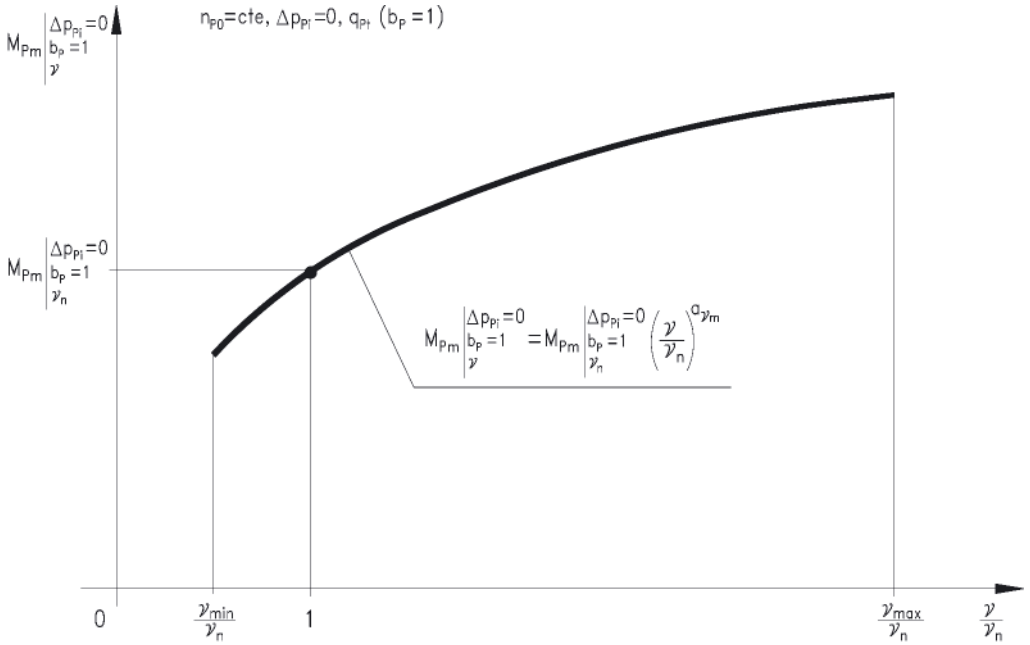

Fig. 3. Torque $M_{Pm|\Delta p_{Pi}=0,b_P=1,\nu}$ of mechanical losses in a piston (axial or radial) pump with crankcase filled with liquid and with constant capacity q_{Pt} per one shaft revolution (b_P = 1), at the indicated increase Δp_{Pi} = 0 of pressure in the pump working chambers, as a function of the ratio of viscosity ν to reference viscosity ν_n – ν/ν_n – graphical interpretation of theoretical model (3); torque $M_{Pm|\Delta p_{Pi}=0,b_P=1,\nu}$ of mechanical losses in the pump without the crankcase filled with liquid is practically independent of the liquid viscosity ν and is determined at the liquid reference viscosity ν_n

(b_P coefficient) per one shaft revolution of a variable capacity pump. **Inertia forces do not depend on the value of increase Δp_{Pi} of pressure in the working chambers, therefore their impact on the torque M_{Pm} of mechanical losses in the pump may be included in the evaluation of the torque $M_{Pm|\Delta ppi=0,bp,\nu n}$ of mechanical losses determined at the increase Δp_{Pi} = 0** (Fig. 5).

The impact of the friction forces between the „working chambers – shaft" assembly elements and the liquid in the casing (crankcase) of the piston pump on the torque M_{Pm} of mechanical losses in the pump can be presented, under the assumption that speed n_P changes in a small range, as a relation of M_{Pm} to the viscosity ν and to the capacity q_{Pgv} (b_P coefficient) per one shaft revolution (Fig. 3, 4, 6, 7).

It is assumed, that the **impact of liquid viscosity ν on the friction forces between the „working chambers – shaft" elements and the liquid in the piston pump casing (crankcase), and in effect on the torque M_{Pm} of mechanical losses in the pump, can be evaluated** at one level of the increase Δp_{Pi} of pressure indicated in the working chambers, e.g. **at the increase Δp_{Pi} = 0** (Fig. 3, 6). This assumption is connected with a simplification assuming that there is no significant impact of the increase Δp_{Pi} of pressure on the liquid viscosity ν and with assuming in the model describing the torque M_{Pm} of mechanical losses the liquid viscosity ν determined in the pump inlet conduit [at pressure p_{P1} equal to zero (at liquid absolute pressure equal to atmospheric pressure)].

The impact of inertia forces of structure elements performing the rotational or reciprocating motion in the pump and also the impact of liquid viscosity ν on the torque M_{Pm} of mechanical losses in the pump is then described in the model of the torque $M_{Pm|\Delta p_{Pi}=0,b_P,\nu}$ of those losses in an unloaded pump (at $\Delta p_{Pi} = 0$) supplied with working liquid of changing viscosity ν.

The proposed **theoretical models describing the torque $M_{Pm|\Delta p_{Pi}=0,b_P,\nu}$ of mechanical losses in an unloaded pump (at the indicated increase $\Delta p_{Pi} = 0$ of pressure in the working chambers) and at changing working liquid viscosity ν** [the impact of liquid viscosity ν occurs in the piston pumps with liquid filling the casing (crankcase)] have the form:

- in the pump with theoretical (constant) capacity q_{Pt} ($b_P = 1$) per one shaft revolution (Fig. 3):

$$M_{Pm|\Delta p_{Pi}=0,b_P=1,\nu} = M_{Pm|\Delta p_{Pi}=0,b_P=1,\nu_n}\left(\frac{\nu}{\nu_n}\right)^{a_{\nu m}} \tag{3}$$

- in the pump with geometrical (variable) capacity q_{Pgv} ($q_{Pgv} = b_P q_{Pt}$) per one shaft revolution (Fig. 6):

$$M_{Pm|\Delta p_{Pi}=0,\,b_P,\,\nu} = \tag{4}$$

$$=(M_{Pm|\Delta p_{Pi}=0,\,b_P=0,\,\nu_n} + \Delta M_{Pm|\Delta p_{Pi}=0,\,b_P,\,\nu_n})\left(\frac{\nu}{\nu_n}\right)^{a_{\nu m}}$$

where:

$$\Delta M_{Pm|\Delta p_{Pi}=0,\,b_P,\,\nu_n} =$$

$$= M_{Pm|\Delta p_{Pi}=0,\,b_P,\,\nu_n} - M_{Pm|\Delta p_{Pi}=0,\,b_P=0,\,\nu_n} = \tag{5}$$

$$= (M_{Pm|\Delta p_{Pi}=0,\,b_P=1,\,\nu_n} - M_{Pm|\Delta p_{Pi}=0,\,b_P=0,\,\nu_n})\,b_P$$

Exponent $a_{\nu m}$ in expressions (3) and (4) **describes the impact of the ratio ν/ν_n of working liquid ν to reference viscosity $\nu_n = 35 mm^2 s^{-1}$ on the value of torque of mechanical losses in a piston displacement machine with liquid filling the casing (crankcase)** (in the pump and in the hydraulic motor).

The increase $M_{Pm|\Delta p_{Pi},b_P,\nu}$ of the torque of mechanical losses in the pump, due to the load of the assembly elements with the indicated torque M_{Pi} resulting from the indicated increase Δp_{Pi} of pressure in the pump working chambers, is independent of the inertia forces of elements performing the rotational or reciprocating motion in the pump. It is also practically independent of the working liquid viscosity ν; therefore, it may be determined at one viscosity value, e.g. at the liquid reference viscosity ν_n (Fig. 4, 7).

The proposed **theoretical models describing the increase $M_{Pm|\Delta p_{Pi},b_P,\nu}$ of the torque of mechanical losses in the pump, resulting from the indicated increase Δp_{Pi} of pressure in the working chambers,** have the form:

- in the pump with theoretical (constant) capacity q_{Pt} ($b_P = 1$) per one shaft revolution (Fig. 4):

$$\Delta M_{Pm|\Delta p_{Pi},\,b_P=1,\,\nu} = \Delta M_{Pm|\Delta p_{Pi},\,b_P=1,\,\nu_n} =$$

$$= M_{Pm|\Delta p_{Pi},\,b_P=1,\,\nu_n} - M_{Pm|\Delta p_{Pi}=0,\,b_P=1,\,\nu_n} = \tag{6}$$

$$= (M_{Pm|\Delta p_{Pi}=p_n,\,b_P=1,\,\nu_n} - M_{Pm|\Delta p_{Pi}=0,\,b_P=1,\,\nu_n})\,\frac{\Delta p_{Pi}}{p_n}$$

- in the pump with geometrical (variable) capacity q_{Pgv} ($q_{Pgv} = b_P q_{Pt}$) per one shaft revolution (Fig. 7):

$$\Delta M_{Pm|\Delta p_{Pi},\,b_P,\,\nu} = \Delta M_{Pm|\Delta p_{Pi},\,b_P,\,\nu_n} =$$

$$= M_{Pm|\Delta p_{Pi},\,b_P,\,\nu_n} - M_{Pm|\Delta p_{Pi}=0,\,b_P,\,\nu_n} =$$

$$= (M_{Pm|\Delta p_{Pi}=p_n,\,b_P=1,\,\nu_n} + \tag{7}$$

$$- M_{Pm|\Delta p_{Pi}=0,\,b_P=1,\,\nu_n})\,b_P\frac{\Delta p_{Pi}}{p_n}$$

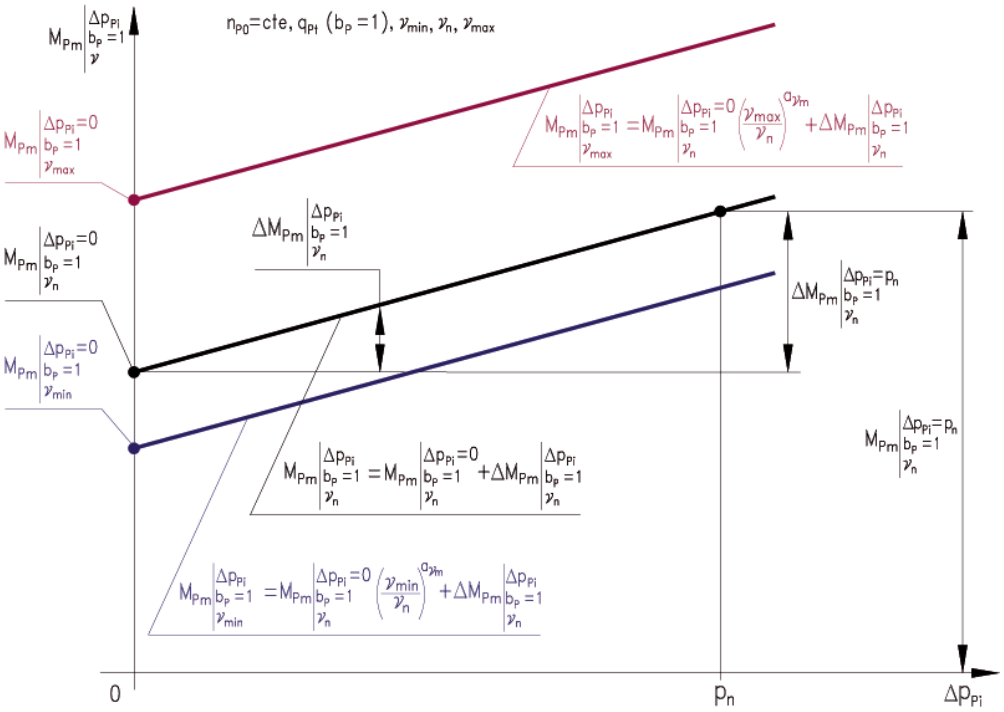

Fig. 4. Torque $M_{Pm|\Delta p_{Pi},b_P=1,\nu}$ of mechanical losses in a piston (axial or radial) pump with crankcase filled with liquid and with constant capacity q_{Pt} per one shaft revolution ($b_P = 1$), as a function of the indicated increase Δp_{Pi} of pressure in the pump working chambers – graphical interpretation of theoretical models (2) and (8); liquid viscosity ν_{min}, ν_n and ν_{max}. Torque $M_{Pm|\Delta p_{Pi},b_P=1,\nu}$ of mechanical losses in the pump without the crankcase filled with liquid is practically independent of the liquid viscosity ν and is determined at the liquid reference viscosity ν_n

In effect, the proposed **theoretical models describing the torque M_{Pm} of mechanical losses in the pump** take the forms:

- in the pump with theoretical (constant) capacity q_{Pt} ($b_P = 1$) per one shaft revolution (Fig. 4):

$$M_{Pm|\Delta p_{Pi}, b_P=1, \nu} = M_{Pm|\Delta p_{Pi}=0, b_P=1, \nu_n} \left(\frac{\nu}{\nu_n}\right)^{a_{vm}} + \tag{8}$$

$$+ \Delta M_{Pm|\Delta p_{Pi}, b_P=1, \nu_n} = M_{Pm|\Delta p_{Pi}=0, b_P=1, \nu_n} \left(\frac{\nu}{\nu_n}\right)^{a_{vm}} +$$

$$+ (M_{Pm|\Delta p_{Pi}=p_n, b_P=1, \nu_n} - M_{Pm|\Delta p_{Pi}=0, b_P=1, \nu_n}) \frac{\Delta p_{Pi}}{p_n}$$

- in the pump with geometrical (variable) capacity q_{Pgv} ($q_{Pgv} = b_P q_{Pt}$) per one shaft revolution (Fig.7):

$$M_{Pm|\Delta p_{Pi}, b_P, \nu} = \tag{9}$$

$$= (M_{Pm|\Delta p_{Pi}=0, b_P=0, \nu_n} + \Delta M_{Pm|\Delta p_{Pi}=0, b_P, \nu_n}) \left(\frac{\nu}{\nu_n}\right)^{a_{vm}} +$$

$$+ \Delta M_{Pm|\Delta p_{Pi}, b_P, \nu_n}$$

where:

$$\Delta M_{Pm|\Delta p_{Pi}=0, b_P, \nu_n} =$$

$$= (M_{Pm|\Delta p_{Pi}=0, b_P=1, \nu_n} - M_{Pm|\Delta p_{Pi}=0, b_P=0, \nu_n}) b_P \tag{10}$$

$$\Delta M_{Pm|\Delta p_{Pi}, b_P, \nu_n} =$$

$$(M_{Pm|\Delta p_{Pi}=p_n, b_P=1, \nu_n} - M_{Pm|\Delta p_{Pi}=0, b_P=1, \nu_n}) b_P \frac{\Delta p_{Pi}}{p_n} \tag{11}$$

MATHEMATICAL MODELS OF THE TORQUE OF MECHANICAL LOSSES

In the mathematical models describing the torque M_{Pm} of mechanical losses in the pump, coefficients k_i of losses are used relating (comparing) the components describing the torque M_{Pm} of losses in theoretical models to the pump theoretical torque M_{Pt}. The pump theoretical torque M_{Pt} is also a reference value used in the description of the torque M_{Pi} indicated in the pump working chambers:

– theoretical torque:

$$M_{Pt} = \frac{q_{Pt} p_n}{2\Pi}$$

of the pump, with theoretical (constant) capacity q_{Pt} per one shaft revolution ($b_P = 1$), is determined with the increase Δp_P of pressure in the pump equal to the system nominal pressure $p_n - \Delta p_P = p_n$, and with the assumption that there are no pressure and mechanical losses in the pump,

– indicated torque:

$$M_{Pi} = \frac{q_{Pt} \Delta p_{Pi}}{2\Pi} = \frac{q_{Pt} p_n}{2\Pi} \frac{\Delta p_{Pi}}{p_n} = M_{Pt} \frac{\Delta p_{Pi}}{p_n}$$

in working chambers of the pump with theoretical (constant) capacity q_{Pt} per one shaft revolution ($b_P = 1$) is determined with the indicated increase Δp_{Pi} of pressure in the working chambers,

– indicated torque:

$$M_{Pi} = \frac{q_{Pgv} \Delta p_{Pi}}{2\Pi} = \frac{b_P q_{Pt} \Delta p_{Pi}}{2\Pi} =$$

$$= \frac{q_{Pt} p_n}{2\Pi} b_P \frac{\Delta p_{Pi}}{p_n} = M_{Pt} b_P \frac{\Delta p_{Pi}}{p_n}$$

in working chambers of the pump with geometrical (variable) capacity $q_{Pgv} = b_P q_{Pt}$ per one shaft revolution is determined with the indicated increase Δp_{Pi} of pressure in the working chambers.

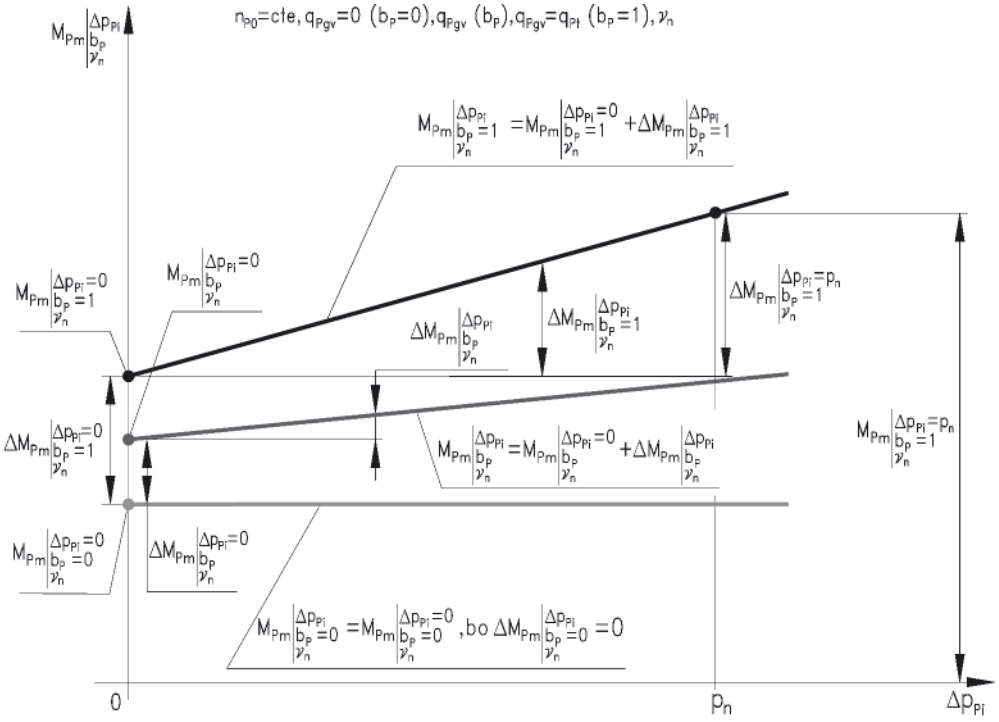

Fig. 5. *Torque $M_{Pm|\Delta p_{Pi}, b_P, \nu}$ of mechanical losses in the pump with variable capacity $q_{Pgv} = b_P q_{Pt}$ per one shaft revolution, with working liquid reference viscosity ν_n, as a function of the indicated increase Δp_{Pi} of pressure in the pump working chambers – graphical interpretation of theoretical models (2) and (7); capacity q_{Pgv} per one shaft revolution (coefficient b_P of pump capacity): $q_{Pgv} = 0$ ($b_P = 0$), q_{Pgv} (b_P), $q_{Pgv} = q_{Pt}$ ($b_P = 1$)*

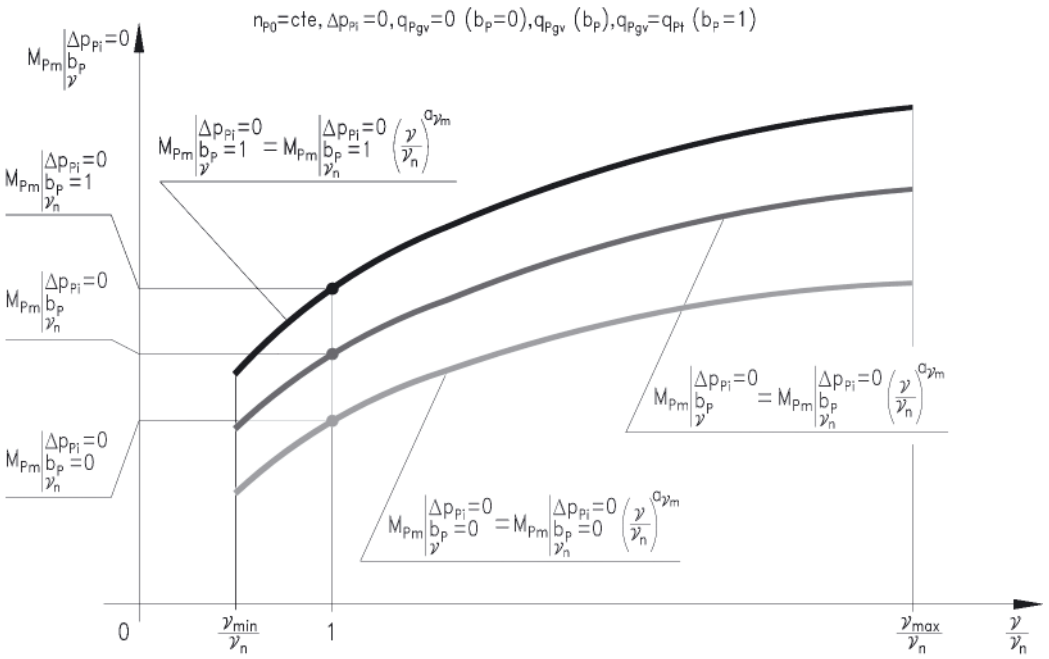

Fig. 6. *Torque $M_{Pm|\Delta ppi=0,bp,\nu}$ of mechanical losses in a piston (axial or radial) pump with crankcase filled with liquid and with variable capacity q_{Pgv}= $b_P q_{Pt}$ per one shaft revolution, at the indicated increase Δp_{Pi} = 0 of pressure in the pump working chambers, as a function of the ratio of viscosity ν to reference viscosity ν_n – ν/ν_n – graphical interpretation of theoretical model (4); capacity q_{Pgv} per one shaft revolution (coefficient b_P of pump capacity): q_{Pgv}= 0 (b_P = 0), q_{Pgv} (b_P), q_{Pgv}= q_{Pt} (b_P = 1). Torque $M_{Pm|\Delta ppi=0,bp,\nu}$ of mechanical losses in the pump without crankcase filled with liquid is practically independent of the liquid viscosity ν and is determined at the liquid reference viscosity ν_n*

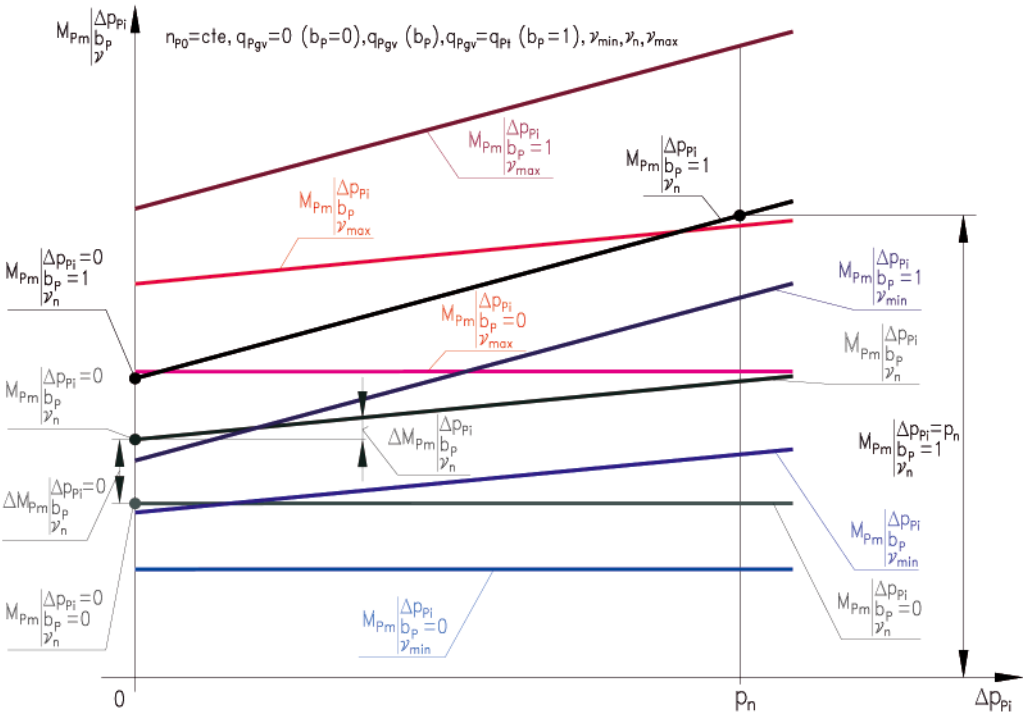

Fig. 7. *Torque $M_{Pm|\Delta ppi,bp,\nu}$ of mechanical losses in a piston (axial or radial) pump with crankcase filled with liquid and with variable capacity q_{Pgv}= $b_P q_{Pt}$ per one shaft revolution, as a function of the indicated increase Δp_{Pi} of pressure in the pump working chambers – graphical interpretation of theoretical model (9); capacity q_{Pgv} per one shaft revolution (coefficient b_P of pump capacity): q_{Pgv}= 0 (b_P = 0), q_{Pgv} (b_P), q_{Pgv}= q_{Pt} (b_P = 1); liquid viscosity ν_{min} , ν_n and ν_{max}. Torque $M_{Pm|\Delta ppi,bp,\nu}$ of mechanical losses in the pump without the crankcase filled with liquid is practically independent of the liquid viscosity ν and is determined at the liquid reference viscosity ν_n*

The theoretical and mathematical models describe the torque M_{Pm} of mechanical losses in the pump with theoretical (constant) capacity q_{Pt} per one shaft revolution or with geometrical (variable) capacity q_{Pgv} = b_P q_{Pt} per one shaft revolution:

– q_{Pt} = $q_{P|\Delta ppi\,=\,0,ppli\,=\,0,bp\,=\,1,vn}$ is a theoretical capacity per one shaft revolution of the pump with constant capacity per one revolution (b_P = 1) determined at Δp_{Pi} = 0, p_{P1i} = 0 and ν_n, which is equal to the working volume of the working chambers created during one shaft revolution,

– q_{Pgv} = b_P q_{Pt} is a geometrical capacity per one shaft revolution of the pump with variable capacity per one revolution at Δp_{Pi} = 0, p_{P1i} = 0 and ν_n, which is equal to the working volume of the working chambers created during one shaft

revolution. Capacity q_{Pgv} per one shaft revolution changes in the $0 \le q_{Pgv} \le q_{Pt}$ range and coefficient $b_P = q_{Pgv}/q_{Pt}$ of the pump capacity changes in the $0 \le b_P \le 1$ range.

The proposed **mathematical models describing the torque M_{Pm} of mechanical losses in the pump, related to theoretical models of the torque of mechanical losses**, take the form:

- in a pump with theoretical (constant) capacity q_{Pt} per one shaft revolution ($b_P = 1$) [referring to theoretical model (8)]:

$$M_{Pm|\Delta p_{Pi},\nu} = k_{4.1}\, M_{Pt}\left(\frac{\nu}{\nu_n}\right)^{a_{vm}} + k_{4.2} M_{Pt}\frac{\Delta p_{Pi}}{p_n} =$$

$$= \left[k_{4.1}\left(\frac{\nu}{\nu_n}\right)^{a_{vm}} + k_{4.2}\frac{\Delta p_{Pi}}{p_n}\right] M_{Pt} = \qquad (12)$$

$$= \left[k_{4.1}\left(\frac{\nu}{\nu_n}\right)^{a_{vm}} + k_{4.2}\frac{\Delta p_{Pi}}{p_n}\right]\frac{q_{Pt}p_n}{2\Pi}$$

where:

$$k_{4.1} = \frac{M_{Pm|\Delta p_{Pi}=0,\, b_P=1,\nu_n}}{M_{Pt}} = \frac{M_{Pm|\Delta p_{Pi}=0,\, b_P=1,\nu_n}}{\frac{q_{Pt}p_n}{2\Pi}} \qquad (13$$

$$k_{4.2} = \frac{\Delta M_{Pm|\Delta p_{Pi},\, b_P=1,\, \nu_n}}{M_{Pi}} = \frac{\Delta M_{Pm|\Delta p_{Pi},\, b_P=1,\, \nu_n}}{\frac{q_{Pt}\Delta p_{Pi}}{2\Pi}} =$$

$$= \frac{M_{Pm|\Delta p_{Pi},\, b_P=1,\nu_n} - M_{Pm|\Delta p_{Pi}=0,\, b_P=1,\, \nu_n}}{\frac{q_{Pt}\Delta p_{Pi}}{2\Pi}} = \qquad (14)$$

$$= \frac{M_{Pm|\Delta p_{Pi}=p_n,\, b_P=1,\, \nu_n} - M_{Pm|\Delta p_{Pi}=0,\, b_P=1,\, \nu_n}}{\frac{q_{Pt}p_n}{2\Pi}} =$$

$$= \frac{M_{Pm|\Delta p_{Pi}=p_n,\, b_P=1,\, \nu_n} - M_{Pm|\Delta p_{Pi}=0,\, b_P=1,\, \nu_n}}{M_{Pt}} =$$

- in a pump with geometrical (variable) capacity q_{Pgv} ($q_{Pgv} = b_P q_{Pt}$) per one shaft revolution [referring to theoretical models (9), (10) and (11)]:

$$M_{Pm|\Delta p_{Pi},\, b_P,\, \nu} = \qquad (15)$$

$$= (k_{4.1.1} + k_{4.1.2}\, b_P)\, M_{Pt}\left(\frac{\nu}{\nu_n}\right)^{a_{vm}} + k_{4.2} M_{Pt} b_P \frac{\Delta p_{Pi}}{p_n} =$$

$$= \left[(k_{4.1.1} + k_{4.1.2}\, b_P)\left(\frac{\nu}{\nu_n}\right)^{a_{vm}} + k_{4.2}\, b_P \frac{\Delta p_{Pi}}{p_n}\right] M_{Pt} =$$

$$= \left[(k_{4.1.1} + k_{4.1.2}\, b_P)\left(\frac{\nu}{\nu_n}\right)^{a_{vm}} + k_{4.2}\, b_P \frac{\Delta p_{Pi}}{p_n}\right]\frac{q_{Pt}p_n}{2\Pi}$$

where:

$$k_{4.1.1} = \frac{M_{Pm|\Delta p_{Pi}=0,\, b_P=0,\, \nu_n}}{M_{Pt}} = \frac{M_{Pm|\Delta p_{Pi}=0,\, b_P=0,\nu_n}}{\frac{q_{Pt}p_n}{2\Pi}} \qquad (16)$$

$$k_{4.1.2} = \frac{M_{Pm|\Delta p_{Pi}=0,\, b_P=1,\, \nu_n} - M_{Pm|\Delta p_{Pi}=0,\, b_P=0,\nu_n}}{M_{Pt}} =$$

$$= \frac{M_{Pm|\Delta p_{Pi}=0,\, b_P=1,\, \nu_n} - M_{Pm|\Delta p_{Pi}=0,\, b_P=0,\nu_n}}{\frac{q_{Pt}p_n}{2\Pi}} \qquad (17)$$

$$k_{4.2} = \frac{\Delta M_{Pm|\Delta p_{Pi},\, b_P,\, \nu_n}}{M_{Pi}} =$$

$$= \frac{\Delta M_{Pm|\Delta p_{Pi},\, b_P,\, \nu_n}}{\frac{b_P\, q_{Pt}\Delta p_{Pi}}{2\Pi}} = \frac{\Delta M_{Pm|\Delta p_{Pi},\, b_P=1,\, \nu_n}}{\frac{q_{Pt}\Delta p_{Pi}}{2\Pi}} = \qquad (18)$$

$$= \frac{M_{Pm|\Delta p_{Pi}=p_n,\, b_P=1,\, \nu_n} - M_{Pm|\Delta p_{Pi}=0,\, b_P=1,\, \nu_n}}{\frac{q_{Pt}p_n}{2\Pi}} =$$

$$= \frac{M_{Pm|\Delta p_{Pi}=p_n,\, b_P=1,\, \nu_n} - M_{Pm|\Delta p_{Pi}=0,\, b_P=1,\, \nu_n}}{M_{Pt}}$$

Commentary:

- The sum ($k_{4.1.1} + k_{4.1.2}$) of coefficients used in mathematical model (15) describing the torque M_{Pm} of mechanical losses in the pump with geometrical (variable) capacity q_{Pgv} ($q_{Pgv} = b_P q_{Pt}$) per one shaft revolution is equal to coefficient $k_{4.1}$ used in the mathematical model (12) describing the torque M_{Pm} of mechanical losses in that pump working as a pump with theoretical (constant) capacity per one shaft revolution:
  $k_{4.1.1} + k_{4.1.2} = k_{4.1}$.
- Coefficient $k_{4.2}$ used in mathematical model (15) describing the torque M_{Pm} of mechanical losses in the pump with geometrical (variable) capacity q_{Pgv} ($q_{Pgv} = b_P q_{Pt}$) per one shaft revolution is equal to coefficient $k_{4.2}$ used in the mathematical model (12) describing the torque M_{Pm} of mechanical losses in that pump working as a pump with theoretical (constant) capacity q_{Pt} per one shaft revolution.

CONCLUSIONS

1. The theoretical and mathematical models have been developed of the torque M_{Pm} of mechanical losses in the „working chambers – shaft" assembly of a displacement pump with constant q_{Pt} (V_{Pt}) and variable $q_{Pgv} = b_P q_{Pt}$ (V_{Pgv}) capacity per one shaft revolution.
   The models describe the relation of the torque M_{Pm} of mechanical losses in the assembly to the torque:
   $$M_{Pi} = \frac{q_{Pgv}\Delta p_{Pi}}{2\Pi} = \frac{b_P\, q_{Pt}\Delta p_{Pi}}{2\Pi}$$
   indicated in the pump working chambers and also to the working liquid viscosity ν at the pump inlet, changing in the $\nu_{min} \le \nu \le \nu_{max}$ range. It is assumed that a small change of the pump driving motor rotational speed n_P (due to the changing pump shaft torque M_P loading the motor) practically does not influence the torque M_{Pm} of losses.
   The indicated torque M_{Pi} in the pump working chambers and the working liquid viscosity ν are parameters independent of the torque M_{Pm} of mechanical losses in the „working chambers – shaft" assembly.

The models describe also the relation of torque M_{Pm} to the capacity q_{Pgv} per one shaft revolution (coefficient $b_P = q_{Pgv}/q_{Pt}$ of the pump capacity) in a pump with variable capacity per onerevolution.
The assumedchange of q_{Pgv} (b_P) is in the $0 \le q_{pgv} \le q_{Mt}$ ($0 \le b_p \le 1$) range.

2. The mathematical models of the torque M_{Pm} of mechanical losses are based on defined coefficients k_i of energy losses relating the torque of mechanical losses to a reference value, i.e. to:
   – theoretical torque M_{Pt} of a pump with theoretical (constant) capacity q_{Pt} per one shaft revolution, determined at the increase Δp_{Pi} of pressure in the pump equal to the nominal pressure p_n of system operation ($\Delta p_{Pi} = p_n$), with:
   - known values of the pump capacity coefficient $b_P = q_{Pgv}/q_{Pt}$,
   - assumption of practically constant pump speed n_P equal to the speed n_{P0} of the unloaded pump shaft ($n_P = n_{P0}$).
3. The mathematical models of the torque M_{Pm} of mechanical losses in the „working chambers – shaft" assembly should correspond with the models of volumetric losses in the working chambers and with the models of pressure losses in the pump channels.

BIBLIOGRAPHY

1. Paszota Z.: *Graphical presentation of the power of energy losses and power developed in the elements of hydrostatic drive and control system. Part I – Rotational hydraulic motor speed series throttling control systems*. Chapter in the monograph: *„Research, design, production and operation of hydraulic systems"* (in Polish), Adam Klich, Edward Palczak and Andrzej Meder editors. „Cylinder" Library. Komag Mining Mechanisation Centre, Gliwice 2008
2. Paszota Z.: *Graphical presentation of the power of energy losses and power developed in the elements of hydrostatic drive and control system. Part II – Rotational hydraulic motor speed parallel throttling control and volumetric control systems*. Chapter in the monograph: *„Research, design, production and operation of hydraulic systems"* (in Polish), Adam Klich, Edward Palczak and Andrzej Meder editors. „Cylinder" Library. Komag Mining Mechanisation Centre, Gliwice 2008
3. Paszota Z.: *Direction of increase of power stream in the hydrostatic drive and control system. Graphical presentation of the power of energy losses and power developed in the elements of hydrostatic drive and control system. Part I – Rotational hydraulic motor speed series throttling control systems* (in Polish), Napędy i sterowanie, scientific monthly, No 10 (114), October 2008
4. Paszota Z.: *Direction of increase of power stream in the hydrostatic drive and control system. Graphical presentation of the power of energy losses and power developed in the elements of hydrostatic drive and control system. Part II – Rotational hydraulic motor speed parallel throttling control and volumetric control systems* (in Polish), Napędy i sterowanie, scientific monthly, No 11 (115), November 2008
5. Paszota Z.: *Graphical presentation of the power of energy losses and power developed in the elements of hydrostatic drive and control system. Part I – Rotational hydraulic motor speed series throttling control systems*. Polish Maritime Research 3 (57) 2008, Vol. 15
6. Paszota Z.: *Graphical presentation of the power of energy losses and power developed in the elements of hydrostatic drive and control system. Part II – Rotational hydraulic motor speed parallel throttling control and volumetric control systems.* Polish Maritime Research 4 (58) 2008,Vol. 15
7. Paszota Z.: *The operating field of a hydrostatic drive system*. Chapter in the monograph: *„Research, design, production and operation of hydraulic systems"* (in Polish), Adam Klich, Antoni Kozieł and Edward Palczak editors. „Cylinder" Library. Komag Mining Mechanisation Centre, Gliwice 2009
8. Paszota Z.: *Parameters of the energy efficiency investigations of pumps and hydraulic motors. The operating field of a hydrostatic drive system* (in Polish), Napędy i sterowanie, scientific monthly, No 11 (127), November 2009
9. Paszota Z.: *The operating field of a hydrostatic drive system parameters of the energy efficiency investigations of pumps and hydraulic motors*. Polish Maritime Research 4 (62) 2009, Vol. 16
10. Paszota Z.: *Energy losses in a rotational hydraulic motor – definitions and relations for evaluation of the efficiency of motor and hydrostatic drive*. Chapter in the monograph: *„Research, design, production and operation of hydraulic systems"* (in Polish), Adam Klich, Antoni Kozieł and Edward Palczak editors. „Cylinder" Library. Komag Mining Mechanisation Centre, Gliwice 2010
11. Paszota Z.: *Theoretical and mathematical models of the torque of mechanical losses in a hydraulic rotational motor for hydrostatic drive*. Chapter in the monograph: *„Research, design, production and operation of hydraulic systems"* (in Polish), Adam Klich, Antoni Kozieł and Edward Palczak editors. „Cylinder" Library. Komag Mining Mechanisation Centre, Gliwice 2010
12. Paszota Z.: *Energy losses in a rotational hydraulic motor – definitions and relations for evaluation of the efficiency of motor and hydrostatic drive* (in Polish), Napędy i sterowanie, scientific monthly, No 10 (138), October 2010
13. Paszota Z.: *Theoretical and mathematical models of the torque of mechanical losses in a hydraulic rotational motor for hydrostatic drive* (in Polish), Napędy i sterowanie, scientific monthly, No 11(139), November 2010
14. Paszota Z.: *Energy losses in the hydraulic rotational motor – definitions and relations for evaluation of the efficiency of motor and hydrostatic drive*. Polish Maritime Research 2 (65) 2010,Vol. 17
15. Paszota Z.: *Theoretical and mathematical models of the torque of mechanical losses in a hydraulic rotational motor for hydrostatic drive*. Polish Maritime Research 3 (66) 2010,Vol. 17
16. Paszota Z.: *Hydrostatic drives as safe and energy saving machines* (in Polish), Napędy i sterowanie, scientific monthly, No 1(141), January 2011
17. Paszota Z.: *Hydrostatic drives as safe and energy saving machines* (in Polish), Proceedings of the „Innovative machines and Technologies - Safety" conference, Szczyrk 03 – 04 February 2011
18. Paszota Z.: *Hydrostatic drives as safe and energy saving machines. The drive investigation method compatible with the diagram of power increase opposite to the direction of power flow*. Polish Maritime Research 1(68) 2011,Vol. 18

CONTACT WITH THE AUTHOR

Prof. Zygmunt Paszota
Faculty of Ocean Engineering
and Ship Technology
Gdansk University of Technology
Narutowicza 11/12
80-233 Gdansk, POLAND
e-mail: zpaszota@pg.gda.pl

POLISH MARITIME RESEARCH 4(71) 2011 Vol 18; pp. 36-42
10.2478/v10012-011-0024-9

The semi-Markov model of energy state changes of the main marine internal combustion engine and method for evaluating its operation during ship voyage

Jerzy Girtler, Prof.
Gdansk University of Technology

ABSTRACT

The article presents a method for evaluating the operation of internal combustion engines used as the main engines in the propulsion systems of sea-going ships in various operating conditions. This method enables calculating the engine operation value based on the theory of semi-Markov processes and mathematical statistics. What is noteworthy, the operation of the examined internal combustion engines is compared to a physical quantity which is expressed in the form of a number with the measure unit called joule-second. a model having the form of a semi-Markov process is proposed to describe the energy state changes taking place in the main engines during their operation. Also proposed is the use of the point and interval estimation at a given confidence level β for determining the value of the energy converted in the engine during its operation for the known and unknown standard energy deviation treated as the random variable. The semi-Markov model of changes of the energy converted in the engine during its operation is presented in a general form. The above model was used for determining the ship's main engine operation, which is in the examined case a function of the energy converted in particular energy states, the expected value of the time of duration of these states and the probability of their existence. These probabilities compose the limiting distribution of the semi-Markov process, the values of which are the specified main engine energy states.

Key words: operation; energy; semi-Markov process; piston internal combustion engine

INTRODUCTION

References [2, 4, 6, 12, 13] present a proposal to investigate the operation of internal combustion engines as the effect of the existence of their energy states which makes it possible to convert the delivered energy E and transmit it in time t to the energy receivers, such as propeller screws, pumps, compressors, etc. For the operation understood in the above way a method was proposed to valuate the operation of diesel engines used in shipbuilding in a general formulation taking into account the engine wear [2, 6]. Ref. [2] discusses the operation of the abovementioned internal combustion engines used as the main engines in the propulsion systems of sea-going ships taking into account the fact that correct operation of these engines requires securing delivery of sufficient amount of energy to its receivers, which are the propeller screws. The method presented in that article makes use of the deterministic model of engine operation which takes into account ship sailing conditions.

This article presents a stochastic model in the form of a semi-Markov process to model the changes of energy states of an arbitrary main engine, and the method for valuating the operation of those engines using this model. Like in Ref. [2], it was assumed here that the operation (D) can be compared to the physical quantity being the product of energy (E) and time (t) of its conversion, i.e. $D = E \cdot t$.

The above interpretation of the operation of piston internal combustion engines results from the application of the analogy method (the intermediate method between induction and deduction), which makes it possible to transmit the observations from one object of investigation (empirical system) to another. Like in Ref. [2], the inspirations for developing the here presented method were proposals by P. L. Maupertius and W. R. Hamilton to consider the operation of a mechanical system as a physical quantity which reflects changes of mechanical energy in time. In classical physics an interpretation of the operation can be found which considers it the effect of the change of energy in time, expressed in the form of the product of energy and time, with the joule-second (joule×second) as the resultant measure unit.

In this formulation distinction is made between the operation [18, 19]:

- of the mechanical system (system of material points) being the result of kinetic and potential energy changes, which is referred to as the Hamilton operation (D_H) and
- resulting from the change of only the kinetic energy of the mechanical system (body), called the Maupertius operation (D_M).

A similar interpretation of the operation was adopted in quantum mechanics with respect to the source of

electromagnetic radiation [8]. There, the equivalent of the operation having a similar sense is the Planck's constant (h), which is also a physical quantity expressed by a number and the measure unit [joule×second].

Achievements in classical physics and quantum mechanics in this area were the motivations for the author to introduce the operation understood in the above way also to the technique, giving it a specific interpretation for particular power generation devices, including diesel engines. During the operation of these engines the energy conversion also takes place. The energy is first converted into heat (Q) and then into work (L). In the former case the chemical energy collected in the fuel-air mixture is converted into the internal energy of the exhaust gas, which bears the name of the thermal energy. This process takes place during fuel combustion. In the latter case, in turn, the internal energy in the exhaust gas is converted into the mechanical (kinetic and potential) energy of the moving piston. Obviously, the above energy conversion processes are accompanied with losses.

Such an approach to engine operation seems to be more favourable, as comparing energy conversion related advantages of particular engines based solely on the analysis and evaluation of their power or work does not give comprehensive information of the engine capability to perform the task. This information can only be obtained from a combined analysis of the work and the time of its realisation, represented by the quantity $D = L \cdot t$ or $D = N \cdot t^2$, as it may happen that the engine is capable to convert the required energy to get the work L, but the time t which it needs for doing this is longer than the required time (for instance, excessively long time of duration of transient processes, so-called unsteady states, in the engine before it is fully loaded). Or, it may happen that the work $L = N \cdot t$ needed for performing the assumed task will not be done by the engine in a given time t (for instance, due to excessively small power output N of the engine resulting from its wear). Hence the conclusion that evaluating the correctness of engine operation based only on its power or work, without simultaneously taking into account the time of engine operation, is insufficient for full assessment of its energy conversion related qualities. Obviously, the engine power is an important parameter, as it contains the information how quickly the work can be done. But the operation in the above presented formulation is also important as it contains the information how long the engine can work. Since obtaining the required work (L) via conversion of the energy (E) is accompanied by energy losses in the form of heat (Q), therefore it is more reasonable to analyse energy changes, and not only engine work during engine operation.

The advantage of the interpretation of the diesel engine operation proposed by the author is that the earlier descriptive evaluation of engine operation, for instance: the operation is good, bad, etc., can be replaced by the assessment based on comparing the engine operation with the reference standard operation using numbers and the measure unit, which is the joule-second.

The sense of the above interpretation of the operation of an engine, and in general any power generation device, can also be justified by the observation that changes of motion of a body depend on the force (F) acting on this body and the time (t) during which this action takes place. Body's capability to move is expressed by the product of force and time ($F \cdot t$) bearing the name of the impulse of force [9]. The measure unit of the impulse of force is the newton-second. By analogy, we can conclude that the operation (D) of the diesel engine depends on work (L) done by this engine and time (t) of its operation, i.e. $D = L \cdot t$.

CONDITIONS OF MAIN ENGINE OPERATION AND THEIR STOCHASTIC NATURE

The conditions of main engine operation depend on the conditions in which it works, which are determined by external conditions of sailing of the sea-going ship and tasks undertaken by ship users (the crew). These conditions and tasks are the reason why different amounts of energy are converted in different times in the working spaces of these engines. In each case, however, the operation of the main engine is defined by the area of its performance [2, 11, 16, 17]. These performance areas are determined by engine speed characteristics, including external and control characteristics. If these characteristics are projected against the propeller characteristics, which also belong to the speed characteristics, then the ranges of operation of these engines are defined [4, 5].

It was shown in Ref [2] that the points of cooperation for a given propeller characteristic are created depending on the injection pump setting. Therefore it may happen that along a given propeller characteristic the main engine can be loaded with power according to the following external power characteristics [11, 16, 17]:

- external characteristic of partial power N_{ec} (h_c = idem, c = 1, 2, …, $N_{ec} < N_{etr}$),
- external characteristic of continuous operating power N_{etr} (h_{tr} = idem),
- external characteristic of nominal power N_{en} (h_n = idem),
- external characteristic of maximal power N_{emax} (h_{max} = = idem).

A sample realisation of power changes of the main engine during its operation is shown in Fig. 1 [2]. The effective power N_e generated by the main engine characterises the engine operation in the aspect of the rate of energy conversion into work, taking into account various types of losses, in particular thermal loss. However, engine operation consisting in energy conversion into work is not possible if this energy is not earlier converted into heat in the engine working spaces [2, 15]. Therefore when analysing the main engine operation we should take into account the energy delivered to the engine in the fuel-air mixture, which is first converted into heat (Q) and then into work (L), rather then the pure engine power output.

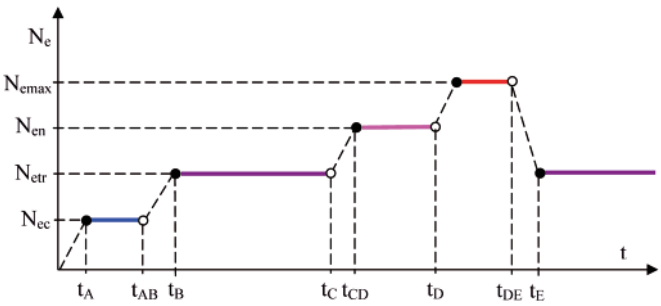

Fig. 1. Sample realisation of the process of main engine load changes during engine operation: N_e – effective power, t – operating time [2]

The analysis should focus on the process of changes of the energy delivered to the engine. Particular states of this process should be the energy states which release the energy E_j(j = 1, …, 4), and secure the generation of particular powers N_{ej} (j = 1, …, 4), which are essential for correct engine operation and secure realisation of the operating task, (Fig. 1):

$$N_1 = N_{ec},\ N_2 = N_{etr},\ N_3 = N_{en},\ N_4 = N_{emax} \quad (1)$$

The analysis can be performed using a deterministic or stochastic model for describing real main engine energy change processes.

The deterministic model of energy state changes taking place in the main engine during its operation was presented and discussed in Ref. [2]. This article presents the stochastic model of these changes having the form of a semi-Markov process.

MODEL OF ENGINE OPERATION IN THE FORM OF A SEMI-MARKOV PROCESS

Developing the model of internal combustion engine operation in the form of the semi-Markov process requires the application of the theory of semi-Markov processes. The publications on the semi-Markov processes give definitions of this process which differ by the range of generality and precision [3, 7]. For the purpose of modelling changes of the internal combustion engine energy states the semi-Markov process (family of random variables) $\{X(t): t \geq 0\}$ at $T = [0, +\infty)$, can be defined using a so-called homogeneous markovian process of recovery [7].

The semi-Markov model of an arbitrary real process can be only constructed when the states of this process can be defined in such a way that the time of duration of the state existing in time τ_n and the state which is to be obtained in time τ_{n+1} do not depend stochastically on the states which earlier took place, nor the time intervals of those states.

Constructing the semi-Markov model $\{X(t): t \geq 0\}$ of the real process of energy state changes taking place in the diesel engine operation phase is possible, because [3]:

1) the Markov condition is fulfilled which says that the future evolution of an arbitrary process of the energy state changes taking place during engine operation depends solely on the engine state at a given time instant and not on the past engine operation, consequently the future state of this process and the time of its duration depend on the present and not on the past,
2) random variables T_i, which represent the time of duration of the state e_i irrespective of the fact which state will be the next, and T_{ij}, which represent the time of duration of the state „e_i" on condition that the next state of this process is the state „e_j", have distributions different than the exponential distribution.

When analysing changes of the main engine energy states e_i resulting from converting particular energies $E_i (i = 1, \ldots, 4)$ in the interpretation expressed by formula (1) for engine operation which enables the ship to perform the transporting task in a relatively long time, theoretically tending to infinity ($t \to \infty$), we can omit time intervals connected with changes of energy states e_i taking place when the energy converted in the engine working spaces increases from E_i to E_{i+1} to generate engine power output corresponding to those energies (1) in given time intervals (Fig. 1). Consecutive power outputs N_{ej} ($j = 1, \ldots, 4$) can be considered the effects of the engine energy states $e_j \in E_e$($j = 1, \ldots, 4$) of the stochastic process $\{X(t): t \geq 0\}$, each of which takes a constant values in the time interval $[\tau_m, \tau_{m+1})$.

That means that the semi-Markov process $\{X(t): t \geq 0\}$ is the process having the realisations constant in intervals and continuous on the right. Therefore the process is discrete in states and continuous in time. a sample fragment of the realisation x(t) of this process is shown in Fig. 2. This realisation reflects the situation when, following the elapsed time t, successive state changes of this process take place in successive time intervals $[\tau_m, \tau_{m+1})$.

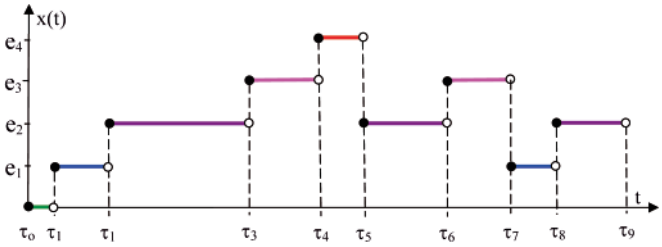

Fig. 2. *Fragment of a sample realisation x(t) of the semi-Markov process {X(t): t ≥ 0}*

In case of marine main engines, in an arbitrary time of their operation the process $\{X(t): t \geq 0\}$ can take one of the energy states existing during engine operation and belonging to the set:

$$E_e = \{e_1, e_2, e_3, e_4\} \tag{2}$$

with elements having the following interpretation (Fig. 1):

- e_1 – engine energy state resulting from generation of energy E_1 corresponding to engine load with partial power $N_1 = N_{ec}$,
- e_2 – engine energy state resulting from generation of energy E_2 corresponding to engine load with (continuous) operating power $N_2 = N_{etr}$,
- e_3 – engine energy state resulting from generation of energy E_3 corresponding to engine load with nominal power $N_3 = N_{en}$,
- e_4 – engine energy state resulting from generation of energy E_4 corresponding to engine load withy maximal power $N_4 = N_{emax}$.

Making distinction between those energy states differing by engine load is important because these states originate from the principles of diesel engine operation and are connected with the need for precise positioning of the fuel lever corresponding to particular loads [11, 15, 16, 17].

According to the presented model of energy state changes in the form of the process $\{X(t): t \geq 0\}$, an arbitrary main engine which is in state e_1 during its operation can reach, due to load increase, the state e_2 with the probability p_{12} after time T_{12}, and then reach the state e_3 with the probability p_{23} after time T_{23}. The state e_4 of the process $\{X(t): t \geq 0\}$ will take place when an arbitrary main engine starts converting energy E_4. In a similar way, from the state e_4 the process can reach the state e_3 with the probability p_{43} after time T_{43}, or the state e_2, which can take place with probability p_{42} after time T_{42}, etc.

A characteristic feature of the presented model of main engine energy state changes $\{X(t): t \geq 0\}$ is that the change of the state e_i into the state e_j only depends on the properties of the state e_i, and not on the previous states. This feature justifies the opinion that it is the semi-Markov process.

In this process the set of states $E_e = \{e_1, e_2, e_3, e_4\}$ is finite. The elements composing this set are the values of the semi-Markov process $X(t): t \geq 0\}$. Changes of states in this process take place at times $\tau_0 = 0, \tau_1, \tau_2, \ldots$ and after the lapse of time intervals of their duration (Fig. 2) being random variables with different distributions. The state changes in this process take place with the following probability:

$$P\{X(\tau_{n+1}) = e_j, \tau_{n+1} - \tau_n < \tag{3}$$

$$< t \left| X(\tau_n) = e_i, X(\tau_{n-1}), \ldots, X(\tau_0), \tau_n - \tau_{n-1}, \ldots, \tau_1, \tau_0 \right\} =$$

$$= P\{X(\tau_{n+1}) = e_j, \tau_{n+1} - \tau_n < t \left| X(\tau_n) = e_i \right\}$$

where:

$e_i, e_j \in E_e$, $i, j = 1, 2, 3, 4$; $e_i \neq e_j$.

As a result, when the state $e_i (i = 0, 1, ..., 4)$ of the process $\{X(t): t \geq 0\}$ is known at time τ_n, the time of its duration and the state e_j reached at time τ_{n+1} do not depend stochastically on the process states taking place at times $0 = \tau_0, \tau_1, ..., \tau_{n1}$, nor the time intervals of their duration.

The stochastic process $\{X(t): t \geq 0\}$ is the process whose states are identical (constant) in intervals and the realisations of these states are continuous on the right. The lengths of the intervals $[\tau_0, \tau_1), [\tau_1, \tau_2), [\tau_2, \tau_3), \ldots, [\tau_n, \tau_{n+1}), \ldots$, in which the process $\{X(t): t \geq 0\}$ takes constant (the same) values are random variables with positive distributions. In case of the loads of the abovementioned engines we can assume [3] that the duration time of an arbitrary state $e_i \in E_e$ (6), which was reached at time τ_n and the state reached at time τ_{n+1} do not depend stochastically on the states which earlier took place, nor the time intervals of their duration. Consequently, the process $\{X(t): t \geq 0\}$ is the model of randomly changing main engine loads, with the set of states $E_e = \{e_1, e_2, e_3, e_4\}$ and the graph of state changes shown in Fig. 3.

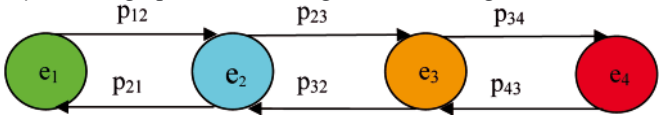

Fig. 3. *Graph of state changes in the process {X(t): t ≥0}*

The specified states $e_i \in E_e$ $(i = 1, 2, 3, 4)$ of the process $\{X(t): t \geq 0\}$ of an arbitrary main engine can be recognised using relevant diagnostic systems (SD), the applicability of which depends on the quality of the adopted diagnosing system (SDG) and its capability to recognise the states of the abovementioned engines as the diagnosed systems (SDN).

During the operation of an arbitrary diesel engine working as the main engine, changes of the states belonging to the set $E_e = \{e_i; i = 1, 2, 3, 4\}$ can be interpreted as the process $\{X(t): t \geq 0\}$ with the realisations constant (identical) in consecutive time intervals and continuous on the right [3, 7]. The lengths of the intervals in which the process $\{X(t): t \geq 0\}$ takes the constant (identical) values are the random variables T_{ij} representing the time of duration of the state $e_i \in E$ of this process, on condition that the next state is $e_j \in E_e$, where $i, j = 1, ..., 4$ and $i \neq j$. These variables are independent random variables with finite expected values $E(T_{ij})$ and have positively concentrated distributions. Moreover, this process reveals a property consisting in the fact that the duration time of the state e_i which took place at time τ_n and the state which started at time τ_{n+1} do not depend stochastically on the states which took place earlier, nor the time intervals of their duration. Therefore we can assume that the future states (situations) depend solely on the presently existing situation. That means that the process $\{X(t): t \geq 0\}$ is the semi-Markov process with the state change graph shown in Fig. 3. Defining this process requires defining its initial distribution P_i and the functional matrix **Q(t)**.

The initial distribution of the process $\{X(t): t \geq 0\}$ is the following:

$$P_i = P\{X(0) = e_i\} = \begin{cases} 1 & \text{for } i = 0 \\ 0 & \text{for } i = 1,2,...,3 \end{cases} \tag{4}$$

According to the state change graph shown in Fig. 3, the functional matrix has the following form:

$$Q(t) = \begin{bmatrix} 0 & Q_{01}(t) & 0 & 0 \\ Q_{10}(t) & 0 & Q_{12}(t) & 0 \\ 0 & Q_{21}(t) & 0 & Q_{23}(t) \\ 0 & 0 & Q_{32}(t) & 0 \end{bmatrix} \tag{5}$$

The elements of the matrix (5) are non-decreasing functions of the variable t which represent the probabilities of switching the process $\{X(t): t \geq 0\}$ from the state c_i to the state e_j $(e_i, e_j \in E_e; i,j = 1, 2, 3, 4; i \neq j)$ in time not longer than t, and are described in the following way [3, 7]:

$$Q_{ij}(t) = P\{X(\tau_{n+1}) = \\ = e_j, \tau_{n+1} - \tau_n < t \,|\, X(\tau_n) = e_i\} = p_{ij}F_{ij}(t) \tag{6}$$

where:
$e_i, e_j \in E_e (i, j = 1, 2, 3, 4; i \neq j)$,
and: p_{ij} is the probability of switching in one step of the homogeneous Markov chain inserted in the process $\{X(t): t \geq 0\}$. $F_{ij}(t)$ is the distribution function of the random variable T_{ij} representing the duration time of the state c_i of the process $\{X(t): t \geq 0\}$ on condition that the next state will be e_j.

The probability p_{ij} is interpreted in the following way:

$$p_{ij} = P\{X(\tau_{n+1}) = e_j \,|\, X(\tau_n) = e_i\} = \lim_{t \to \infty} Q_{ij}(t) \tag{7}$$

In this situation solving the problem consist in finding the limiting distribution of the process $\{X(t): t \geq 0\}$ having the following interpretation:

$$P_j = \lim_{t \to \infty} P\{X(t) = e_j\}, \quad j = \overline{1.4}$$

This distribution can be calculated using the formula [7]:

$$P_j = \frac{\pi_j E(T_j)}{\sum_{k=0}^{3} \pi_k E(T_k)}, \quad j = 1,\ 2,\ 3,\ 4 \tag{8}$$

where:

$$\pi_j = \lim_{n \to \infty} \frac{1}{n} \sum_{k=1}^{n} P\{X(\tau_n) = e_j | X(0) = e_i\}$$

$[\pi_j; j = 1, 2, 3, 4]$ – the stationary distribution of the Markov chain $\{X(\tau_n): n \in N\}$ inserted in the process $\{X(t): t \geq 0\}$.

The matrix (5) is the stochastic matrix, therefore this distribution is fulfilled by the following equation system (19) [7]:

$$\left.\begin{aligned} [\pi_1, \pi_2, \pi_3, \pi_4] \begin{bmatrix} 0 & 1 & 0 & 0 \\ p_{21} & 0 & p_{23} & 0 \\ 0 & p_{32} & 0 & p_{34} \\ 0 & 0 & 1 & 0 \end{bmatrix} &= [\pi_1, \pi_2, \pi_3, \pi_4] \\ \pi_1 + \pi_2 + \pi_3 + \pi_4 &= 1 \end{aligned}\right\} \tag{9}$$

After solving the equation system (9) we obtain the following relations according to the formula (8):

$$P_1 = \frac{p_{21}p_{32}E(T_1)}{M};\ P_2 = \frac{p_{32}E(T_2)}{M}; \\ P_3 = \frac{p_{23}E(T_3)}{M};\ P_4 = \frac{p_{23}p_{34}E(T_4)}{M} \tag{10}$$

where:
$M = p_{21}p_{32}E(T_1) + p_{32}E(T_2) + p_{23}E(T_3) + p_{23}p_{34}E(T_4)$;
p_{ij} – probability of switching the process $\{X(t): t \geq 0\}$ from state e_i to state e_j $(e_i, e_j \in E_e; i, j = 1, 2, 3, 4; i \neq j)$;
$E(T_j)$ – expected value of the random variable $T_j (j = 1, 2, 3, 4)$ representing the duration time of the state $e_j \in E_e$ $(j = 1, 2, 3, 4)$ of the process $\{X(t): t \geq 0\}$ irrespective of the next state to which this process switches.

The expected values $E(T_j)$ are related with the expected values $E(T_{ij})$ and the probability p_{ij} in the following way:

$$E(T_j) = E(T_i) = \sum_j p_{ij} E(T_{ij}), \quad i, j = \overline{1,4}; \quad i \neq j \tag{11}$$

Therefore, according to the adopted interpretation of the internal combustion engine operation [2, 10], the main engine operation can be defined in the following general way, see (Fig. 4) and formula (7):

$$\begin{aligned} D[\tau_1, \tau_9) = {} & P_1 E_1 E(T_1) + P_2 E_2 E(T_2) + P_3 E_3 E(T_{33}) + \\ & + P_4 E_4 E(T_4) + P_2 E_2 E(T_2) + P_3 E_3 E(T_3) + \\ & + P_1 E_1 E(T_1) + P_2 E_2 E(T_2) \end{aligned} \tag{12}$$

The main engine operation defined by formula (12) takes place when we can assume that the changes of the propeller characteristic, resulting from changes of sailing conditions, do not affect considerably the changes of energy conversion in the engine working spaces, i.e. we can assume that the energy E = idem.

When changes of the energy E are larger and cannot be omitted, the formula (12) is to be modified by introducing the average value of this energy, which, as the random variable, is the statistics $\overline{E}$. Then the operation will be defined in the following way:

$$\begin{aligned} \overline{D}[\tau_1, \tau_9) = {} & P_1 \overline{E}_1 E(T_1) + P_2 \overline{E}_2 E(T_2) + P_3 \overline{E}_3 E(T_3) + \\ & + P_4 \overline{E}_4 E(T_4) + P_2 \overline{E}_2 E(T_2) + P_3 \overline{E}_3 E(T_3) + \\ & + P_1 \overline{E}_1 E(T_1) + P_2 \overline{E}_2 E(T_2) \end{aligned} \tag{13}$$

A more accurate definition of the operation requires introducing probabilities $P_j (j = 1, ..., 4)$ given by formula (20) to equations (12) and (13).

Particular probabilities $P_j (j = 1, ..., 4)$ have the following interpretations:

$$P_1 = \lim_{t\to\infty} P\{X(t) = e_1\}, \; P_2 = \lim_{t\to\infty} P\{X(t) = e_2\},$$

$$P_3 = \lim_{t\to\infty} P\{X(t) = e_3\}, \; P_4 = \lim_{t\to\infty} P\{X(t) = e_4\}$$

The probability P_1 can be interpreted as the probability of engine load according to the partial power characteristic, and the three remaining probabilities P_2, P_3 and P_4 can have similar interpretations referring to the operating power, nominal power, and maximal power characteristics, respectively.

Obtaining the (obviously approximate) values of the probabilities $P_j (j = 1, 2, 3, 4)$ requires valuating p_{ij} and $E(T_j)$.

Valuating the probabilities p_{ij} and the expected values $E(T_j)$ is possible when we have the realisation x(t) of the process $\{X(t): t \geq 0\}$ in a relatively long time interval of investigations, i.e. for $t \in [0, t_b]$, where $t_b >> 0$. Then we can obtain numbers $n_{ij} (i,j = 1, 2, 3, 4; i \neq j)$, which represent the number of changes from the state e_i to the state e_j in the relatively long time.

The estimator of the highest likelihood of the probability of change p_{ij} is the statistics: [7]

$$\hat{P}_{ij} = \frac{N_{ij}}{\sum_j N_{ij}}, \quad i \neq j; \; i, j = 1, \; 2, \; 3, \; 4 \tag{14}$$

the value:

$$\hat{P}_{ij} = \frac{N_{ij}}{\sum_j N_{ij}}$$

of which is the assessment of the unknown probability p_{ij} of switching the process $\{X(t): t \geq 0\}$ from the state e_i to the state e_j.

From the abovementioned realisation x(t) we can also obtain realisations $t_{ij}^{(m)}$, $m = 1, 2, ..., n_{ij}$ of the random variables T_j. The application of point estimation provides opportunities for easy assessment of $E(T_j)$ as the arithmetic mean of the realisation $t_{ij}^{(m)}$.

The expected value of energy in formula (12) is the observed value of the statistics $\overline{E}_k (k = 1, 2, 3, 4)$. Obviously, this statistics is the random variable [1, 7] having the following general formula:

$$\overline{E}_k = \frac{1}{n} \sum_{i=1}^{n} E_{ki} \tag{15}$$

where:

E_{ki} – random variables having the same (arbitrary) distributions, with the same expected value $E(E_{ki}) = m_{1ki}$ and variance:

$$D^2(E_{ki}) = \sigma_{ki}^2 \neq 0$$

This way the random variable $\overline{E}_k$ (statistics) is the arithmetic mean of n independent random variables E_{ki} having the same distributions. The expected value and the variance of the random variable $\overline{E}_k$ are given by the relations [1, 14]:

$$\begin{aligned} E(\overline{E}_k) &= E(E_k) = m_{1k}, \\ D^2(E_{kn}) &= \frac{1}{n} D^2(E_{ki}) = \frac{\delta_k^2}{n} \end{aligned} \tag{16}$$

It results from the Lindeberg-Levy theorem [1] that the random variable $\overline{E}_k$ has the asymptotically normal distribution $N(m_{1k}, \sigma_k/\sqrt{n})$ irrespective of the nature of the random variable E_k. That means that the arithmetic mean of n independent random variables E_{ki} having an arbitrary but the same distribution and the same expected value, $E(E_{ki}) = m_{1k}$ and the variance $D^2(E_{ki}) = \sigma_k^2$, has the asymptotically normal distribution $N(m_{1k}, \sigma_k/\sqrt{n})$.

Applying the proposed methodology to the analysis of energy changes during the main engine operation seems attractive due to the fact that the convergence of the distribution of the statistics $\overline{E}_k$ to the normal distribution $N(m_{1k}, \sigma_k/\sqrt{n})$ is very fast and we can use it for all $n \geq 4$, i.e. always in practice [1].

When the value σ_k is known, taking into account the distribution $N(m_{1k}, \sigma_k/\sqrt{n})$ of the statistics $\overline{E}_k$ we can calculate the confidence interval for the unknown expected value $m_{k1} = E(E_k)$ using the formula [1, 10]:

$$P\left\{ \bar{e}_k - y_\alpha \frac{\sigma_k}{\sqrt{n}} \leq E(E_k) \leq \bar{e}_k + y_\alpha \frac{\sigma_k}{\sqrt{n}} \right\} = \beta \tag{17}$$

where:

β – confidence level,

y_α – standardised variable of the normal distribution, which corresponds to the confidence level $\beta = 1 - \alpha$ (α - significance level),

$\bar{e}_k$ – value of the statistics $\overline{E}_k$, which is the arithmetic mean of the performed measurements.

In experimental practice, as a rule, the value σ_k is not known, but it can be evaluated using the formula [1, 14]:

$$s_k = \sqrt{\frac{1}{n-1} \sum_{i=1}^{n} (e_{ki} - \bar{e}_k)^2} \tag{18}$$

Since the statistics $\overline{E}_k$ has always the asymptotically normal distribution $N(m_{1k}, \sigma_k/\sqrt{n})$, and its convergence to the normal distribution $N(m_1, \sigma)$ is very fast, we can assume in practice that

the investigated energy E_k has normal distribution $N(m_{1k}, \sigma_k)$. It is noteworthy, however, that adopting the above assumption is not a limitation in experimental practice, as the statistics $\overline{E}_k$ has always statistically normal distribution $N(m_{1k}, \sigma_k/\sqrt{n})$. Moreover, the convergence of this distribution to the normal distribution is very fast [3]. Therefore the random variable:

$$\frac{\overline{E}_k - E(E_k)}{s_k}\sqrt{n-1}$$

has the t-Student distribution with $k = n - 1$ degrees of freedom [1, 10]. That means that the confidence interval for the unknown expected value $E(E_k)$ of the random variable E_k can be calculated using the formula [1, 10]:

$$P\left\{\bar{e}_k - t_{\alpha,n-1}\frac{s_k}{\sqrt{n-1}} \le E(E_k) \le \bar{e}_k + t_{\alpha,n-1}\frac{s_k}{\sqrt{n-1}}\right\} = \beta \quad (19)$$

In practice, the formula (19) is more applicable for assessing the energy changes during engine operation in real conditions of ship sailing than the commonly used formula (15), as it not only reflects the randomness of the results obtained in operating conditions, but also determines the error in estimating the expected value of the energy converted in the engine in its particular states. This error, which in the present case is equal to $1 - \beta$, is the not covering of the expected value $E(E_k)$ by the confidence interval given by the formula (19).

The application of the estimation in intervals makes it possible to determine the expected value $E(E_k)$ in the form of an interval with random limits, which means that the following inequality is to be fulfilled with probability β:

$$E_d \le E(E_k) \le E_g \quad (20)$$

It results from the inequality (20) that the main engine operation which can be considered safe can be assessed in the following way, according to formula (13):

$$\begin{aligned}\overline{D}[\tau_1, \tau_9) = {} & P_1E_{1d}E(T_1) + P_2E_{2d}E(T_2) + P_3E_{3d}E(T_3) + \\ & + P_4E_{4d}E(T_4) + P_2E_{2d}E(T_2) + P_3E_{3d}E(T_3) + \\ & + P_1E_{1d}E(T_1) + P_2E_{2d}E(T_2)\end{aligned} \quad (21)$$

On the other hand, the optimistic engine operation can be assessed, according to formula (13), as:

$$\begin{aligned}\overline{D}[\tau_1, \tau_9) = {} & P_1E_{1g}E(T_1) + P_2E_{2g}E(T_2) + P_3E_{3g}E(T_3) + \\ & + P_4E_{4g}E(T_4) + P_2E_{2g}E(T_2) + P_3E_{3g}E(T_3) + \\ & + P_1E_{1g}E(T_1) + P_2E_{2g}E(T_2)\end{aligned} \quad (22)$$

If necessary, processes of this type with a larger number of states e_i, $i = 1, 2, 3, \ldots K$ can be investigated. Taking theoretically into account these needs, we can most generally discuss the process $\{X(t): t \ge 0\}$ with the set of states $E_{eK} = \{e_1, e_2, e_3, \ldots, e_K\}$. This process will be fully defined if, like in previous cases, a formula is given for the functional matrix:

$$Q_{ij} = [Q_{ij}(t)] \quad i, j = 1, 2, 3, \ldots, K \quad (23)$$

and the initial distribution:

$$P_i = P\{X(0) = e_i\} \quad i = 1, 2, 3, \ldots, K$$

For this generalised case the matrix of the process $\{X(t): t \ge 0\}$ is the following:

$$\mathbf{Q(t)} = \begin{bmatrix} 0 & Q_{12}(t) & 0 & \ldots & 0 & 0 & 0 \\ Q_{21}(t) & 0 & Q_{23}(t) & \ldots & 0 & 0 & 0 \\ \ldots & \ldots & \ldots & \ldots & \ldots & \ldots & \ldots \\ 0 & 0 & 0 & \ldots & Q_{K-1K-2}(t) & 0 & Q_{K-1K}(t) \\ 0 & 0 & 0 & \ldots & 0 & Q_{KK-1}(t) & 0 \end{bmatrix} \quad (24)$$

and its initial distribution has the form:

$$P_i = P\{X(0) = e_i\} = \begin{cases} 1 \text{ for } i = 1 \\ 0 \text{ for } i = 2,3,\ldots,K \end{cases} \quad (25)$$

Consequently, $P\{X(0) = e_1\} = 1$.

Like in previous analyses, we have to assess the limiting distribution of the process [7]:

$$P_j = \frac{\pi_j E(T_j)}{\sum_{k=1}^{K} \pi_k E(T_k)}, \quad j = 1, 2, \ldots, K \quad (26)$$

Using the same procedure as in previous cases we arrive at the relation:

$$P_j = \frac{\left[\prod_{k=2}^{j} \frac{(1 - p_{k-1k-2})}{p_{kk-1}}\right] E(T_j)}{E(T_1) + \left[\sum_{j=2}^{K}\prod_{k=2}^{j} \frac{(1 - p_{k-1k})}{p_{kk-1}}\right] E(T_j)} \quad j = 2, 3, \ldots, K \quad (27)$$

It results from formula (27) that, for instance, the probability of engine load resulting from the appearance of the state e_1 can be calculated as [7]:

$$P_1 = \frac{E(T_1)}{E(T_1) + \left[\sum_{j=2}^{K}\prod_{k=2}^{j} \frac{(1 - p_{k-1k-2})}{p_{kk-1}}\right] E(T_j)} \quad (28)$$

The presented considerations reveal that after adopting the interpretation of the operation in the here proposed version and making use of the theory of semi-Markov processes we can determine the operation of marine main engines in probabilistic formulation, which is more adequate than the deterministic formulation, as it reflects random conditions of operation of engines of this type.

REMARKS AND CONCLUSIONS

- The article presents the probabilistic method for evaluating the operation of an internal combustion engine used as the main engine on a ship. This method can be applied to an arbitrary piston internal combustion engine of both spark-ignition and compression-ignition type. The method takes it into account stochastic nature of energy conversion processes observed during engine operation. It was proved that a very useful model for investigating those processes is the model having the form of a stochastic process which is discrete in states and continuous in time. The analyses presented in the article reveal that this model can be the semi-Markov process which has the abovementioned features.
- The operation of the internal combustion engine was interpreted as generation of the required energy in a given time and its delivery (transmission) to the receiver. That means that when analysing the operation of these engines in given time and taking into account both the energy generated by these engines and time of its generation, we can compare (in a valuating formulation) this operation to a physical quantity which has a numerical value and the measure unit called joule-second [joule×second].
  When analysing energy related qualities of internal combustion engines we should analyse their whole

operation, and not only their work, as the engine operation includes not only the energy conversion into work, but also into heat.

- The process of changes of energy states during the operation of an arbitrary diesel engine is a random process with continuous, positive and limited realisations.
- The models of changes of energy states may refer to the operation of an arbitrary engine, and include various numbers and interpretations of energy states. In each case, however, a model can be constructed in the form of a semi-Markov process, continuous in time and discrete in states, i.e. having a limited number of states.
- The developed semi-Markov model of the process of energy state changes during the main engine operation is the process with limited number of states and continuous in time.

  Another approach to investigating the energy converted in the main engine and transmitted to the propeller screw was also proposed. This approach consists in considering this energy a random variable. The applicability of the Lindeberg-Levy theorem was proved which says that the statistics created based on the results of the investigations of a given energy is the random variable having the asymptotically normal distribution, irrespective of the nature of the random variable representing this energy. This enables using the estimation in intervals to evaluate the unknown expected value of the random variable, which can be the energy converted in the main engine and transmitted to the propeller screw during engine operation.
- The application of the estimation in intervals to the evaluation of engine operation has made it possible to assess its value in an optimistic version (22) and a safe version (21).

BIBLIOGRAPHY

1. Firkowicz S.: Statistic evaluation of quality and reliability of electron tubes (in Polish). WNT, Warszawa 1963.
2. Girtler J.: a method for evaluating the performance of a marine piston internal combustion engine used as the main engine on a ship during its voyage in different sailing conditions Polish Maritime Research. Vol. 17, iss. 4(67), 2010.
3. Girtler J.: Physical aspect of application and usefulness of semi-Markovian processes for modelling the processes occurring in operational phase of technical objects. Polish Maritime Research. 2004 nr 3(41), vol. 11, pp. 25-30.
4. Girtler J.: Possibility of valuation of operation of marine diesel engines. Journal of POLISH CIMAC, Vol. 4, No 1, 2009.
5. Girtler J.: Energy-based aspect of operation of diesel engine. COMBUSTION ENGINES No 2/2009 (137).
6. Girtler J.: Conception of valuation of combustion engine operation. Journal of KONES. Powertrain and Transport. Editorial Office Institute of Aeronautics BK, Warsaw 2008.
7. Grabski F.: Theory of semi-Markov processes of operation of technical objects (in Polish). ZN AMW nr 75A, Gdynia 1982.
8. Gribbin J.: In Search of Schrödinger's Cat Quantum Physics Reality. (Polish issue). Zysk i S-ka Wydawnictwo s.c. Poznań 1 997.
9. Helwitt P.G.: Physics around us (in Polish). PWN, Warszawa 2001.
10. Pawłowski Z.: Mathematical statistics (in Polish). PWN, Warszawa 1980.
11. Piotrowski I., Witkowski K.: Operation of marine internal combustion engines (in Polish). AM, Gdynia 2002.
12. Rosłanowski J.: Identification of ships propulsion engine operation by means of dimensional analysis. Journal of POLISH CIMAC, Vol 4, No 1, 2009.
13. Rudnicki J.: On making into account value of operational applied to ship main propulsion engine as an example. Journal of POLISH CIMAC, Vol 4, No 1, 2009.
14. Volk W.: Applied statistics for engineers (in Polish). WNT, Warszawa 1965.
15. Wajand J.A.: Compression-ignition engine (in Polish). WNT, Warszawa 1988.
16. Włodarski J.K.: Operating states of marine internal combustion engines (in Polish). WSM, Gdynia 1998.
17. Wojnowski W.: Marine internal-combustion power plants, Pt I. (in Polish). AMW, Gdynia 1999.
18. Encyclopaedia of contemporary physics (in Polish). Collective work. Editor: Redakcja Nauk Matematyczno-Fizycznych i Techniki Zespołu Encyklopedii i Słowników PWN. PWN, Warsaw 1983.
19. Scientific and technical lexicon with supplement (in Polish). Collective work. Editor: Zespół redaktorów Działu Słownictwa Technicznego WNT. WNT, Warsaw 1989.

CONTACT WITH THE AUTHOR

Jerzy Girtler, Prof.
Faculty of Ocean Engineering
and Ship Technology
Gdansk University of Technology
Narutowicza 11/12
80-233 Gdansk, POLAND
tel.: (+48 58) 347-24-30; fax: (+48 58) 347-19-81
e-mail: jgirtl@pg.gda.pl

POLISH MARITIME RESEARCH 4(71) 2011 Vol 18; pp. 43-48
10.2478/v10012-011-0025-8

Comparing combined gas tubrine/steam turbine and marine low speed piston engine/steam turbine systems in naval applications

Marek Dzida, Assoc. Prof.
Wojciech Olszewski, M. Sc.
Gdansk University of Technology

ABSTRACT

The article compares combined systems in naval applications. The object of the analysis is the combined gas turbine/steam turbine system which is compared to the combined marine low-speed Diesel engine/steam turbine system. The comparison refers to the additional power and efficiency increase resulting from the use of the heat in the exhaust gas leaving the piston engine or the gas turbine. In the analysis a number of types of gas turbines with different exhaust gas temperatures and two large-power low-speed piston engines have been taken into account. The comparison bases on the assumption about comparable power ranges of the main engine.

Key words: marine power plants, combined systems, piston internal combustion engine, gas turbine, steam turbine

INTRODUCTION

In recent years combined systems consisting of a gas turbine and a steam turbine have started to be used as marine propulsion systems. In inland applications the efficiency of these systems can exceed 60%. In naval applications such a system was used in Millenium, a passenger liner. But it is, so far, a unique case of propulsion system related with the highest efficiency. However, this system requires a more expensive fuel, which is the marine Diesel oil.

Another possible combined system can consist of a piston engine which cooperates with the steam turbine utilising the heat in the exhaust gas leaving the piston engine. The leading engine in this is system is always the piston internal combustion engine. The objects used as the main engines will be large low-speed piston engines which burn heavy fuel. At present, the efficiency of these engines reaches 45-50%. In case of such large main engine power ranges, the exhaust gas leaving the piston engine contains huge amount of heat which can be the object of further utilisation.

Another possible solution of a combined system which can be applied in shipbuilding consists of a gas turbine, and a steam turbine which utilises the heat leaving the gas turbine. This heat can be used for production of steam which, in turn, can be used in the steam turbine cycle.

CONCEPT OF A COMBINED SYSTEM

Combined propulsion systems in naval applications are first of all used in fast special ships and in the Navy as the systems being the combination of a Diesel engine and a gas turbine (CODAG, CODOG) or gas turbines (COGOG, COGAG). The propulsion applied in the passenger liner Millenium makes use of a COGES system which increases the efficiency and operating abilities of the ship by combining the operation of a gas turbine with a steam turbine which drives the electric generator, while the propeller screws are driven by electric motors. In this system the steam turbine cycle is fed with the steam produced in the waste heat boiler supplied with the exhaust gas from the gas turbines.

Fig. 1 shows sample efficiency curves of the combined gas turbine/steam turbine systems as functions of power plant load, as compared to the gas turbine working in a simple open cycle and the marine low-speed Diesel engine. The analysis of the efficiency changes reveals that the combined system composed of a gas turbine and a steam turbine has the highest efficiency, which can reach up to 60% for maximal loads. Gas turbines working in a simple open cycle have the lowest efficiency, of an order of 33÷35% on average, and about 40% as the maximum [7]. Low-speed Diesel engines reach efficiency of an order of 47÷50% [5, 6]. At the same time their efficiency characteristics as functions of load are flat, which is of highest importance in marine propulsion systems working in heavily changing load conditions. For instance, the relative efficiency drop $\Delta\eta/\eta_{GT}$ is equal to 15÷20% when the load changes from 100% down to 50% in the combined gas turbine/steam turbine systems and gas turbines working in a simple cycle, while for a low-speed Diesel engine this efficiency drop is equal to 1÷2%. This property of the Diesel engine and utilisation of additional heat contained in its exhaust gas makes the application of this

system very useful for marine propulsion systems working in extremely changing load conditions.

The temperatures of the exhaust gas from the gas turbines are equal to 450÷600°C on average, while for the low-speed Diesel engine these temperatures are of an order of 220÷300°C [5, 6], Fig. 2. But in the gas turbines this temperature remarkably decreases with decreasing load, while in the Diesel engine its changes are not high, nor monotonic: initially the temperature decreases and then starts increasing with the decreasing load.

This property of the Diesel engine in partial loads makes it possible to keep the temperature of the live steam at a constant level within a wide range of steam turbine cycle loads.

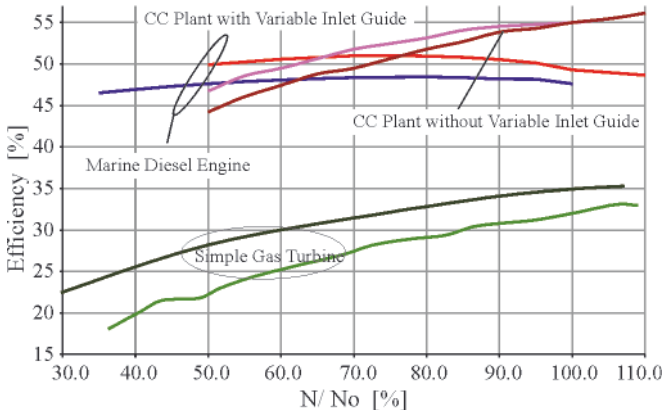

Fig. 1. *Part-load efficiency of a combined-cycle plant (GT&ST), simple gas turbine and marine Diesel engine*

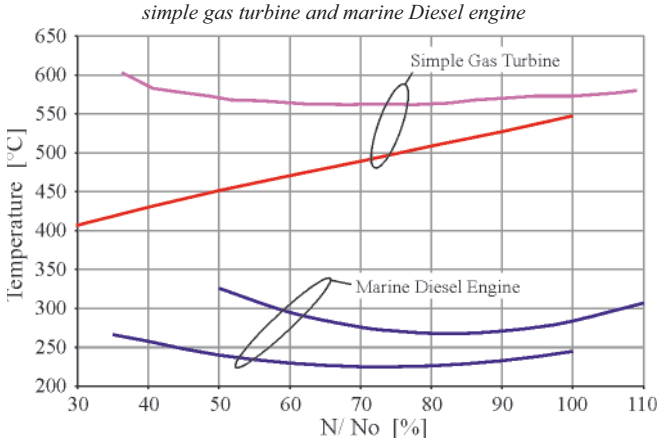

Fig. 2. *Temperatures of the exhaust gas from the marine Diesel engine and the simple gas turbine as functions of power plant load*

Power evaluation of the combined propulsion system

The power of the combined propulsion system is calculated by adding up particular power outputs of the system components, i.e. the main engine and the steam turbine:

$$N_{combi} = N_C + N_{ST} \tag{1}$$

while the efficiency of the combined system is:

$$\eta_{combi} = \frac{N_{combi}}{m_f \cdot Wu} = \eta_D \cdot \left(1 + \frac{N_{ST}}{N_C}\right) \tag{2}$$

where:

η_C, m_f – are the efficiency and mass flow rate of the main engine.

It results from the relation (2) that each additional power in the propulsion system increases the efficiency of the system and, consequently, decreases the fuel consumption. The higher the additional power obtained from utilisation of the heat contained in the main engine exhaust gas, the lower the fuel consumption. In these circumstances we should tend to reach maximal power also from the steam turbine, in which the power output largely depends on proper selection of live steam parameters and condenser parameters.

Steam turbine cycle

The combined cycle makes use of the waste heat in the exhaust gas from the Diesel engine or the gas turbine. Adding a steam cycle to the combined Diesel engine or gas turbine cycle makes it possible to increase the power of the combined system, i.e. increase the system efficiency according to formula (2).

In case of small powers and low live steam temperatures in combined systems, single pressure systems are used [1, 2, 3], Fig. 3. Such a system consists of a single pressure waste heat boiler), a condensing steam turbine, a water cooled condenser, and a single stage feed water preheater in the deaerator.

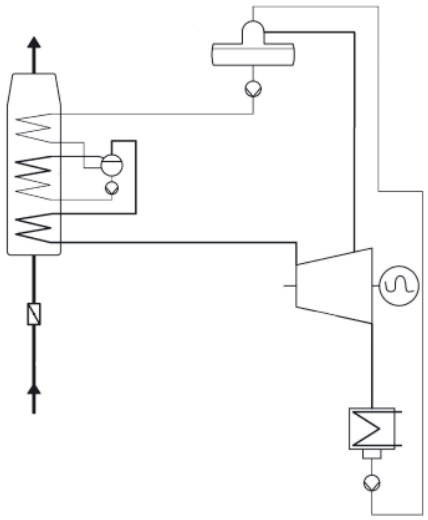

Fig. 3. *Flow diagram of a single pressure system*

The application of the single pressure system does not secure optimal utilisation of the energy in the exhaust gas when its temperature is high. The system which is most frequently used in these cases includes an additional low pressure evaporator [2, 3], Fig. 4, which not only increases the utilisation of the waste heat in the exhaust gas, but also provides opportunities for better thermodynamic use of the low-pressure steam.

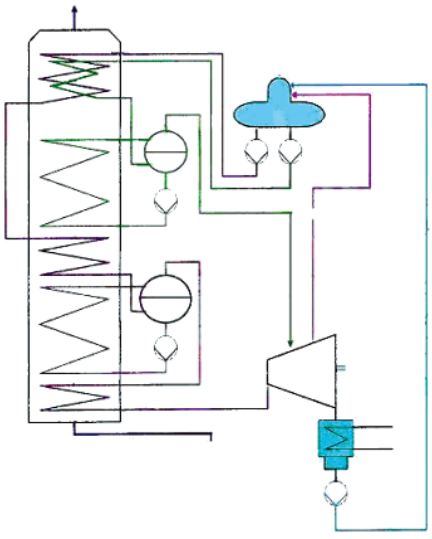

Fig. 4. *Flow diagram of a two-pressure system*

Limits of steam cycle parameters

Limits of steam cycle parameters result from strength, technical, and durability conditions for particular system elements, but also from constructional and economic restrictions.

The temperature difference between the exhaust gas and the live steam was assumed equal to $\Delta t = 10°C$ in utilisation boilers used in shipbuilding, following the literature [3, 4]. The "pitch point" value recommended by MAN B&W [4] for marine boilers was assumed equal to $\delta t = 10°C$. The limit of the steam dryness factor x behind the steam turbine was assumed equal to $x_{limit} = 0.86\text{-}0.88$. For marine condensers cooled with salt water, the company MAN B&W [4] recommends assuming the condenser pressure equal to $p_K = 0.065$ bar. The temperature of the water which feeds the boiler is of high importance for the lifetime of the feed water heater in the boiler. MAN B&W [4] recommends assuming that the feed water temperature is not lower than 120°C, when the content of sulphur exceeds 2%. The caloric value of the fuel was assumed constant and equal to Wu = 42700 kJ/kg in the calculations.

Steam cycle optimisation

The combined systems, in this case the steam cycles, should make maximal use of the heat contained in the exhaust gas from the main engine. Therefore the optimisation is reduced to calculating steam cycle parameters for which the steam turbine reaches the maximal power output. The area within which optimal steam cycle parameters are searched for is to be narrowed to the area in which all above listed limits and restrictions imposed on the steam cycle are fulfilled.

In case of combined systems with gas turbines, a two-pressure steam turbine cycle is used. The calculations for the combined system with Diesel engines were performed for both the single- and the two- pressure variant. The steam turbine cycles in the combined systems were calculated based on the same schemes, and the same above listed assumptions and parameters.

COMBINED GAS TURBINE/STEAM TURBINE SYSTEMS

In the calculations of the combined systems with gas turbines a number of types of gas turbines produced by Alstom and GE were taken into account. The analysed turbines represented different power outputs and different exhaust gas temperatures. The total power output of the gas turbines in the combined system was kept close to each other in all variants. The gas turbine parameters which were assumed in the calculations are collected in Table 1.

Tab. 1. *Parameters of gas turbines used in the combined gas turbine/steam turbine cycle [7]*

Type of turbine	N_{GT}	m_{GT}	t_4	η_{GT}	be_{GT}
	kW	kg/s	°C	-	g/kWh
CYCLON	12900	39.7	570	0.340	248.0
GTX100	43000	122.0	546	0.370	227.9
GT10B	24400	80.4	538	0.347	243.0
LM2500	22400	68.0	528	0.365	230.9
GT35	17000	92.3	378	0.320	263.5

Tab. 2. *Combined gas turbine/steam turbine cycle with two-pressure boiler*

Type		CYCLON	GTX100	GT10B	LM2500	GT35
Number of engines		4	1	2	1	3
N_{GT}	kW	51600	43000	48800	44800	51000
m_{TG}	kg/s	158.80	122.00	160.80	136.00	276.90
m_f	kg/s	3.5542	2.7217	3.2935	2.8729	3.7324
t_4	°C	570	546	538	528	378
t_o	°C	560	536	528	518	368
p_o	bar	160	134	128	114	30
p_I	bar	4	4	3	3	2
t_{FW}	°C	120	120	120	120	120
Pu	bar	2.09	2.09	2.09	2.09	2.09
Mo	kg/s	20.88	14.58	18.57	15.23	18.28
m_d	kg/s	3.88	2.87	3.75	3.1	4.14
m_{IT}	kg/s	5.78	5.1	7.270	6.2	10.74
N_{ST}	kW	25304	17523	22232	18047	17713
N_{ST}/N_{TG}	-	0.4904	0.4075	0.4556	0.4028	0.3473
η_{combi}	-	0.5067	0.5208	0.5051	0.5123	0.4311
be_{combi}	g/kWh	166.4	161.9	166.9	164.6	195.6
m_o/N_{GT}	kg/kWh	1.4567	1.2207	1.3699	1.2238	1.2904
m_d/m_o	%	18.58	19.68	20.19	20.35	22.65
m_{IT}/m_o	%	27.68	35.12	39.15	40.71	58.75
m_{GT}/N_{GT}	kg/kWh	11.08	10.21	11.86	10.93	19.55

In this case the steam turbine system was analysed in the cycle with the two-pressure boiler, see Fig. 4, for the feed water temperature t_{FW} = 120°C. The results of the combined cycle calculations are given in Table 2. The power output of the steam turbine with respect to that of the gas turbine changes between 35% and 49%. The power output of the steam turbine increases mainly due to the increase of the gas turbine exhaust gas temperature, but also depends on the ratio of the mass flow rate of the gas turbine exhaust gas to the turbine power output. The live steam pressure depends on the gas turbine exhaust gas temperature and increasers with the increase of this temperature. The pressure p_I of the low-pressure stage also increases with the increasing exhaust gas temperature (t_4), but this increase is not large.

The mass flow rates m_d of the heating steam taken from the turbine extraction point for heating the condensate in the deaerator are relatively comparable. The mass flow rate m_{IT} of the low-pressure steam which is passed from the boiler to the steam turbine decreases with the increasing temperature of the gas turbine exhaust gas.

The combined cycle applied to a system with the gas turbines makes it possible to increase the system efficiency by 35-49% with respect to the simple gas turbine cycle.

COMBINED MARINE DIESEL ENGINE/ STEAM TURBINE SYSTEMS

The calculations of the combined Diesel engine/steam turbine systems took into account two marine low-speed engines: 9RTA96C made by Warstsila [6] and 9K98MC made by MAN Diesel & Turbo [5] which revealed similar power outputs as the gas turbines. The analyses were performed in the combined system with the steam turbine cycle with a single pressure boiler, according to a scheme shown in Fig. 3, and the two-pressure boiler, see Fig. 4. The calculations were performed based on the producer's data for the reference point according to ISO Conditions: ambient air temperature equal to 25°C and barometric pressure equal to 1 bar, Table 3.

Tab. 3. *Parameters of marine low-speed Diesel engines used in the combined Diesel engine/steam turbine system [5, 6]*

Type of engine	N_D	m_D	t_4	η_D	be_D
	kW	kg/s	°C	-	g/kWh
9K98MC	48762	134.25	232.8	0.482	174.9
9RTA96C	46332	104.50	271.0	0.506	166.8

In that case the steam turbine system was analysed for the feed water temperature equal to t_{FW} = 120°C. The results of the combined cycle calculations are given in Table 4. Like for the combined system with gas turbines, the caloric value of the fuel was assumed equal to Wu = 42700 kJ/kg.

The power of the steam turbine in the combined system ranges from 5.3% to 6.8% of the piston engine power. The steam turbine power is larger for the steam turbine cycle with the two-pressure boiler, but this increase in not significant as compared to the power of the turbine with the single–pressure boiler. The turbine power increases with the increasing temperature of the piston engine exhaust gas. The pressure of the live steam for the two-pressure cycle is about 2.5 times as high as that for the single-pressure cycle and it increases with the increase of the temperature t_4 of the engine exhaust gas.

Tab. 4. *Combined Diesel engine – steam turbine cycle*

Type		9K98MC		9RTA96C	
N_D	kW	48762		46332	
m_D	K kg/s	134.25		104.504	
m_f	kg/s	2.369		2.1467	
t_4	°C	232.8		271	
Steam cycle		**Single-pressure**	**Two-pressure**	**Single-pressure**	**Two-pressure**
t_o	°C	223	223	261	261
p_o	bar	2.5	6	4	10
p_I	bar		2		2
t_{FW}	°C	120	120	120	120
pu	bar	2.09	2.09	2.09	2.09
mo	kg/s	5.37	3.89	5.225	3.979
m_d	kg/s	0.714	0.940	0.700	0.941
m_{IT}	kg/s		2.28		2.91
N_{ST}	kW	2566	2717	2906	3147
N_{ST}/N_D	-	0.0526	0.0557	0.0627	0.0679
η_{combi}	-	0.5074	0.5089	0.5372	0.5398
be_{combi}	g/kWh	166.2	165.7	157.0	156.2
m_o/N_D	kg/kWh	0.3965	0.2872	0.4060	0.3092
m_d/m_o	%	13.30	24.16	13.40	23.65
m_{IT}/m_o	%		58.61		73.13
m_D/N_D	kg/kWh	9.91		8.12	

The live steam mass flow rate for the single-pressure system is larger than that for the two-pressure system. When related to the engine power, this parameter differs insignificantly for the two examined engines. The extraction steam mass flow rate m_d, as related to that of the live steam, is almost twice as small in the single-pressure system as in the two-pressure system. In the two-pressure system the mass flow rate m_{IT} of the low-pressure steam which feeds the steam turbine is equal to 59 ÷ 73 % of the live steam mass flow rate and increases with the increase of the piston engine exhaust gas temperature.

In the combined system the cycle efficiency increases by 5.6 ÷ 6.7% with respect to the power plant with only a Diesel engine.

COMPARISON OF COMBINED GAS TURBINE/STEAM TURBINE AND MARINE LOW-SPEED DIESEL ENGINE/STEAM TURBINE SYSTEMS

The use of combined systems with the gas turbine or the Diesel engine cooperating with the steam turbine cycle increases the power of the system, and simultaneously increases the power plant efficiency.

In the systems with gas turbines the efficiency increase with respect to the simple gas turbine cycle (35 ÷ 49%) is much larger than that observed in the combined cycle with the Diesel engine, the increase of an order of 5.5 ÷ 6.7% with respect to the Diesel engine power, see Table 5.

Tab. 5. *Comparing combined cycles*

type	t_4	$\Delta\eta/\eta_C$	$\Delta be/be_C$	N_{combi}/N_C	t_{exh}
	°C	%	%	%	°C
Combined gas turbine/steam turbine system					
CYCLON	570	49.03	-32.91	149.0	139
GTX100	546	40.76	-28.96	140.8	139
GT10B	538	45.56	-31.31	145.6	135
LM2500	528	40.28	-28.73	140.3	135
GT35	378	34.72	-25.79	134.7	131
Combined Diesel engine/steam turbine system					
9K98MC	232.8	5.58	-5.28	105.6	131
9RTA96C	271	6.68	-6.36	106.8	131

The two combined systems reveal comparable overall efficiencies, and the resultant specific fuel consumption is also similar. It is noteworthy, however, that the heavy fuel burned in the marine low-speed engines is cheaper than the marine Diesel oil burned in gas turbines. This, in combination with comparable fuel consumption rates, results in lower fuel costs of the combined system with the Diesel engine.

Table 6 gives the energy balance of the combined system with the gas turbines or the marine low-speed Diesel engine.

In the energy balance of the combined system, the power of the main engine is equal to 35%, on average, for the gas turbine and 49% for the Diesel engine in relation to the energy delivered in the fuel to the engine, while the steam turbine power is equal to 15% for the system with the gas turbine and 3% for the system with the Diesel engine. The stack loss and the condenser loss amount to 15% and 33% respectively in the system with the gas turbine, and to 15% and 11% in the systems with the Diesel engine. The comparable levels of the stack losses for these two systems result from their comparable exhaust gas temperatures.

Other losses in the system with the Diesel engine amount to about 21%, as compared to 3% in the systems with gas turbines. In the Diesel engine the other losses include the heat taken over in the scavenge air coolers - about 15%, in the lubricating oil cooler – about 3%, and in the jacket water cooler 4%.

Tab. 6. *Energy balance of the combined cycle*

Type of engine	Energy input	Engine Power	Steam Turbine Power	Condenser Loss	Stack Loss	Others
	%	%	%	%	%	%
CYCLON	100	34.00	16.67	32.04	13.25	4.04
GTX100	100	37.00	15.08	30.90	13.30	3.72
GT10B	100	34.70	15.81	33.59	13.99	1.91
LM2500	100	36.52	14.71	31.96	13.63	3.18
GT35	100	32.00	11.11	33.94	20.28	2.66
	Single-Pressure Combined-Cycle Plant					
9K98MC	100	48.20	2.54	10.77	16.50	21.99
9RTA96C	100	50.55	3.17	11.42	15.68	19.18
	Two-Pressure Combined-Cycle Plant					
9K98MC	100	48.20	2.69	11.38	15.65	22.07
9RTA96C	100	50.55	3.43	13.16	13.58	19.28

Steam turbine cycles used in the combined system composed of gas turbines should include a two-pressure boiler, the least, to allow good utilisation of the energy of the high-temperature exhaust gas.

In the combined systems comprising a low-speed Diesel engine, a single-pressure boiler can be used in the steam turbine cycle, as it can secure good utilisation of the exhaust gas heat (much lower temperatures of the exhaust gas, compared to those recorded in the gas turbine).

The live steam parameters in the combined system with gas turbines are much higher than those in the system with the Diesel engine.

The power outputs of the steam turbines in the systems with gas turbines are many times higher than those in the systems with the Diesel engine, compare Tables 2 and 4. For comparable powers of the combined system, the power of the steam turbine amounts to 26 ÷ 33% of the power of the entire power plant for the systems with the gas turbines, and to 5.3 ÷ 6.9% in the systems with the Diesel engine. In those latter systems the power output of the Diesel engine amounts to 94% of the power plant power, while in the systems with the gas turbines the power of the gas turbine amounts to 67 ÷ 74%. For the same total powers of the combined system the power of the Diesel engine is larger 1.3÷1.4 times than that of the gas turbine.

The exit temperatures t_{EXH} of the exhaust gas in the combined system for the cases with the gas turbine or the Diesel engine are comparable, Table 5.

FINAL CONCLUSIONS

There is a possibility to use a combined system composed of the Diesel engine or a gas turbine as the leading engine, and the steam turbine cycle which utilises the heat contained in the engine exhaust gas. These systems reach thermodynamic efficiency comparable with the combined systems of gas turbines cooperating with steam turbines.

Power outputs of the combined systems

Depending on the adopted variant and main engine load, the use of the combined system can increase the power output of the power plant by 35 ÷ 49% in the systems with gas turbines, and by 5 ÷ 7% in systems with Diesel engines, with respect to a conventional power plant for the same fuel mass flow rate. Additional power output is generated due to recovery of the energy contained in the exhaust gas from the piston internal combustion engine or the gas turbine. This way the combined system reduces the specific fuel consumption by 26 ÷ 36% for cycles with gas turbines and by 5 ÷ 6.4% for the cycle with a Diesel engine, with respect to the conventional power plant.

Efficiencies of the combined systems

The use of the combined system for ship propulsion increases the system efficiency, which leads to the reduction of the specific fuel consumption and, additionally, increases the power of the of propulsion system, without additional fuel consumption. Like the power output, the efficiency of the combined system increases with respect to the conventional power plant, reaching the level of about 43 ÷ 54% for maximal power outputs. The efficiency levels for the combined gas turbine/steam turbine and Diesel engine/steam turbine systems are comparable.

Overall power plant dimensions

The power plant with the combined system with gas turbines is smaller both in mass and dimensions than that with the Diesel engine.

Economic aspects

The technical and economic analysis of power plant operation should be performed to justify the use of such a power plant. The analysis should take into account both investment and operating costs. At comparable fuel consumption in both combined systems, the cost of burning the heavy fuel oil in the marine power plant with the Diesel engine is lower, as the combined systems with gas turbines burn more expensive marine Diesel oils. But in case of sailing in zones with limits imposed on heavy fuel burning, the use of a combined power plant with gas turbines can be more economically justified.

Depending on the adopted solution, the use of the combined power plant makes it possible to reach the assumed power of the propulsion system at smaller load of the main internal combustion engine, and to reduce the fuel consumption.

NOMENCLATURE

be	–	specific fuel consumption
m	–	mass flow rate
m_{IT}	–	mass flow rate of the low-pressure steam in the turbine
N	–	power
N_C	–	power of the gas turbine or of the piston internal combustion engine
p	–	pressure
p_I	–	low-pressure steam pressure
t_4	–	temperature of the exhaust gas from the piston internal combustion engine or the gas turbine
η	–	efficiency

SUBSCRIPTS

combi	–	combined system
D	–	deaerator
D	–	piston internal combustion engine
exh	–	outlet duct
F	–	fuel
FW	–	feed water
GT	–	gas turbine
K	–	parameters in the condenser
o	–	live steam, calculation point
ST	–	steam turbine

BIBLIOGRAPHY

1. Advances in Gas Turbine Technology. Chapter (Dzida M.) Possible Efficiency Increasing of Ship Propulsion and Marine Power Plant with the System Combined of Marine Diesel Engine, Gas Turbine and Steam Turbine. ISBN 978-953-307-611-9. Book edited by: Dr. Ernesto Benini. INTECH, 2011
2. Dzida, M.: *On the possible increasing of efficiency of ship power plant with the system combined of marine diesel engine, gas turbine and steam turbine at the main engine - steam turbine mode of cooperation*. Polish Maritime Research, Vol. 16, No.1(59), (2009), pp. 47-52, ISSN 1233-2585
3. Kehlhofer, R.: *Combined-Cycle Gas & Steam Turbine Power Plants*, The Fairmont Press, INC., ISBN 0-88173-076-9, USA, 1991
4. MAN B&M. The MC Engine. Exhaust Gas Date. Waste Heat Recovery System. Total Economy, *MAN B&W Publication S.A.,* Danish, 1985
5. MAN Diesel & Turbo & Turbo. Stationary Engine. Programme 4th edition, *Branch of MAN Diesel & Turbo & Turbo SE,* Germany, Available from www.mandieselturbo.com, 2010
6. Sulzer RTA 96C*, Engine Selection and Project Manual,* June 2001, Wartsila.
7. ABB ALSTOM POWER Ltd. *Gas Turbine and Combined-Cycle Power Plants, Switzerland, CH-50 5401,* Baden.

CONTACT WITH THE AUTHORS

Marek Dzida, Assoc. Prof.
Wojciech Olszewski, M. Sc.
Faculty of Ocean Engineering
and Ship Technology
Gdansk University of Technology
Narutowicza 11/12
80-233 Gdansk, POLAND
e-mail: dzida@pg.gda.pl

POLISH MARITIME RESEARCH 4(71) 2011 Vol 18; pp. 49-53
10.2478/v10012-011-0026-7

Exhaust gas temperature measurements in diagnostic examination of naval gas turbine engines

Part III
Diagnostic and operating tolerances

Zbigniew Korczewski, Prof.
Gdansk University of Technology

ABSTRACT

The third part of the article presents a method for detecting failures of the automatic engine control system with the aid of an exhaust gas temperature setter, specially designed and machined for this purpose. It also presents a procedure of identifying the operating tolerances and determining the diagnostic tolerances for the exhaust gas temperature recorded in the naval turbine engine during the start-up and acceleration processes. The diagnostic tolerances were determined using the statistic inference, based on the hypothesis about the normal distribution of the starting exhaust gas temperature dispersion at the initial time of engine operation. The above hypothesis was verified using the non-parametric statistic test χ^2 for examining the consistency of the empirical distribution with the assumed normal distribution. As a result of the examination, satisfactory convergence of the compared distributions was obtained which made the basis for assuming the three-sigma limits of the diagnostic tolerance for the analysed engine control parameter.

Key words: technical diagnostics; naval turbine engines; exhaust gas temperature; operating and diagnostic tolerances

INTRODUCTION

The general assessment of the technical state of a naval turbine engine can be done based on the values of basic parameters, such as power, specific fuel consumption, rotational speeds of rotating units, and/or mass flow rates of the delivered fuel or the thermodynamic medium flowing through the engine. All these parameters characterise, in a general way, the quality of engine operation [1, 2, 3, 6]. However, in case of most serial engines, the above parameters cannot be directly measured (their measurement is extremely complicated and/or economically unjustified) in conditions of engine operation in the naval power plant. Moreover, these parameters do not deliver sufficiently precise information on the real course of the physical processes taking place in basic functional modules of the engine (flow part, kinematic system, fuel installation, automatic control system, etc.) [4, 5, 7, 8, 14]. That is why the operational diagnostics of turbine engines makes use of a set of auxiliary control parameters which indirectly define the basic parameters and, additionally, provide opportunities for indicating the areas in which the largest energy losses are observed, as well as for identifying and localising known and recognisable failures of engine sub-assemblies and constructional elements during engine operation.

The real value of each control parameter differs from its calculated value, which results from differences in machining (inaccuracies of the realised technological process), the action of external agents (temperature, humidity, dust, vibrations, sea undulation, etc.), impurities, and/or wear and tear of constructional elements (reversible and irreversible changes of the surface layer) [7,8,9]. These actions are of random nature (random events) and, as a consequence, generate random changes of values of the structure parameters [2, 7]. Their effect on the technical state of the engine can also be observed as changes of the probability distribution of the occurrence of these parameters – the expected value and the average deviation (dispersion around the mean value for the set of engines in operation). The smaller the changes of the expected value and the mean deviation of the control parameter, the higher the correctness of engine operation and, consequently, its lifetime and reliability.

The correctness of operation of a constructional module or unit, as well as that of the entire turbine engine, is defined by the tolerances of parameters which reflect the most desirable and permissible courses of the realised physical processes:

- Operating tolerances (maximal permissible) – determined by the producer (designer) based on the tests done on prototype copies. They define precisely the maximum ranges within

which the values of the control parameters are to be kept during the engine operation process to secure that the engine performance parameters do not drop below permissible levels, the engine operation is undisturbed and reliable, and that the technical durability is good and in line with the limits of the operating potential for particular hours and days. When the value of any control parameter exceeds the set operating tolerance limits, it is a signal of unacceptable disturbance of energy conversion processes realised in the engine, which threats with its failure (unstable operation of the compressor, for instance) [3, 7, 8, 11, 12, 14].

- Diagnostic tolerances – determined via statistical inference of the results of the tests done on a sufficiently numerous set of new and correctly adjusted engines (revealing full technical ability), compared with the results of operating tests of the same engines is successive stages of their use, provided that they still maintain a good functioning level, which is assessed from changes of basic parameters. During the time of engine operation the values of the control parameters shift towards the diagnostic tolerance limits, which signals the symptoms of small changes of engine's technical state, characteristic for the "approaching" state of inability. At the same time, the above changes of the basic parameters reflect the dependence of the technical state of the engine on the time of its operation, which manifests itself as changes of the expected values of the control parameters and their average deviations.

Consequently, a conclusion can be formulated that the tolerances of the control parameters for diagnostic purposes should be much smaller (more restrictive) that the operating tolerances.

IDENTIFYING FAILURES OF THE AUTOMATICS SYSTEM (OPERATING TOLERANCES)

Some most typical operating failures of the engine automatics system can be identified using simulation analyses done with the aid of specially designed setters (testers) on the non-operating engine [15]. These devices control the correctness of operation of the engine protection system against the excessive increase of the exhaust gas temperature. The tests aim at checking correct threshold settings for the (maximal) exhaust gas temperatures behind the exhaust gas generator, and the temperature grow rates at which the final control units in the automatics system open:

- the fuel overflow valve (ZPP),
- the main fuel valve (ZGP),
- the immediate (emergency) engine switch-off valve (ZA).

The values determined in the above way are considered the limits of the operating tolerance zone for permissible changes of parameters in the process of engine start-up and acceleration. Sample results of these tests are shown in Fig. 1 in the form of simulated dynamic time-histories of exhaust gas temperature changes. To assess the ability of the examined engine, the time-histories obtained from the simulation test are compared with the real curves recorded during earlier start-ups (see: part II – Unsteady states).

The comparison analysis of the results recorded during many years of operation of the UGT type ZORYA naval engines which were the object of diagnostic supervision [15] has made it possible to recognise characteristic thresholds for initiating certain actions of the protection system. These thresholds are

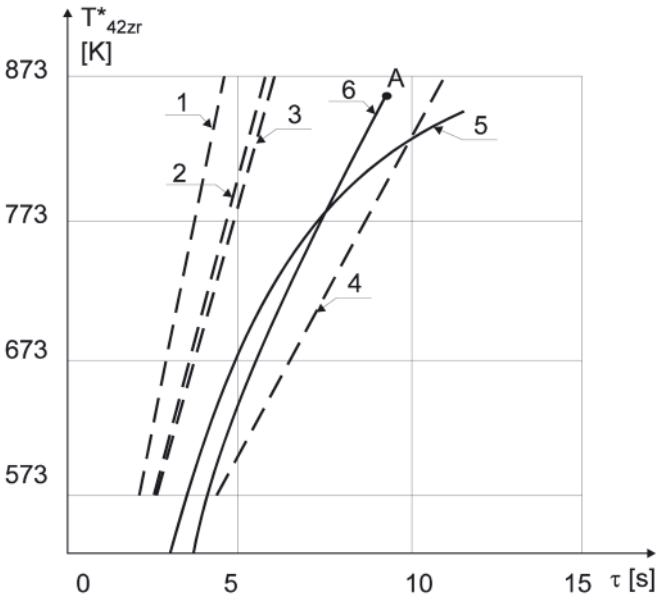

Fig. 1. *Simulated (dashed lines) and real (solid lines) time-histories of the exhaust gas temperature recorded behind the low pressure turbine during diagnostic start-up tests of the UGT type ZORYA engine.*

1 *– input function $dT^*_{42}/d\tau$ = 112 K/s - ZPP(-), ZGP(+), ZA(+);*

2 *– input function $dT^*_{42}/d\tau$ = 88 K/s - ZPP(-), ZGP(+), ZA(+);*

3 *– input function $dT^*_{42}/d\tau$ = 84 K/s - ZPP(+), ZGP(+), ZA(+);*

4 *– input function $dT^*_{42}/d\tau$ = 48 K/s - ZPP(-), ZGP(-), ZA(-);*

5 *– successful engine start-up $dT^*_{42}/d\tau$ = 64 K/s ;*

6 *– unsuccessful start-up $dT^*_{42}/d\tau$ = 82 K/s;*

A *– automatic engine switch-off*

considered the limits of the operating tolerance zone for the time derivative of the averaged exhaust gas temperature behind the exhaust gas generator:

- $dT^*_{42}/d\tau > 80$ K/s – the engine is automatically switched-off - ZPP(+), ZGP(+), ZA(+);
- $dT^*_{42}/d\tau = 50 \div 80$ K/s – the engine can be started with automatic fuel dosage - ZPP(+), ZGP(-), ZA(-);
- $dT^*_{42}/d\tau < 50$ K/s – the engine is starter automatically without the action of the protection system - ZPP(-), ZGP(-), ZA(-).

Having analysed the data shown in Fig. 1 we can conclude that the system of thermal engine protection is out of order in this case. The fuel overflow valve (ZPP) does not work, irrespective of the rate of exhaust gas temperature grow (curves 1 and 2). After a detailed analysis of the recorded symptoms of engine inability, the damaged engine automatics elements were localised and replaced. The next simulation tests confirmed the correctness of the formulated diagnosis, which is illustrated in Fig. 1 by the line 3 recorded after removing the defect.

It also results from the performed tests that the system has the zone of insensitivity ranging between 273 and 593 K, irrespective of the dynamics of exhaust gas temperature grow.

METHOD OF DEFINING DIAGNOSTIC TOLERANCES

Measurements of the control parameters which characterise the quality of the turbine engine operation in the processes of start-up, acceleration and deceleration of rotor units, the operation at steady-load ranges, and the engine switch-off are done in the very initial stage of engine use, directly after its installation in the power plant room [14, 15]. Discrete values

of the diagnostic parameters recorded in these measurements are modelled as continuous and one-dimensional random variables with the certain probability distribution, expected value, and variance being the measure of the dispersion of the measured results. In this situation the diagnostic tolerance calculation method is mainly limited to finding the form of the distribution of the dispersion of the observed discrete values of the diagnostic parameter around the average value for the entire population of engines in operation, and then to determining the parameters of this distribution. One of methods making use of the statistic inference to find the form of the distribution of the random variable consists in verifying the hypothesis that the examined distribution of the discrete values of the diagnostic parameter can be approximated using an assumed theoretical distribution which is described by a known random variable probability density function at time t = 0 [2, 10]. Once the form of the function of the theoretical distribution and its characteristic parameters (the expected value m and the average deviation σ) are known, we can determine the interval of tolerance for the values of the diagnostic parameters, for instance m ± 3σ for the normal distribution.

A method for determining the limits of the diagnostic tolerance zone for the rate of grow of the exhaust gas temperature behind the exhaust gas generator in the start-up process[1)], $dT^*_{42}/d\tau$, which take into account the unrepeatability of production and the effect of external operating agents, will be demonstrated on the population of 46 UGT3000 type Zorya turbine engines which were introduced to operation in naval power plants [14,15]. Table 1 collects a set of realisations of the numerical values of the starting temperatures recorded in the start-up process of the new engines (or directly after general overhaul) in the state of full technical ability (the values are reduced to normal atmospheric conditions) [3, 13].

Tab. 1. *Set of realisations of numerical values of the starting temperature $dT^*_{42}/d\tau$ (random variable X(t)) recorded during the start-up in the initial time of operation of UGT3000 engines installed in naval power plants*

Item	x_i [K/s]	n_i	Item	x_i [K/s]	n_i
1	12	1	8	20	5
2	13	2	9	21	4
3	14	3	10	22	3
4	15	4	11	23	3
5	16	4	12	24	3
6	17	5	13	25	2
7	19	6	14	29	1

Assuming that the distribution of the values of the analysed diagnostic parameter in time t = 0 is normal, which is confirmed by diagnostic tests of aircraft engines [2], a zero hypothesis H_0 is formulated that the distribution function of the empirical distribution shown in Table 1 is consistent with the normal distribution function. The zero hypothesis was verified using the non-parametric statistical test χ^2, which does not require the information on normal distribution parameters, i.e. the expected value m and the variance σ^2 [10]. In this situation the statistical estimation of the expected value and the variance for the calculated statistics is made based on the arithmetic mean $\overline{x}$ and the standard deviation $\overline{\sigma}$ of the measured results.

For testing purposes, the interval within which the values of the random variable are included $X(t) = \{x_i\}$ was divided into six equal sub-intervals of 3,0 K/s in length (the widths of the intervals do not have to be equal) – Table 2. The limits of the intervals were chosen in such a way that the numbers of the results of measurement in successive intervals were not excessively small (5-8 results in each interval as the minimum).

Tab. 2. *Scheme of χ_o^2 statistics calculations*

Number of interval	Limits of intervals x_i [K/s]	Number of results of measurement in i-th interval n_i	Normalised limits of intervals $z_i = \frac{x_i - \overline{x}}{\sigma}$	Value of Laplace function for beginnings of intervals Φp(zi)
1	2	3	4	5
1	11…14	6	-∞…-1.32	-0.5
2	14…17	13	-1.32…-0.52	-0.4064
3	17…20	11	-0.52…+0.27	-0.1985
4	20…23	10	0.27…1.06	0.1065
5	23…26	5	1.06…1.86	0.3507
6	26…29	1	1.86…+∞	0.4687
Sum	-	46	-	-

Number of interval	Theoretical probability to obtain the result from i-th interval $p_i = \Phi_p(z_{i+1}) - \Phi_p(z_i)$	Theoretical number of results in i-th interval $n \cdot p_i$	Value of statistics for i-th interval $\chi_i^2 = \frac{(n_i - n \cdot p_i)^2}{n \cdot p_i}$
1	6	7	8
1	0.0936	4.3056	0.6668
2	0.2079	9.5634	1.2349
3	0.3050	14.0300	0.6544
4	0.2442	11.2332	0.1354
5	-	-	-
6	0.1493	6.8678	0.1097
Sum	1.0000	46	2.8012

• arithmetic mean $\overline{x}$ = 18.97826, • standard deviation $\overline{\sigma}$ = 3.784919

[1)] Further in the text, more briefly referred to as the "starting temperature".

If the number of the results of measurement in the interval is smaller than 5, this interval is to be linked with one of the neighbouring intervals [10].

In successive steps we calculate:

- the normalised limits of the intervals with respect to $\overline{x}$, re-calculated to $\overline{\sigma}$ units:

$$z_i = \frac{x_i - \overline{x}}{\overline{\sigma}} \tag{1}$$

The beginning of the first interval is -∞, while the end of the last interval is +∞. The end of the previous interval is simultaneously the beginning of the next interval;

- the normalised Laplace function of the normal distribution for the beginnings Φp(zi) of the intervals – from statistical tables [10];
- the theoretical probability to obtain the result from the i-th interval:

$$p_i = \Phi_p(z_{i+1}) - \Phi_p(z_i) \tag{2}$$

- the theoretical number of results in the i-th interval: $n \cdot p_i$;
- the χ_i^2 statistics for each interval:

$$\chi_i^2 = \frac{(n_i - n \cdot p_i)^2}{n \cdot p_i} \tag{3}$$

The last step includes calculating the value of the statistics for the analysed set of random variable realisations:

$$\chi_0^2 = \sum_{i=1}^{n} \chi_i^2 = 2.8012 \tag{4}$$

The calculated value of the χ_0^2 statistics should be compared with its critical value determined from the statistical tables [10], at the assumed significance level α and the number of freedom degrees f calculated from the following relation:

$$f = l - k - 1 \tag{5}$$

where:

l – number of intervals in the distributive series,

k – number of estimated parameters of the verified distribution.

Two parameters characterising the normal distribution: $\overline{x}$ and $\overline{\sigma}$, were evaluated based on the empirical data. For the number of degrees of freedom: f = 2 (l = 5, k = 2) and the assumed significance level: α = 0.05 the critical value of the statistics which was read in the χ^2 distribution tables is equal to $\chi_{kr}^2 = 5.991$ [10].

The calculated value of the statistics is equal to $\chi_o^2 = 2.8012$ and is smaller than the critical value $\chi_{kr}^2(\alpha = 0.05, f = 2) = 5.991$. That means that there is no ground for rejecting the zero hypothesis and, consequently, that the analysed empirical distribution can be considered consistent with the normal distribution. Therefore the probability density function of the random variable $X(t) = \{x_i\}$ in the initial operation stage (time t = 0) can be given by the formula:

$$f(x) = \frac{1}{\sigma \cdot \sqrt{2\pi}} \cdot \exp\left[-\frac{(x - \overline{x})^2}{2 \cdot \sigma^2}\right] \tag{6}$$

Having known the formula for the distribution and its basic parameters we can calculate the limits of the diagnostic tolerance zone assuming the value interval m±3σ as the diagnostic limiting conditions for the control parameter of interest. For the analysed starting temperature the calculated expected value was equal to $m = \overline{x} = 18.98$ K/s and the average deviation was $\sigma = \overline{\sigma} = 3.78$ K/s, which gives the following diagnostic tolerances of the analysed control parameter:

$$7.64 \le x_{t=0} \le 30.32 \tag{7}$$

It results from the performed calculations that the diagnostic tolerances of the rate of exhaust gas temperature grow in the start-up process of the turbine engine of UGT3000 type are limited from one side, which means that the limiting value of this parameter assessed for diagnostic purposes must not exceed 30 K/s in a new engine.

Taking advantage, in turn, of the symmetry of the normal distribution and the values of the Laplace function $\Phi_p(z_i)$ we can calculate the probability that the random variable X(t) takes a value from within this interval:

$$P\{X \in (m \pm 3\sigma)\} = \Phi_p(3) - \Phi_p(-3) = 0.9973 \tag{8}$$

Thus, assuming the three-sigma limits for the diagnostic tolerances of the analysed control parameter means that less than 3 $^0/_{00}$ (3 out of 1000 as the maximum) of possible results of measurement differ from the expected value by more than 3σ.

In the process of engine operation on a ship, the action of unfavourable operating agents leads to ageing, wear, and pollution of constructional elements. These processes are permanent and irreversible, and they always accompany the operation of internal combustion engines in marine conditions. All this leads to the decrease of the usable potential, the measure of which are the deformations of the shape of probability density function defined by the changes of the expected value and the average deviation, while the normal distribution of the random variable (dispersion of the analysed control parameter) is still being preserved. As a consequence, the dispersion of the exhaust gas temperature grow rate in the engine start-up process increases, and the limits of the diagnostic tolerances, which under no circumstances can exceed the operating tolerances, become wider – Fig. 2. We accept that with the increasing total time of engine operation its functioning is getting less correct, but still preserves all requirements of safe use.

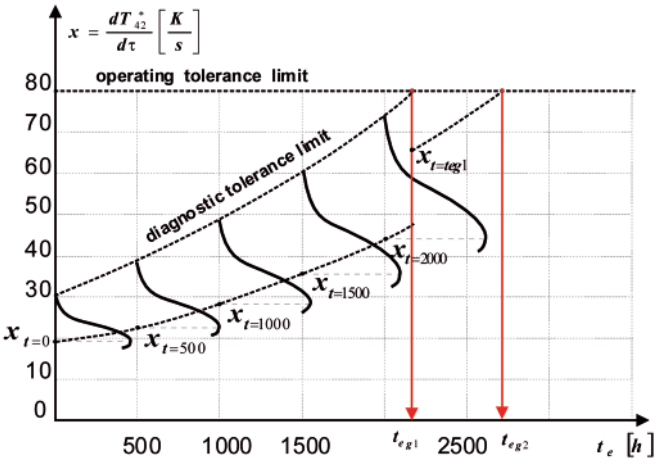

Fig. 2. Deformations of the shape of the probability density function for the analysed random variable vs. the total time of operation of the turbine engine

It results from the numerical data shown in Fig. 1 that after calculating the shapes of the probability density function of the random variable in successive stages of engine operation (for instance, in annual control and measurement cycles, or after each 500 hours of operation) we can determine the trend lines for the changes of the expected value and the upper tolerance limit of the set or realisations of the diagnostic parameter. We can also assess the horizon for the prognosis of correct engine operation (without failures) until time t_{eg1} based on the crossing point of the line of upper diagnostic tolerance limit with the line of the operating tolerance limit. For this purpose the value

of the diagnostic parameter is to be measured on the examined engine - for instance, the point:

$$x_{t=teg1} = \left(\frac{dT_{42}^{*}}{d\tau} \right)_{t=teg1}$$

and the upper diagnostic tolerance limit is to be extrapolated until it crosses the line of the operating tolerance limit (time t_{eg2}) etc. This way we formulate the strategy of engine operation based on its current technical state, the reconstruction of which (adjustment, repair, replacement of an element) depends on individual features of constructional structure degradation, mainly connected with the nature of changes of engine load (number of start-ups, stop-down, accelerations and decelerations of rotor units, manoeuvres of the separate power turbine, etc.).

CONCLUSIONS

The presented sample application of the statistical method for determining the diagnostic tolerances of the rate of grow of the exhaust gas temperature recorded in the start-up process of a naval turbine engine can be extended onto remaining control parameters recorded during engine operation. A necessary condition for statistical inference is to adopt the assumption that in the initial stage of operation the examined engines maintain correct functioning, which is assessed from the values of basic parameters. In this situation the value of the observed control parameter shifts towards the limit of the diagnostic tolerance zone, thus generating a symptom of small changes of the technical state, characteristic for the "approaching" inability state. Simultaneously it reflects the dependence of the technical state of the engine on the time of its use, which manifests itself by changes of the expected values of the control parameter and its average deviations in successive engine operation stages.

BIBLIOGRAPHY

1. Balicki W., Szczeciński S.: *Diagnosing aircraft turbine engines. Rotor machines*. (in Polish). Scientific Library of the Institute of Aviation. Warsaw 2001.
2. Boliński B., Stelmaszczyk Z.: *Aircraft propulsion systems. Operation of turbine engines* (in Polish). WKiL, Warsaw 1981.
3. Cohen H., Rogers G.F.C., Saravanamuttor H.I.H.: *Gas turbine theory*. Longman Scientific & Technical, New York 1987.
4. Dzida M.: *Influence of gas turbine controller adjustment on ship propulsion system behavior in rough sea conditions Part 2. The simulation investigations*. Polish Maritime Research, No 1(39), 2004, Vol.11.
5. Dzida M.: *Simulation of ship propulsion gas turbine dynamics - an educational laboratory model*. Polish Maritime Research, No 4(22), 1999, Vol.6.
6. Hardin J.R. and others.: *A gas turbine condition - monitoring system*. Naval Engineers Journal, November, USA 1995.
7. Korczewski Z.: *Method of diagnosing the flow part of a naval turbine engine in operation* (in Polish). AMW (Ph.D. thesis), Gdynia 1992.
8. Korczewski Z.: *Identifying gasodynamic processes in the compressor system of a naval turbine engine for diagnostic purposes* (in Polish). AMW Gdynia 1999.
9. Korczewski Z.: *Endoscopy of naval engines* (in Polish). AMW Gdynia 2008.
10. Korzyński M.: *Methodology of experiment* (in Polish). WNT Warszawa 2006.
11. Orkisz M.: *Selected problems in the theory of naval jet engines* (in Polish). ITE, Radom 1995.
12. Pawlak W., Wiklik K., Morawski J.M.: *Synthesis and investigations of aircraft turbine engine control systems using computer simulation methods* (in Polish). Institute of Aviation, Warsaw 1996.
13. Szczeciński S.: *Aircraft turbine engines* (in Polish). Wydawnictwo MON, Warsaw 1965.
14. *Technical and operating documentation of naval turbine engines GTU6a, DE59, ZORYA of UGT type, General Electric LM2500* (in Polish).
15. *Reports on diagnostic tests of piston and turbine engines in operation on Polish Navy vessels – Research activities of AMW* (in Polish), Gdynia 1992 ÷ 2008.

CONTACT WITH THE AUTHOR
Zbigniew Korczewski, Prof.
Faculty of Ocean Engineering
and Ship Technology
Gdansk University of Technology
Narutowicza 11/12
80-233 Gdansk, POLAND
e-mail: z.korczewski@gmail.com

POLISH MARITIME RESEARCH 4(71) 2011 Vol 18; pp. 54-58
10.2478/v10012-011-0027-6

Influence of pitting corrosion on strength of steel ships and offshore structures

Marek Jakubowski, Assoc. Prof.
Gdansk University of Technology

ABSTRACT

The present paper deals with the influence of pitting corrosion on mechanical properties of mild and low alloy steels and strength of steel structures under static and quasi-static loads. Pitting corrosion is a very important phenomenon that influence local strength of ship hull members. The present paper is based mainly on Japanese publications. Analyzing the standard tensile diagrams one can see that that pitting corrosion reduces the load corresponding to yield stress (YS) and, even more markedly, tensile strength UTS, reduces almost to zero plastic flow strains at YS load level and dramatically reduces the total elongation to fracture. Nominal UTS load for uniformly corroded specimens is higher than that for pitted specimens at the same average thickness loss. The strength related to the true fracture surface area (i.e. reduced by pits, taking into account real path of the crack through the pits) is almost independent of the thickness loss and is almost the same as for uniform thickness loss. For wide specimens the tensile strength depends mainly on the local deformation ability, and the maximum loading ability for large members, predicted on the base of the total true fracture surface area, can be overestimated. Concept of equivalent thickness loss for plates under bending and compression and for more complex structural models as well as relation between the average and the equivalent thickness losses has been presented. Approach based on degree of pitting (ratio of pitted area to total plate surface area) has been shown as a real and more convenient than the approach based on the thickness loss.

Keywords: pitting corrosion, strength, shipbuilding steels, ship structures

INTRODUCTION

There are two groups of actions that can lead to damages of real structures:

- Chemical or electrochemical, if undesirable, are identified with corrosion
- mechanical, usually identified with stresses or strains

Interaction of corrosive and mechanical factors is the most general case. Almost all corroding structures are stressed. Almost all stressed structures are exploited in any environment that is not neutral in mechanical damage process. Pure mechanical or pure corrosive damage can be considered as specific and unusual cases. In case of vacuum or eventually inert gas environment we can assume that damage is purely mechanical in nature, while for very low stress levels we can assume that damage is purely corrosive.

The above is especially true for ships and offshore structures that are the main object of the present paper. Corrosive environment of these structures is also the main source of service loads, i.e. static or dynamic pressure of sea water.

The present paper concerns the influence of pitting corrosion on strength of steels and steel structures under static or quasi-static loads. The mild and low alloy steels used for welded marine structures are considered as insensitive to stress corrosion cracking in marine environment. Therefore only the pit nucleation and growth process should be considered as a complex mechanical-electrochemical phenomenon. Fracture process occurs in a relatively short time and influence of corrosive environment on this process can be considered as negligible. Pitting corrosion incubation and growth and the role of strain and/or stress in this process has been discussed elsewhere [1, 2]. The present paper is focused on the influence of pre-existing pits on mechanical properties of mild and low alloy steels and strength of the steel structures.

Previous pitting corrosion influences the fatigue strength and life by the following ways:

I reduction of the average material thickness that influence the nominal stress in the structure;
II pitting-corrosion-induced roughness of the material surface that leads to local stress concentrations at some locations at the surface.

The role of pitting in fatigue of materials and structures is commonly appreciated. The problem has been discussed in [2] on the wide base of references concerning different materials. In common opinion, pits, if they are present at the material, are almost always the potential sites of the fatigue crack initiation, thus they reduce the fatigue life. If strength of steel structures under static or quasi-static loadings is considered, the opinion is not so unanimous.

Melchers [3] has formulated opinion that pitting corrosion has very little influence on the strength of well maintained structures, such as ships – general corrosion (loss of thickness) is more important. This opinion has been accepted by Wang et al. [4]. These authors have elaborated models for the time-related growth of the maximum depth of pitting because, in their opinion, the main menace is perforation of the structure walls and it can be dangerous especially for pipelines and tanks. However, extensive studies of the influence of pitting corrosion on the behaviors of materials and structures under static loading has been carried out in Japan by Nakai, Matsushita, Yamamoto and, in some papers, Arai [5 - 10], and they have shown that the influence of pitting on the steel strength is not negligible. General strength of ship hull is mainly affected by general corrosion that reduce thickness of shell and stiffeners therefore reduce midship section modulus. Pitting corrosion is a very important phenomenon that influence local strength of ship hull members.

International Association of Classification Societies (IACS) [11, 12] and Polish Register of Shipping (PRS) [11, 12] have defined the required minimum thickness of plating in pits or other local corrosion areas (is to be greater than 70-75% of the as-built thickness), or average thickness across any cross section in the plating (is to be greater than the renewal thickness for general corrosion). These requirements are surely based on unknown considerations of strength of pitted steel.

TENSILE DIAGRAM FOR PITTED STEEL

The mentioned Japanese authors tested only conical pits that are observed on hold frames of bulk carriers. The pits were generated artificially by spot drilling of the both steel surfaces. Different pit patterns were manufactured with different values of degree of pit intensity DOP (ratio of pitted area to entire area of the specimen). In the Rules of Classification Societies DOP is called simply the pitting intensity. In order to verification of validity of such artificial pits testing, the results were compared to the results for actually corroded specimens [9]. It has appeared that specimens with orderly located artificial pits which had a fixed diameter equal to the average pit diameter in actual corroded specimens could simulate the actual corroded specimen where the pit size and distribution are random. Results of standard static tensile tests of pitted and smooth specimens are described in [6, 7, 9]. Exemplary tensile diagrams (load versus displacement) for small specimens are shown in Fig. 1 [7]. It is evident that pitting:

(i) reduced the load corresponding to yield stress;
(ii) reduced almost to zero plastic flaw strain at the level of yield strength;
(iii) reduced load, corresponding to ultimate tensile strength, even stronger than yield stress;
(iv) markedly reduced total elongation to fracture;
(v) total elongation for 13mm and 11mm uniformly thick specimens is the same.

The same investigations [7] have shown that the effect of pitting depends on the specimen thickness, i.e. the nominal tensile strength and total elongation dropped more

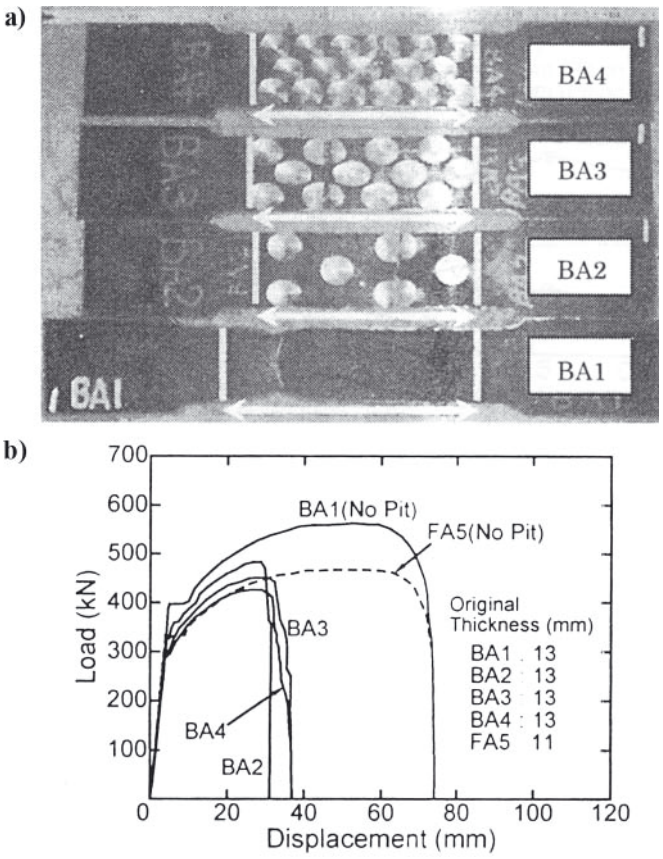

Fig. 1. *Results of small tensile specimens testing:* ***a)*** *view of specimens after testing;* ***b)*** *tensile diagram "load – displacement" [7]*

significantly for higher pit-depth-to-plate-thickness ratios. For thinnest plated (10 mm) total elongation dropped from 30% to about 5%.

Matsushita et al [6] realized tensile tests of specimens with different DOP from a single one-side pit up to more than 80% of two-side surfaces covered by pitting. Pitting corrosion causes not only unevenness of the material surface but reduction of the average thickness too. The larger DOP leads to the larger average thickness loss. Results are plotted as a function of the thickness loss in Fig. 2 and Fig. 3.

Trend lines for ideally uniform corrosion are also plotted in Fig. 2. All over the range of thickness loss values, the nominal strength for pitted specimens is lower than for "uniformly corroded" ones. The specimens fractured at the smallest area where the local thickness reduction was larger than the average value. Meanwhile, strength of the "uniform corrosion" specimen with a value of uniform thickness loss is always compared with the pitted specimen strength of the same average (not local) thickness loss. True fracture surface does not develop close to one surface approximately perpendicular to load axis, as that in non-pitted specimens, but jumps from one plane to another according to pits distribution. True fracture surface area can be evaluated as the area of the fracture surface before loading projected to the plane perpendicular to the load axis and practically can be substituted by the minimum cross-sectional area (i.e. locally reduced by pits) before loading perpendicular to the load axis [9]. In Matsushita et al opinion, the true strength that is based on the true fracture surface area is the same for uniform and non-uniform thickness loss (Fig. 2b). In our opinion, however, the above explanation is only partially valid. If the only specimen of another type (wide specimen – type B) is not taken into account, the strength of pitted specimens for average thickness loss below 2 mm will be 527-600 MPa, while for average thickness loss above 2 mm

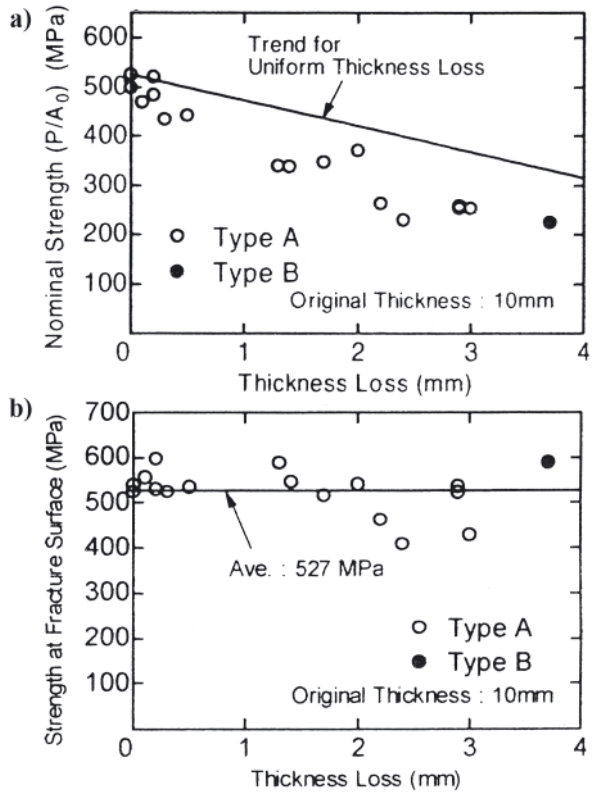

Fig. 2. *Tensile strength of pitted steel versus thickness loss for type A (small specimens) and type B (wide specimens):* ***a)*** *nominal strength P/A_0 (P is the load, A_0 is the initial cross-section area);* ***b)*** *true strength P/A (A is the true area of fracture surface, i.e. reduced by pits) [6]*

the strength will be 400-527 MPa thus it is not independent of the intensity of pitting. In spite of that, the maximum load that can be carried by a specimen can be approximately predicted by the above approach based on true fracture surface or minimum cross-sectional area [6, 9].

The last conclusion concern so called small specimens. The situation is more complex in case pf large (much more wide) specimens. Fracture of small specimen occurs when plastic deformation develops throughout the minimum cross section. In much more wide specimens, having areas with pits of different size and distribution, the deformation ability differ from location to location. As a result, fracture occur locally at this regions where elongation reaches critical value first, i.e. where the elongation ability is the lowest due to local pits sizes and distribution, this local fracture is the dominant factor that determines the maximum load ability of the specimen modeling a structural member [9]. That is why the maximum loading ability for large members, predicted on the base of total true fracture surface area, is overestimated, while for small members this approach was successful [10].

Analogous diagram for total elongation is shown in Fig. 3. The uniform thickness loss does not cause reduction of total elongation (see also Fig. 1). Thus the observed very significant drop of values of total elongation has to be entirely attributed to non-uniform character of pitting corrosion. The drop is very rapid for small values of thickness loss (also values DOP are small). Then relationship saturates and the total elongation does not depend on thickness loss and DOP. Nakai et al [7] noted the minimum, and next even an increase of total elongation as DOP is increased further. This is perhaps due to decrease of the ratio of pit depth to average thickness loss. These data are for 10 mm thick material. For thicker materials the reduction of elongation is also evident but not so dramatic.

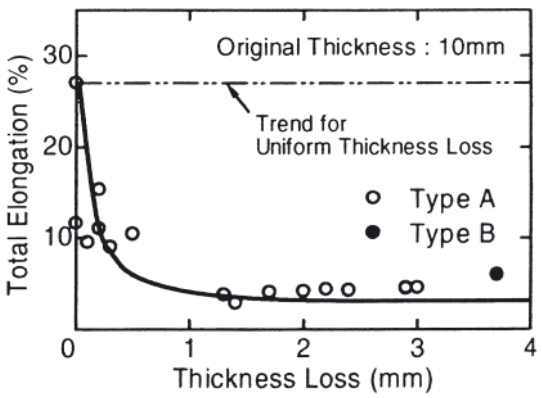

Fig. 3. *Relationship between thickness loss and total elongation in tensile test [6]*

ULTIMATE STRENGTH OF STRUCTURAL MODELS

Lateral-torsional buckling of whole hold frames, and local buckling and fracture of web and face plates in the lower parts of hold frames, is damage typically seen in the hold frames of bulk carriers [5]. Therefore extensive program of FE analyses has been realized [5] with square plates containing conical corrosion pits (aspect ratio depth-to-width of pit equal to 0.125) of different size and distribution. Compressive load plus bending moment have been applied in different proportions: from pure compression (stress gradient equal 0) to pure bending (gradient equal 2).

As for tensile test, for these loads it also has appeared that ultimate strength of pitted plates is smaller than or equal to that of uniformly corroded plate for the same average thickness loss. There is a tendency for the strength reduction to increase as the pit diameter and depth is increased. Thus a prediction of the strength of pitted plates using the average thickness loss would lead to non-conservative results. However, the average thickness loss or maximum pit depths are not always dominant factors for ultimate strength but the strength depends also on type of pit distribution on the both sides of the plate [5, 9].

Nakai and co-workers analyse equivalent thickness of plate for ultimate tensile strength (t_e) that is defined as the thickness of an uniformly corroded plate whose ultimate strength is the same as that of pitted plate. Value of the equivalent thickness is almost independent of the loading mode: from pure compression, through different combinations of compression and bending, up to pure bending [5]. Nakai and co-workers have compared these values of equivalent thickness to the values evaluated by tensile test, where the following proportion is valid:

$$t_e / t_0 = \sigma_u / \sigma_{u0} \tag{1}$$

where t_0 is the original plate thickness, σ_u and σ_{u0} are the nominal UTS for the plate with and without pits, respectively. The comparison has been made for the same degree of pit intensity (DOP). It has appeared that equivalent thickness evaluated in tensile test of pitted specimens is smaller than that for evaluated for plates subjected to in-plane compression and bending, especially for the thinnest specimens. Thus tensile test represent the most dangerous case. If an evaluation method for the effect of pitting corrosion on the equivalent thickness (t_e) under tensile loading is established, a reduction of t_e of pitted plates under in-plane compression, bending and shear will be predicted conservatively by the same method.

Equivalent thickness of plates with pitting corrosion (t_e) for the tensile strength is almost equal to average thickness at the minimum cross section ($t_{ave,min}$)[10]:

$$t_e = t_{ave,min} \quad (2)$$

Equivalent thickness loss (t_{el}) is defined as thickness loss of uniformly corroded plate that has the same tensile strength as a plate with pitting corrosion. It can be calculated by:

$$t_{el} = t_0 - t_e \quad (3)$$

Average thickness loss (t_{al}) of pitted plates is defined by:

$$t_{al} = t_0 - t_{ave} \quad (4)$$

where:
t_{ave} – the average thickness of the pitted plates.

Finite Element (FE) analyses of pitted square plates under uniaxial compression, biaxial compression, shear and combinations if the above mentioned loadings showed that the equivalent thickness can conservatively be predicted by equation (3) and the following equation [10]:

$$t_{el} = 1.25 \cdot t_{al} \quad (5)$$

Thus ultimate strength of pitted plate of an average thickness (t_{ave}') is lower than the strength of uniformly corroded plate of the same thickness. This means that unevenness of the plate surface due to pitting corrosion reduce ultimate strength of the plate.

FE analyses of structural model: beam (web plate, face plate and shell) under 4-points bending has been done [10]. Web plates were pitted. It has appeared that for the following cases: (i) the ultimate strength is reached accompanying local buckling; (ii) the structural models collapse without buckling; (iii) shear buckling of web plates occurs; and (iv) web crippling occurs, equivalent thickness of the web plates can be predicted by equation (3) and the following equation:

$$t_{el} = 1.44 \cdot t_{al} \quad (6)$$

The above equations mean that the influence of the pitting-corrosion-induced unevenness of the plate surface on the ultimate strength of more complex structural models is more detrimental than for simple square plates.

APPROACH BASED ON DEGREE OF PITTING (DOP) INSTEAD THICKNESS LOSS

Nakai and co-workers conclude that for non-uniform random pitting, the average thickness loss of a whole plate, or for the minimum cross section, is often difficult to determine. Each pit is covered with a heavy rust blister which is difficult to remove, even with hammers. Even if the rust blisters and rust from non-pitted areas are removed, correct thickness measurement is difficult due to great unevenness of the surface. [9, 10]. The average thickness loss or the average thickness loss at the minimum cross section cannot be determined directly by observation of the plate surface. Meanwhile, degree of pitting (DOP) can be approximately evaluated by observation of the plate surface also without removing the heavy rust blisters, because Nakai and co-workers has shown that the diameter of the rust blisters and that of the corresponding pits are almost the same [10] and degree of blisters intensity (ratio of the surface area covered with rust blisters to the entire surface area) corresponds to DOP. Therefore, to elaborate a method of evaluating the tensile strength of pitted members using the value of DOP, is a task of primary importance.

First attempt to solve this problem has been made by the same authors [10]. Diagrams of thickness loss of plates versus values of DOP are shown in Fig. 4. The diagrams include average thickness loss t_{al} and effective thickness loss t_{el} for ultimate strength calculated for different cases: square plates under combined loading of compression and shear [equation (5)], more complex structural models (equation (6)) and for ultimate tensile strength. From ultimate-strength point of view, average thickness loss is not so important as effective thickness loss. Equivalent thickness loss for all three cases is increases almost linearly with the increase of DOP when DOP is smaller than approximately 75% [10]. The trend is especially evident foe equivalent thickness loss for ultimate tensile strength. Equivalent thickness loss for tensile strength (that equals to average thickness loss at minimum cross section) is larger than that for other loading conditions; only for largest values of DOP it is equal to $1.44t_{al}$ that is specified for structural models The same observation has been made for plates under in-plane compression and bending [5] described above. Therefore, it is possible to ensure the structural integrity if the average thickness loss at the minimum cross section is within the allowable corrosion level specified in rules for uniformly corroded members [10]. Allowable value of DOP could be evaluated on the base of allowable thickness loss for uniform corrosion, equivalent thickness loss for the pitted plate, and Fig. 4.

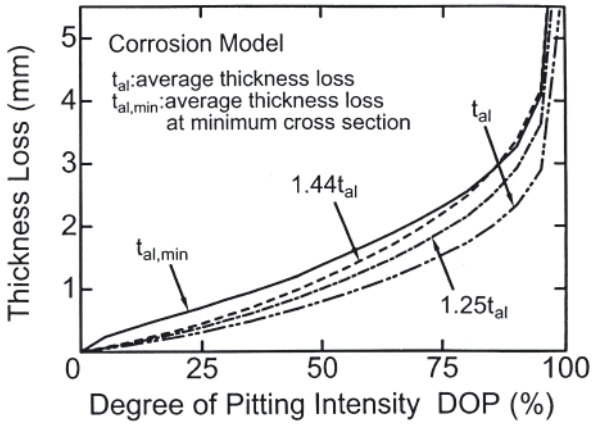

Fig. 4. *Diagram of average thickness loss t_{al}, equivalent thickness loss under combination of compression and shear ($1.25t_{al}$), equivalent thickness loss for ultimate strength of structural models ($1.44t_{al}$) and equivalent thickness loss for tensile strength at minimum cross section ($t_{al,\,min}$) versus degree of pitting (DOP) [10]*

Analyzing progress of pitting corrosion as a function of DOP, it has appeared [10] that average thickness loss and standard deviation of the thickness loss vary with small scatter band, while large scatter band is observed for extreme values like maximum pit depth or average thickness loss at the minimum cross section. When average thickness loss exceeds about 2 mm for one side of plate, then DOP equals about 100%. After this stage the form of corrosion tends to a change from pitting corrosion to general corrosion.

The same authors [8] have investigated experimentally and analytically (FEM) strength of 4 point bent welded frames contained of web plate, face plate and shell (tensile load act on the face plate). Artificial pits were made over a separated areas of the web plate. Lowest strength had a frame with a band of pits close to the compressed shell, higher strength had the frame with a band of pits situated at the center of the web height, highest strength had the frame with pits close to tensed face plate. Pits situated at the center of the frame length (pure bending segment) more significantly reduced strength than that situated close to ends (high shear stress). It means that localization of pitting corrosion at the web plate surface is an additional factor influencing the strength of frame. Influence

of this position of pitting corrosion on the frame strength for longer, slender frames is less pronounced than for short frames.

CONCLUSIONS

1. Uniform thickness loss dos not influence the total elongation of specimens in tensile test. Pitting corrosion, even of small degree of pit intensity, very significantly reduce total elongation of the specimens. Pitting corrosion reduces the ultimate tensile strength of steels stronger than the uniform corrosion
2. For tension and any combination of in-plane compression and bending, the ultimate strength of pitted plate is smaller than that of uniformly corroded plate with the same average thickness loss. There is a tendency for the strength reduction to increase with the as the pit diameter and depth is increased. Thus a prediction of the strength of pitted plates using the average thickness loss would lead to non-conservative results
3. The equivalent thickness (t_e), defined as the thickness of uniformly corroded plate whose ultimate strength is the same as that of pitted plate, for tensile loading is smaller than for any combination of in-plane compression and bending. Therefore it can be applied for conservative prediction of strength of members subjected to each of the loading modes.
4. It is possible and convenient to analyze the ultimate strength of pitted structures as a function of degree of pitting (DOP – the ratio of the total pitted area to the entire area of the plate) instead as a function of the plate thickness loss.
5. Ultimate buckling strength of pitted plates and frames depends also of the position of the pitted areas and the type of pit distribution in every area.

Acknowledgements

This work has been performed in the scope of the project RISPECT "Risk-Based Expert System for Through-Life Ship Structural Inspection and Maintenance and New-Build Ship Structural Design" which has been financed by the UE under the contract SCP7-GA-2008-218499

BIBLIOGRAPHY

1. Jakubowski M.: *Influence of pitting corrosion on fatigue and corrosion fatigue of ship structures. Part I: Mechanism and modeling of pitting corrosion of ship structures*. To be published in Polish Maritime Research
2. Jakubowski M.: *Influence of pitting corrosion on fatigue and corrosion fatigue of ship structures. Part II: Loading – pitting – cracking interaction*. To be published in Polish Maritime Research
3. Melchers R.E.: *Pitting corrosion of mild steel in marine immersion environment – Part 1: Maximum pit depth*. Corrosion, 2004, Vol.60, No 9, pp.824-836.
4. Wang Y., Wang Y., Huang X. Cui W.: *A simplified maximum pit depth model of mild and low alloy steels in marine immersion environment*. Journal of Ship Mechanics, 2008, Vol.6, No.1, pp.401-417.
5. Nakai T., Matsushita H., Yamamoto N.: *Effect of pitting corrosion on the ultimate strength of steel plates subjected to in-plane compression and bending*. J. Marine Science and Technology, 2006, pp.52-64.
6. Matsushita H., Nakai T., Yamamoto N., Arai H.: *Effect of corrosion on static strength of hull structural members (1st report)*. J. Society of the Naval Architects of Japan, 2002, Vol.192, pp.357-365 (in Japanese)
7. Nakai T., Matsushita H., Yamamoto N., Arai H.: *Effect of corrosion on static strength of hull structural members (2nd report)*. J. Society of the Naval Architects of Japan, 2004, Vol.195, pp.221-231(in Japanese)
8. Nakai T., Matsushita H., Yamamoto N., *Arai H.: Effect of corrosion on static strength of hull structural members (3rd report)*. J. Society of the Naval Architects of Japan, 2004, Vol.195, pp.233-242 (in Japanese).
9. Nakai T., Matsushita H., Yamamoto N., *Arai H.: Effect of pitting corrosion on local strength of hull structural members*. ClassNK Technical Bulletin, 2005, pp.29-49.
10. Nakai T., Matsushita H., Yamamoto N.: *Assessment of corroded conditions of webs of hold frames with pitting corrosion*. ClassNK Technical Bulletin, 2007, pp.23-32.
11. Polish Register of Shipping (PRS) Rules: *Publication No. 84/P, Requirements concerning the construction and strength of the hull and hull equipment of sea-going bulk carriers of 90 m length and above*, 2009, Chapter 13.2.3.2.3.; as well as International Association of Classification Societies (IACS): Common Structural Rules for Bulk Carriers, Chapter 13.2.3.2.3.
12. Polish Register of Shipping (PRS) Rules: Publication No. 85/P, *Requirements concerning the construction and strength of the hull and hull equipment of sea-going double hull oil tankers of 150 m in length and above*, 2010, Chapter 12.1.3. – 13.1.6.; as well as International Association of Classification Societies (IACS): Common Structural Rules for Double Hull Tankers, Chapter 12.1.3. – 13.1.6.

CONTACT WITH THE AUTHOR
Marek Jakubowski, Assoc. Prof.
Faculty of Ocean Engineering
and Ship Technology
Gdansk University of Technology
Narutowicza 11/12
80-233 Gdansk, POLAND
e-mail: marjak@pg.gda.pl

On November 29th, 2011
at the age of 84, passed away

Former Editor (1994 – 2007) of the Quarterly "Polish Maritime Research"

Mr **Zbigniew Witold Kirkor**, M. Sc.

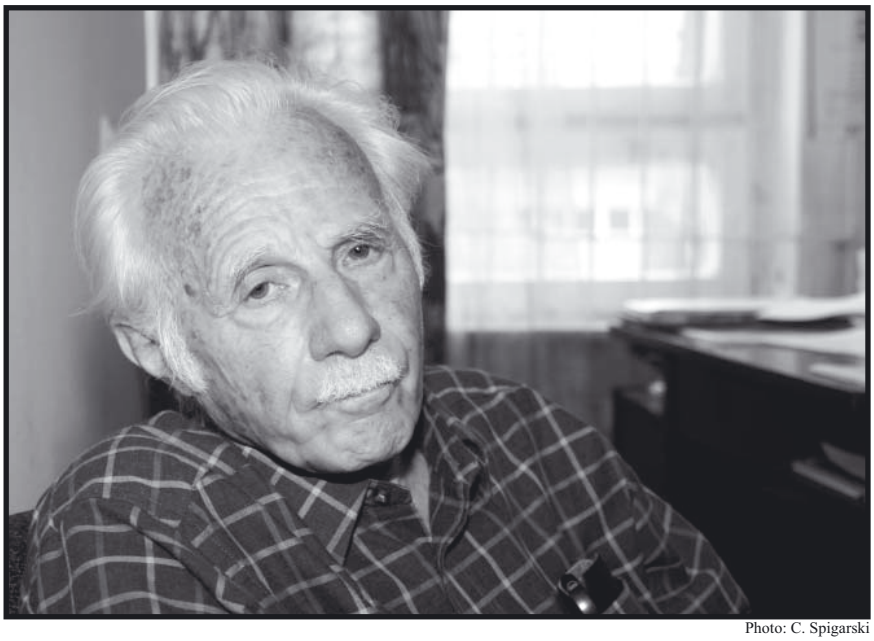

Photo: C. Spigarski

Mr Zbigniew W. Kirkor graduated from the Faculty of Ocean Engineering and Ship Technology, Gdansk University of Technology in 1956.

He was awarded the Knight's Cross of the OOP, the Gold Cross of Merit and was honoured with many other sport-related distinctions.

Dean

Faculty of Ocean Engineering
and Ship Technology,
Gdansk University of Technology

Editorial Board

Polish Maritime Research

The Ship Handling Research and Training Centre at Ilawa is owned by the Foundation for Safety of Navigation and Environment Protection, which is a joint venture between the Gdynia Maritime University, the Gdansk University of Technology and the City of Ilawa.

Two main fields of activity of the Foundation are:

- Training on ship handling. Since 1980 more than 2500 ship masters and pilots from 35 countries were trained at Iława Centre. The Foundation for Safety of Navigation and Environment Protection, being non-profit organisation is reinvesting all spare funds in new facilities and each year to the existing facilities new models and new training areas were added. Existing training models each year are also modernised, that's why at present the Centre represents a modern facility perfectly capable to perform training on ship handling of shipmasters, pilots and tug masters.

- Research on ship's manoeuvrability. Many experimental and theoretical research programmes covering different problems of manoeuvrability (including human effect, harbour and waterway design) are successfully realised at the Centre.

The Foundation possesses ISO 9001 quality certificate.

Why training on ship handling?

The safe handling of ships depends on many factors - on ship's manoeuvring characteristics, human factor (operator experience and skill, his behaviour in stressed situation, etc.), actual environmental conditions, and degree of water area restriction.

Results of analysis of CRG (collisions, rammings and groundings) casualties show that in one third of all the human error is involved, and the same amount of CRG casualties is attributed to the poor controllability of ships. Training on ship handling is largely recommended by IMO as one of the most effective method for improving the safety at sea. The goal of the above training is to gain theoretical and practical knowledge on ship handling in a wide number of different situations met in practice at sea.

For further information please contact:
The Foundation for Safety of Navigation and Environment Protection

Head office:
36, Chrzanowskiego Street
80-278 GDAŃSK, POLAND
tel./fax: +48 (0) 58 341 59 19

Ship Handling Centre:
14-200 IŁAWA-KAMIONKA, POLAND
tel./fax: +48 (0) 89 648 74 90
e-mail: office@ilawashiphandling.com.pl
e-mail: office@portilawa.com